Targeting Kv2.1/Syntaxin Interaction for Neuroprotection

by

Chung-Yang Yeh

B.A., Rutgers University, 2014

Submitted to the Graduate Faculty of

School of Medicine in partial fulfillment

of the requirements for the degree of

Doctor of Philosophy

University of Pittsburgh

2019

UNIVERSITY OF PITTSBURGH

SCHOOL OF MEDICINE

This thesis/dissertation was presented

by

Chung-Yang Yeh

It was defended on

June 27, 2019

and approved by

Dandan Sun, Professor, Neurology

Thanos Tzounopoulos, Professor, Otolaryngology

Michael Palladino, Professor, Pharmacology & Chemical Biology

Amantha Thathiah, Assistant Professor, Neurobiology

Rajesh Khanna, Professor, Pharmacology, University of Arizona

Dissertation Director: Elias Aizenman, Professor, Neurobiology

Targeting Kv2.1/Syntaxin Binding for Neuroprotection

Chung-Yang Yeh, PhD

University of Pittsburgh, 2019

The regulation of cytosolic potassium is a convergent factor in cell death programs of many mammalian cell types including central nervous system neurons. Physiological levels of potassium concentrations can suppress the activation of critical caspases and nucleases necessary for cell death. Under physiological conditions, several ion channels and exchangers sustain intracellular potassium levels. Conversely, tightly regulated molecular pathways facilitate the depletion of intracellular potassium after injury to very low concentrations, enabling cell death mechanisms to proceed. Several research groups have shown that preventing the loss of intracellular potassium after injury through various approaches can increase the survivability of several cell types. In neurons, the main regulator of intracellular potassium after injury is the delayed rectifier potassium channel Kv2.1. Strategies aimed to ameliorate Kv2.1-dependent neuronal cell death have been investigated over the past several years. We have come to understand that lethal oxidative damage set forth unique, zinc-dependent phosphorylation of Kv2.1, leading to enhanced membrane channel insertion and elevated potassium efflux currents. Critical to this pathway is the protein-protein interaction between Kv2.1 and the cell surface soluble NSF attachment protein receptor (SNARE) syntaxin 1A (syntaxin). Interrupting this interaction has been shown to improve neuronal survival in vitro. In this dissertation, I report several studies that further clarify the molecular interactions between Kv2.1 and syntaxin, and provide the first in vivo evidence that disrupting the Kv2.1-syntaxin binding is a viable neuroprotective strategy. We explored several approaches using both peptide-based and synthetic small molecules as the protective agent. To cap off these findings, I provide preliminary data that leverages the hepatitis virus protein NS5A to

suppress Kv2.1-dependent cell death in ischemic stroke. We intend for the work presented here to serve as the basis to further unravel the role of Kv2.1 in other neurodegenerative conditions and eventually make the translational leap to improve clinical treatments.

Table of Contents

List of Figures

Preface

I would like to first and foremost thank my thesis advisor, Dr. Elias Aizenman, for not only providing excellent scientific guidance throughout my studies, but also for being such a caring mentor for me and for everyone else in the lab. I will always look up to Elias for his abilities to treat others kindly and maintain a persistent optimism. I would like to thank Karen Harnett, the Aizenman lab manager. Karen is the glue that has kept the lab together for decades and none of our works would be possible without her. I would like to acknowledge the other members of the Aizenman lab: the two previous postdocs Jason Justice and Kai He, the graduate student Becca Krall, the medical student Tony Schulien, and the many undergraduate students for sharing their times with me in the past five years.

I would like to thank my committee chair Dr. Dandan Sun for her continual support from the beginning, her collaboration with the animal works, and for including me in her lab activities. I am very grateful for my committee members Drs. Thanos Tzounopoulos, Michael Palladino, Amantha Thathiah, and Rajesh Khanna for making their resources available to me and supporting my studies over the years. I feel truly blessed that the labs of every one of my committee members have contributed to the works presented here. Finally, I would like to acknowledge the many friends I have made along the way, both in and out of science, and the unending support from my family: Orchid, Jack, and Chiuchen. Thank you all.

1.0 Introduction

1.1 The increasing burden of neurodegenerative diseases

Historical advances in medical practice have led to a very different quality of living from merely a century ago. Improved sanitation and disease counter measures have decreased mortality across all age groups. While the maximum human lifespan have not increased significantly in recent times (Dong et al., 2016), the proportion of the elderly in the population today is the highest it has ever been. In 1950, the world's 65 and over age group accounted for roughly 5% of the world's population, in 2015, this number steadily increased to 8.5% and is projected to reach 12% by 2030 and 16.7% by 2050 (He et al., 2016). More nations will begin to have a constriction of the population pyramid, and even inversions of the age structure will be observed. This demographic transition necessarily indicates a change in the prevalence of certain illnesses and contributes to a critical shift in the central focus of modern medicine. Currently in the United States and many similar developed nations, heart disease and cancer-related illnesses are the top leading causes of death by a large margin, as reported by the Center for Disease Control (CDC). Stroke and Alzheimer's disease, two highly age-correlated neurodegenerative diseases (Murphy et al., 2018), are also consistently ranked as leading causes of death, currently at 5 and 6, respectively. With increases in the average human life span and the population growth rate, neurodegenerative diseases are set to rapidly become towering medical and economic burdens in the coming decades.

Age is, by far, the strongest predictor for most idiopathic neurodegenerative diseases. More than three quarters of stroke occurs in the population of ages 65 and up, and the risk for stroke doubles for each successive decade after the age of 55 (CDC). Projection of stroke patients in the

United States population suggests a rising trend from 3.22% in 2012 to 3.88% in 2030, an increase of 3.4 million individuals, accounting for a doubling in direct medical cost from 71.55 billion to 157.30 billion US dollars (Ovbiagele et al., 2013). Individuals suffering from Alzheimer's disease and related dementias in the United States numbered approximately 5 million in 2014 (1.6% of US population) and will expand to 13.9 million people in 2060 (3.3% of US population) (Matthews et al., 2019). Direct cost of care for Alzheimer's disease and related dementias is projected to grow from 109 billion in 2010 to 259 billion US dollars by 2040 (Deb et al., 2017). This projected increase in the prevalence of ischemic stroke and Alzehimer's disease represents a lost in the quality of life for a large afflicted population and their family members. Despite these growing needs, our current treatment options for all these neurodegenerative conditions are wholly unsatisfactory.

The paucity in treatment options for neurodegenerative diseases is not for the lack of attempts in development. Preclinically, drug developmental research has had numerous successes. But translation of these findings to the clinic has been difficult. Between 1995 and 2005, 430 potential stroke drugs were evaluated for efficacy in clinical trials globally. Nineteen (4%) have reached the market. The few treatments that are mechanistically neuroprotective are currently unavailable in the United States for clinical use (Citicoline, a naturally occurring intermediate to cell membrane lipids, has been discontinued due to the lack of effect across several clinical trials (Shi et al., 2016); Fasudil, a Rho kinase inhibitor and vasodilator, has not been approved in the United States after a lengthy legal battle and concerns over liver toxicity (Chen & Wang, 2016)). In fact, most currently accepted ischemic stroke treatments rely on the physical re-establishment of blood flow, the so-called clot buster drugs or variations of thrombectomy, rather than neuroprotective agents. Treatments for Alzheimer's disease are in a similar state. From 1998 to

2017 there have been 146 failed attempts at developing Alzheimer's drugs (PhRMA report 2018). Current treatments for Alzheimer's disease include the use of cholinesterase inhibitors (galantamine, rivastigmine, and donepezil) and the NMDA antagonist memantine. Both groups of drugs are known cognitive enhancers (Repantis et al., 2010) and memantine also confer some neuroprotective activity by counteracting excitotoxicity (Danysz & Parsons, 2003). Treatments designed to target Alzheimer's disease etiology directly have been the most disappointing (recently, see the abandoned projects CREAD 1 and 2, β-amyloid antibodies by Roche, Jan 2019). These costly failed clinical trials highlight a rapidly growing need for more effective neuroprotective therapies, urgently calling for innovative approaches in combating neurodegenerative conditions.

1.2 Apoptotic cell death in neurodegenerative diseases

The complexity of the cell death process in neurodegeneration is central to the difficulties in developing effective treatments. Distinguished biological features allow us to place the event of cell death on a spectrum ranging from the highly precise and contained apoptosis to the uncontrolled process that is necrosis. The apoptotic cell death has the specific goal of minimizing secondary damage, such as the release of inflammatory factors, to surrounding cells upon cell lysis. This is achieved by the activation of a specific class of proteases known as caspases, and caspase-activated endonucleases that cause DNA degradation (Elmore, 2007). Molecular signals such as phosphatidylserine are also presented on membrane surfaces as "eat me" signals to encourage phagocytosis by macrophages (Segawa & Nagata, 2015). While apoptotic programs are a necessary part of the developmental process and in tissue turnover homeostasis in adults, excessive

activation of the cell death program can be observed in pathological states. On the other hand, necrotic cell death releases intracellular contents undeterred and can be detrimental to the whole organism. More recent experiments found programmed molecular pathways can also lead to inflammatory forms of cell death, called necroptosis, and it has been observed in neurodegenerative diseases such as Alzheimer's disease (Caccamo *et al.*, 2017). Realistically, each disease is considered to have unique fingerprints of cell death characteristics, including features of both apoptosis and necrosis, making a comprehensive neuroprotective treatment exceedingly difficult to develop (Chi *et al.*, 2018).

Focal ischemic stroke is a prominent example of a neurodegenerative condition that contains heterogenous cell populations that are undergoing different modes of cell death. At the ischemic core, cells experience rapid necrotic cell death due to the severity of the insult and will die within a few hours. In contrast, cells in the ischemic penumbra, the perimeter of the ischemic site, go through apoptotic programs that can be observed for days (Radak *et al.*, 2017). Elevated protein expression related to the activation of caspase activity, including signs of nuclease-dependent DNA fragmentation, can be found in stroke patient post-mortem brain tissues (Mitsios *et al.*, 2007). In Alzheimer's disease, apoptotic mechanisms are thought to be a significant mode of cell death (McCord & Aizenman, 2014; Obulesu & Lakshmi, 2014). Elevated activation of executioner caspases can be found in post-mortem patient tissues (Rohn & Head, 2009). β-amyloid, the central protein underlying several proposed mechanisms of Alzheimer's disease, induces caspase-dependent apoptosis in neurons (Allen *et al.*, 2001). In all cases, the goal of neuroprotection is to either reduce the region afflicted by necrotic cell death by alleviating the insult or, in the many cases where this is not possible, improve the likelihood of survival in cells undergoing apoptotic cell death by limiting the excessive activation of cell death programs.

Classical features of cell death programs can be the result of convergent intrinsic and extrinsic caspase activation pathways. In the intrinsic pathway, lethal insults such as severe oxidative stress cause irreversible damage to mitochondria, leading to the loss of mitochondrial membrane potential and the release of cytochrome c into the cytosol. This internal cell death signal of cytosolic cytochrome c directly participates in the formation of the apoptotic protease activating factor 1 (Apaf-1) oligomeric apoptosome. The Apaf-1 apoptosome then binds and cleaves pro-caspase-9, activating it and the subsequent executioner caspase cascades (Zou *et al.,* 1999). The extrinsic pathway relies on extracellular ligands binding to death receptors of the tumor necrosis factor (TNF) receptor superfamily such as TNFR1 and Fas Receptor (FasR). While each of these death receptors have specific mechanisms, whether it be regulated gene expression through NF-kb or extranuclear signal transduction to the mitochondria/apoptosome, they all converge to the activation of executioner caspases (Obulesu & Lakshmi, 2014). As cell death programs are underway, many stereotypical features of apoptosis can be observed, such as chromosome condensation, membrane blebbing, and, perhaps the most visually impressive, the dramatic loss of cell volume. While originally assumed to be a passive process, apoptotic cell volume decrease is now known as a robust and highly regulated active event during cell death. This dissertation focuses on a key contributor to apoptotic volume decrease, particularly in neurons.

1.3 Apoptotic cell volume decreases and potassium regulation

Apoptotic volume decrease is an isoelectric loss of cell volume that begins prior to caspase activation and is a characteristic observed in most physiological models of programmed cell death (Bortner & Cidlowski, 2007). The phenomenon of apoptotic volume decrease is distinct from that

of regulatory volume decrease, which only occurs in response to anisotonic conditions, albeit they can involve similar molecular pathways (Szabò et al., 1998; Maeno et al., 2000). Compared to the rapid adjustments in regulatory volume decrease (within seconds), apoptotic volume decrease occurs slowly, within 12-20 minutes of the insult depending on the cell type and death-inducing stimulus studied (Bossy-Wetzel et al., 2004; Hessler et al., 2005). While slower, apoptotic volume decrease is an active process that is necessary for the activation of caspases and the efficiency of apoptotic nucleases (Bortner & Cidlowski, 2002). In fact, typical regulatory elements are often overridden during cell death processes, such as the suppression of mechanisms that maintains cell volume in healthy conditions (Bortner et al., 2001; Mann et al., 2001).

Early work evaluating the contributors of apoptotic volume decrease found intracellular potassium to be the key ionic component mediating this process, as it is the most abundant and osmotically important cation in the cell (Franco et al., 2006). This critical loss of intracellular potassium is coupled with the early inhibition of the cell's ability to uptake potassium through the Na-K-ATPase (Nobel et al., 2000; Bortner et al., 2001). Because this loss of cell volume is electroneutral, outwardly rectifying chloride channels have been observed to accompany intracellular potassium efflux and apoptosis (Szabò et al., 1998). Although chloride blocker can prevent cell shrinkage, they do not suppress the activation of caspase and the subsequent DNA fragmentation, suggesting that potassium ions specifically are required for suppression of apoptotic mechanisms in healthy cells (Wei et al., 2004b).

Blocking potassium efflux in various ways have been shown to suppress apoptosis and the many associated biomarkers. In a number of model systems, the presence of cytoplasmic levels of high extracellular potassium (100 mM+) has been shown to prevent the activation of apoptotic components, including the externalization of phosphatidylserine, mitochondrial depolarization,

and the release of cytochrome c from mitochondria (Thompson et al., 2001). Importantly, caspase-3 activation is inhibited by physiological levels of intracellular potassium (Bortner & Cidlowski, 2002). Apoptotic nuclease activity was also shown to be prevented by physiological concentrations of intracellularpotassium (100-150 mM) in cell-free assays (Hughes et al., 1997). Oligomerization of Apaf-1 and the assembly of the active apoptosome complex is suppressed by physiological intracellular concentrations of potassium as well, preventing activation of downstream caspase-9 cell death cascades (Cain et al., 2001). Interestingly, once assembled, the apoptosome was shown to be relatively insensitive to the ionic effects surrounding this complex (Cain et al., 2001).

The identification of a single potassium channel or mechanism that is universally responsible for the efflux of intracellular potassium in all apoptotic model systems has been elusive. Early studies showed that the N-type potassium channel Kv1.3 in jurkat T lymphocytes and prostate cancer cells appears to mediate cell death. Kv1.2 appears to play a role in the cell death of SH-SY5Y neuroblastoma cells following hypoxia and glucose deprivation and Kv1.5 contributes to the cell death of COS-7 and pulmonary artery smooth muscle cells (Bortner & Cidlowski, 2007). Kv1.1 and Kv1.3 contribute to retinal ganglion neuron degeneration after injury through both neuronal and inflammatory microglia mechanisms (Koeberle & Schlichter, 2010). Potassium channels that are not voltage-gated have also been implicated, such as the calcium-activated IKCa1 channels in T lymphocytes (Elliot & Higgins, 2003). These plethora of reports across various cell types indicate that ion channel-mediated loss of intracellular potassium is likely a redundant mechanism and one may compensate for another during prolonged inhibition of one channel during cell death. Furthermore, reports indicate that mechanisms of apoptotic volume decrease can occur independently from the cell nucleus and other organelles (Bratosin et al., 2001; Lang et al., 2003). Interestingly, in some model systems, the inhibition of potassium channels has

been shown to induce cell death (Choi et al., 1999; Kim et al., 2000). However, in the example of these studies, it is expected that the disruption of basal functions to be deleterious in healthy cells.

1.4 Kv2.1 in neuronal cell death

Kv2.1 is a delayed rectifier potassium channel with 6 transmembrane domains that can form both homomers and heterotetramers with other Kv, such as Kv2.2 (Kihira et al., 2010), the electrically silent voltage gated potassium channel subunits (KvS) (Kv5, Kv6, Kv8, and Kv9 (Bocksteins, 2016), and the EAG family channels Kv10.1 and Kv11.1 (Ottschytsch et al., 2002)). Kv2.1 also contains large intracellular N- and C-terminal domains for non-conducting functions (Feinshreiber et al., 2010; Fox et al., 2015; Greitzer-Antes et al., 2018) and for phosphoregulation of its ion channel functions (Park et al., 2006). Kv2.1 is encoded by KCNB1, found on the long arm of the human chromosome 20q13.13, and it is widely expressed throughout the central nervous system, exclusively in neurons. Kv2.1 is also expressed in several other organs, including the lung, the pulmonary artery, the heart, the pancreas, and the liver. De novo mutations of the KCNB1 gene have been reported to cause frequent infantile epileptic seizures (~11 months) that subside later in age (~4-6 years) but evolve into encephalopathy with severe intellectual disabilities and autism (Calhoun et al., 2017; Marini et al., 2017). Experimental findings revealed that Kv2.1 is an important regulator of intrinsic excitability (Mohapatra et al., 2009), and that Kv2.1 knockout mice exhibit seizure propensity (Speca et al., 2014). Besides its functions in regulating neuronal excitability, Kv2.1 is important in many cell types for the depletion of intracellular potassium concentration during cell death. Various routes of blocking Kv2.1 efflux have been found to be protective. In neurons, lethal insults induce a Kv2.1-dependent pronounced increase in potassium

currents that can be blocked with the expression of a dominate negative Kv2.1 construct (Pal et al., 2003). These findings suggest that Kv2.1 is a key mediator for the apoptotic depletion of intracellular potassium in neurons.

The upstream pathways leading up to the enhanced Kv2.1 current in neurons have been carefully dissected. After significant oxidative insults, oxidized metal-binding proteins release free zinc into the cytosol from various compartments of the cell, such as metallothionine, mitochondria, and other organelles (McCord & Aizenman, 2014; Maret, 2019). This rise in free zinc activates zinc-dependent signaling pathways that can generate an optimal environment for cell death. These pathways include the zinc-dependent dual phosphorylation of Kv2.1 specifically by Src and p38 MAPK at Kv2.1 residues Y124 and S800, respectively and sequentially (McLaughlin et al., 2001; Pal et al., 2003; Redman et al., 2007; Redman et al., 2009; He et al., 2015). These modifications to the channel increase the interaction between Kv2.1's intracellular C-terminus domain and the SNARE protein syntaxin 1A (syntaxin). Subsequently, an upregulation of de novo channel insertion into the plasma membrane leads to the critical enhancement of K+ efflux in damaged neurons, generating the aforementioned necessary low potassium intracellular environment for caspase and nuclease activity. The topic of the Kv2.1-syntaxin interaction is the core interest of this dissertation and is further elaborated upon in section 1.7.

As mentioned, many potassium channels may mediate the loss of intracellular potassium in dying cells. Kv2.1 is particularly important because it is responsible for mediating the majority of the delayed rectifier currents in Kv2.1-expressing neurons, such as those in the hippocampus (Murakoshi & Trimmer, 1999), which are especially sensitive in neurodegenerative conditions. The cell death mechanisms of Kv2.1 has also been shown to be ubiquitous, as transient introduction of Kv2.1 in Chinese Hamster Ovary (CHO) cells, which does not endogenously

express any voltage-gated ion channels, increases the susceptibility of the CHO cell to apoptotic agents (Pal et al., 2003). This is indicative of an intimate and highly refined relationship between the Kv2.1 cell death pathway and the endogenous cell death programs. Combined with the fact that Kv2.1 is widely expressed in many cell types and in CNS neurons, studying Kv2.1-mediated cell death represents an important facet of understanding and treating many diseases involving cellular degeneration.

1.5 Oxidative stress and zinc dysregulation in neurodegenerative diseases

The involvement of elevated zinc signaling in Kv2.1-dependent neuronal cell death is an important indication of the Kv2.1-dependent pathway's relevance in neurodegenerative diseases. Zinc is the second most abundant biological trace element after iron, and its homeostasis is regulated by large families of transporters (Kambe et al., 2015). It is known to serve indispensable roles in the function of over 2000 proteins, including more than 300 enzymes (Andreini et al., 2006; Marreiro et al., 2017). Zinc has been recognized for its abilities to activate the metal-transcription factor-1 (MTF-1), which governs the expression of metallothionine, a potent heavy metal chelator and free radical scavenger (Ruttkay-Nedecky et al., 2013). MTF-1 also activates the expression of the selenoprotein-1 (Sepw1) gene, which encodes an antioxidant glutathione-binding protein that scavenges free radicals (Bonaventura et al., 2015). Zinc and copper are also core structural components of the Cu/Zn type superoxide dismutase (Cu-Zn-SOD), which is essential for antioxidant functions and its mutations has been found to be associated with neurodegenerative diseases such as amyotrophic lateral sclerosis (Valentine & Hart, 2003).

Oxidative stress is a ubiquitous component of almost all neurodegenerative diseases. While generally accepted as an important regulator of proper cellular response to oxidative stress, zinc, when in dyshomeostasis, has been shown to also play detrimental roles in brain diseases (Marreiro et al., 2017; Portbury & Adlard, 2017). Heightened activity in glutamatergic terminals in excitotoxic conditions can promote excess co-release of zinc, which enters through kainate and/or calcium-permeable AMPA receptor channels (Galasso & Dyck, 2007). This disruptive rise in cytosolic zinc can not only cause overactivation of certain zinc-dependent pathways, including those that promotes cell death (Portbury & Adlard, 2017), but also cause prolonged mitochondria dysfunction and reactive oxygen species generation (Galasso & Dyck, 2007). In Alzheimer's disease, zinc appears to be a key structural component in the massive insoluble β-amyloid aggregates (Craddock et al., 2012). Because of the zinc dyshomeostasis and the general increase in detrimental roles of zinc during many disease states, we believe that the zinc-dependent Kv2.1 cell death pathway can be ubiquitously activated as well. Indeed, evidence of Kv2.1-dependent cell death have been found in many cellular injury models specific to several diseases in the past decades, some of these examples are discussed below.

1.6 Evidence of Kv2.1 in neurodegenerative diseases

While the importance of zinc signaling in neurodegenerative diseases is a well-established fact, direct evidence for the involvement of Kv2.1 is just beginning to surface. Initial studies in vitro found that insults that simulate specific diseases can both raise intracellular zinc levels as well as elicit the death-permitting increase in potassium currents. In rat primary culture cortical neurons, treatments with a thiol-oxidant can induce cytosolic zinc release and enhance Kv2.1

currents (Aizenman et al., 2000). Activated microglia, a strong indicator of neuroinflammation in several diseases (Perry et al., 2010), can also induce an increase in cytosolic zinc and in Kv2.1 currents (Knoch et al., 2008). The neurotoxin 6-hydroxydopamine (6-OHDA) acts as an inhibitor to mitochondria complex I and IV and auto-oxidizes to generate damaging free-radicals (Glinka et al., 1997). Because of its ability to cause massive degeneration of dopaminergic neurons, 6-OHDA has been used in models of Parkinson's disease for decades (Simola et al., 2007). Not surprisingly, treatments of 6-OHDA can induce an increase in cytosolic zinc (Sheline et al., 2013) and elicit the increase in death-permitting Kv2.1 currents, which can be blocked to ameliorate neuronal cell death (Redman et al., 2006). Oxygen-glucose deprivation (OGD), an in vitro model of cerebral ischemia, also induces cytosolic zinc release and Kv2.1-dependent cell death that can be ameliorated by blocking Kv2.1 currents (Wei et al., 2004a; Yuan et al., 2011). In vivo evidences are beginning to surface. In rats, elevated delayed rectifier current can be observed after ischemic stroke in the hippocampus (Wu et al., 2015), where Kv2.1 is the major contributor of delayed rectifier currents (Murakoshi & Trimmer, 1999). This is consistent with the fact that broad spectrum potassium channel blockers are known to be protective in various stroke models (Wei et al., 2003). With relevance to Alzheimer's disease, treatments of neurons with β-amyloid also elicits neurotoxicity dependent on enhanced Kv2.1 current (Yu et al., 1998).

An alternate model of Kv2.1-dependent neuronal cell death, focuses on the oligomerization of Kv2.1 after oxidative damage and has also found convincing evidence in several neurological diseases. Unlike the channels in the enhanced potassium currents pathway, oligomerized Kv2.1 do not conduct (Wu et al., 2013). Through the use of transgenic animals that express a Kv2.1 point mutation that cannot be oxidized (Kv2.1 Tg-C73A), experimental findings confirmed the involvement of Kv2.1 oligomerization in neuronal cell death in a mouse traumatic brain injury

model (Yu et al., 2016) and in aging-related cognitive impairments (Yu et al., 2019). Decreased Kv2.1 function was found in Alzheimer's disease mouse model (3xTg-AD) and increases neuronal excitability in the hippocampus (Frazzini et al., 2016). The Kv2.1 Tg-C73A mice was later shown to resistant to the neurological deficits of the 3xTg-AD genotype and that increased oligomerized Kv2.1 was found in human patients of Alzheimer's disease (Yu et al., 2018). Altogether, we believe these findings are strong indications that Kv2.1-dependent cell death mechanisms are present in several neurodegenerative diseases and is therefore an important topic of study.

1.7 The Kv2.1-syntaxin interaction

Kv2.1 has several binding partners through its large cytosolic domains. For example, the neuronal adhesion protein amphoterin-induced gene and ORF (AMIGO) acts as an auxiliary subunit to increase Kv2.1 conductance (Peltola et al., 2011). Non-conducting submicron Kv2.1 clusters are formed by the interaction between Kv2.1 and the endoplasmic reticulum anchoring proteins VAPA and VAPB, which has been observed to act as a protein trafficking hub (Fox et al., 2013; Fox et al., 2015; Johnson et al., 2018; Kirmiz et al., 2018). And perhaps most prominently studied are the direct interactions between Kv2.1 and members of the SNARE complex, including SNAP-25 (MacDonald et al., 2002), VAMP2 (Lvov et al., 2008), and, of interest to this dissertation, syntaxin 1A (Leung et al., 2003). These interactions, particularly the one with syntaxin, have been shown to be important for exocytosis and vesicle fusion in several cell types. In neuroendocrine cells, the Kv2.1-syntaxin interaction facilitates exocytosis of dense core vesicles independently of Kv2.1's ion channel role (Singer-Lahat et al., 2008). In pancreatic β-cells, the Kv2.1-syntaxin interaction modulates the release of insulin. Specifically, clustered Kv2.1 domains

in secretory β-cells are known to facilitate insulin granule release through the selective binding of specific Kv2.1 regions to syntaxin 1A or syntaxin 3 to elicit the secretion of selective granules populations (Zhu et al., 2013; Greitzer-Antes et al., 2018).

In dying neurons, the interaction between Kv2.1 and syntaxin is essential for increasing Kv2.1 channel insertion and the expression of enhanced currents. Blocking the increase in interaction between Kv2.1 and syntaxin by mutating either Y124 or S800 to alanine prevents the currents from becoming large and halts the cell death functions of Kv2.1 (Redman et al., 2007; Redman et al., 2009). Pseudo-phosphorylated S800D or S800E Kv2.1 constitutively express enhanced potassium currents (Redman et al., 2007). The interaction between Kv2.1 and syntaxin is mediated by the proximal Kv2.1 C-terminus domain termed C1a (a.a. 411-522; as opposed to the more distal C1b (a.a. 523-621) and C2 (a.a. 634-853) regions or the N-terminus (a.a. 1-182)) (Leung et al., 2003). We demonstrated that the Kv2.1 C1a domain disrupts the Kv2.1-syntaxin interaction in co-immunoprecipitation and suppresses the enhanced death-permitting currents (McCord et al., 2014). The overexpression of C1a is neuroprotective in cortical culture neurons challenged with activated microglia (McCord et al., 2014). By evaluating the ability of smaller Kv2.1 C1a fragments to inhibit enhanced Kv2.1 currents, the binding region was further narrowed down to residues 441-522 (McCord et al., 2014). These results indicate that disrupting the Kv2.1-syntaxin interaction may be a viable neuroprotective strategy. To realize this translational opportunity, we look to successful examples of targeting protein-protein interactions in neuropathies based on ion channel functions.

1.8 Channel-targeted investigative approaches to neuroprotection

Ion channel modulation has been a prominent focus in the treatment of many diseases, including those neuronal in origin. For example, in the treatment of epileptic seizure through anti-epileptic drugs (AED), the AEDs includes those that targets sodium channels, calcium channels, and both GABA and glutamate receptors (Waszkielewicz et al., 2013). Traditionally, drug treatments for these conditions focused on the direct blockade or opening of the channel in question. However, this approach can detrimentally affect typical channel activity and cause debilitating side effects, such as arrhythmia and respiratory failure, as has been found in the case of blocking potassium channels systemically (Graham, 1950; Iwaki et al., 1987; Nattel, 2008). More recently, a new peptide-based approach has emerged for targeting the interactions of the channel with a regulatory protein as a non-direct approach to modulate channel function. To do this, it is sometimes necessary to further understand the specific interactions between the binding partners. In 1990, Frank and colleagues presented the SPOT synthesis method that greatly improved the feasibility of these studies (Frank et al., 1990; Frank, 2002). SPOT synthesis allows the rapid and cost-effective synthesis of peptide arrays that transverse a known region of a protein, the array can then be probed using a protein of interest. The results of these experiments provide insights to the amino acid sequences that can interact with the protein used in the probing, which can be further leveraged to design a peptide-based molecule capable of competitive binding to the target protein, thus blocking a specific interaction with the channel.

There are a few highly successful examples of using this research approach to target ion channels in neuronal disorders. In the expression of neuropathic pain, the interaction between CaV2.2 and collapsing response mediator protein-2 (CRMP2) was found to increase calcium influx and enhance excitability in small-diameter sensory neurons in the spinal cord. It is known

that CRMP2 binds CaV2.2 via a region within its three CaV-binding domain (CBD1-3) (Brittain et al., 2009). Using the peptide SPOT array, the essential binding sequence between CRMP2 and CaV2.2 was found to be a 15-amino acids sequence within CBD3. By conjugating this sequence (CBD3) to the cell- and blood brain barrier-permeant domain HIV TAT (TAT), the resulting peptide (TAT-CBD3) can competitively bind CaV2.2, effectively preventing its interactions with CRMP2 and reduce pain sensitivity after injury (Brittain et al., 2011b). TAT-CBD3 was later found to also have neuroprotective properties in rodent models of traumatic brain injury and ischemic stroke (Brittain et al., 2011a; Brittain et al., 2012a).

In a clinical example, the discovery of NA-1 (TAT-NR2B9c) is a breakthrough evidence that TAT-linked peptides can be translationally successful for neurodegenerative diseases (Ballarin & Tymianski, 2018). TAT-NR2B9c is made up of the TAT domain and the last 9 C-terminal residues of NMDAR GluN2B, allowing the peptide to disrupt the binding between GluN2B and the N-terminus of nNOS, which is known to confer NMDA receptor-mediated excitotoxicity. Tymianski and colleagues proceeded to evaluate TAT-NR2B9c in various models of ischemic stroke, in which excitotoxicity is a prominent player (Sattler & Tymianski, 2001). Rigorous evaluation of TAT-NR2B9c found effectiveness in ameliorating stroke damage in several rodent models as well as in rhesus macaques (Cook et al., 2012). TAT-NR2B9c then demonstrated clinical effectiveness in phase II clinical trials (ENACT, NCT00728182) completed in 2012, which found TAT-NR2B9c to significantly reduce embolic stroke infarct size in patients that undertook an endovascular procedure against brain aneurysm. Current phase III clinical trials are being carried out in cities around the world for use in neuroprotection after ischemic stroke (USA, Australia, Canada, Germany, Ireland, Korea, Sweden, and the UK; ESCAPE-NA1 NCT02930018, FRONTIER NCT02315443). This rare, potentially successful story of TAT-

NR2B9c's translation demonstrated that TAT-linked peptides based on the disruption of an ion channel's interaction with another protein is a proven therapeutic strategy for clinical applications.

1.9 Thesis Goals

The goal of this dissertation is to explore the neuroprotective potentials of interrupting the Kv2.1-syntaxin interaction. While it has been known for decades that the modulation of potassium movement can improve survivability in several cell types, a translatable molecular target has not been identified. Finding a treatment that does not directly interfere with the channel's physiological roles is an important aspect of a well-tolerated treatment, as side effects themselves can be as debilitating as the symptoms, by way of which many clinical trials may have failed. Furthermore, while the Kv2.1 cell death pathway has been extensively studied in rodent primary neuronal cultures, it has, heretofore, not been shown as a viable therapeutic method in vivo. To begin, we utilized the SPOT peptide synthesis method to identify the interacting entity between Kv2.1 and syntaxin. From this, we generate a channel-derived TAT-linked peptide to disrupt Kv2.1-syntaxin binding, as with the strategy described above (Chapter 2). Using details observed in the peptide SPOT array, we further carried out molecular simulations of Kv2.1 and syntaxin, uncovering precise molecular mechanisms in the binding of these two proteins (Chapter 3). Lastly, we explored an alternative solution for neurodegenerative diseases in the form of adeno-associated virus treatment with a cargo that inhibits the Kv2.1-syntaxin interaction upstream (Chapter 4). These are important studies in the scope of a world where neuroprotective treatments are sparse, and the burden of neurodegenerative diseases is continuing to climb at an alarming rate.

2.0 Targeting a Potassium Channel/Syntaxin Interaction Ameliorates Cell Death in Ischemic Stroke

2.1 Section Summary

The voltage-gated K^+ channel Kv2.1 has been intimately linked with neuronal apoptosis. After ischemic, oxidative, or inflammatory insults, Kv2.1 mediates a pronounced, delayed enhancement of K^+ efflux, generating an optimal intracellular environment for caspase and nuclease activity, key components of programmed cell death. This apoptosis-enabling mechanism is initiated via Zn^{2+}-dependent dual phosphorylation of Kv2.1, increasing the interaction between the channel's intracellular C-terminus domain and the SNARE (soluble *N*-ethylmaleimide-sensitive factor activating protein receptor) protein syntaxin 1A. Subsequently, an upregulation of *de novo* channel insertion into the plasma membrane leads to the critical enhancement of K_ efflux in damaged neurons. Here, we investigated whether a strategy designed to interfere with the cell death-facilitating properties of Kv2.1, specifically its interaction with syntaxin 1A, could lead to neuroprotection following ischemic injury *in vivo*. The minimal syntaxin 1A-binding sequence of Kv2.1 C terminus (C1aB) was first identified via a far-Western peptide screen and used to create a protherapeutic product by conjugating C1aB to a cell-penetrating domain. The resulting peptide (TAT-C1aB) suppressed enhanced whole-cell potassium currents produced by a mutated form of Kv2.1 mimicking apoptosis in a mammalian expression system, and protected cortical neurons from slow excitotoxic injury *in vitro*, without influencing NMDA-induced intracellular calcium responses. Importantly, intraperitoneal administration of TAT-C1aB in mice following transient middle cerebral artery occlusion significantly reduced ischemic stroke damage and improved

neurological outcome. These results provide strong evidence that targeting the proapoptotic function of Kv2.1 is an effective and highly promising neuroprotective strategy.

2.2 Introduction

Voltage-gated potassium channels (Kv), key regulators of cellular excitability, play an important role in cell death processes underlying several neurodegenerative conditions, including stroke (Shah & Aizenman, 2014). At physiological concentrations, intracellular K+ suppresses caspase function, inhibits active nuclease activity, as well as limits apoptosome formation (Hughes & Cidlowski, 1999; Yu, 2003). Thus, in order for cell death cascades to proceed, intracellular K+ concentrations must decrease. In the central nervous system, the delayed rectifier K+ channel Kv2.1 plays a prominent role in this process, particularly in cortical, hippocampal, and nigral neurons (Pal et al., 2003; Redman et al., 2006; Shen et al., 2009; Shepherd et al., 2012). This cell death-enabling mechanism is initiated by intracellular free Zn2+ released from oxidized metal-binding proteins and compromised organelles (Aizenman et al., 2000; Sensi et al., 2003; Knoch et al., 2008; Aras et al., 2009a; McCord & Aizenman, 2013; Granzotto & Sensi, 2015; Medvedeva et al., 2017). Zn2+, in turn, activates a dual kinase-mediated process, resulting in the sequential phosphorylation of the intracellular Kv2.1 residues Y124 and S800 by Src and p38 MAPK, respectively (Redman et al., 2007; Redman et al., 2009; Shepherd et al., 2012; He et al., 2015). These channel phosphorylation events increase a Ca2+/CaMKII-dependent interaction between the proximal C-terminus of Kv2.1, termed C1a (Singer-Lahat et al., 2007; Singer-Lahat et al., 2008), and the SNARE protein syntaxin 1A (STX1A), promoting de novo channel incorporation into the plasma membrane and the associated apoptosis-permitting K+ efflux in dying cells (Pal et

al., 2006; McCord & Aizenman, 2013; McCord et al., 2014). Notably, the increased surface expression of functional Kv2.1 channels in vitro generally occurs after a delay of approximately three hours following the initiation of the injurious event (McLaughlin et al., 2001).

Experimental manipulation of this pathway at several checkpoints has strongly suggested that inhibition of the pro-apoptotic function of Kv2.1 has therapeutic potential. Non-phosphorylatable point mutations of either Y124 or S800 Kv2.1 residues, inhibition of upstream kinases, or interfering with STX1A function have all led to a blockade of pro-apoptotic channel trafficking and are protective in in vitro models of neurodegeneration (McLaughlin et al., 2001; Aras & Aizenman, 2005; Redman et al., 2007; Redman et al., 2009; McCord & Aizenman, 2014). Not surprisingly, suppressing delayed rectifier currents directly is sufficient for improving neuronal survival both in vitro (Pal et al., 2003; Yuan et al., 2011) and in vivo (Wei et al., 2003). However, blockers of delayed rectifier currents can have significant effects on cardiomyocyte repolarization, and are associated with potentially serious side effects, such as ventricular tachycardia and respiratory failure (Graham, 1950; Iwaki et al., 1987; Nattel, 2008), making them less than ideal candidates for central nervous system pharmacotherapy. As such, the identification of an approach to target the cell death-specific elements of Kv2.1 is an essential step towards realizing the neuroprotective potential of targeting this channel. With this in mind, we report the generation of a cell-permeant, highly neuroprotective peptide construct (TAT-C1aB), derived from a heretofore unidentified minimal, 9 amino acid (a.a.), STX1A-binding Kv2.1 sequence coupled to the cell-permeable transactivator of transcription (TAT) domain from the human immunodeficiency virus.

2.3 Results

2.3.1 Establishing the sequence of TAT-C1aB

To identify the minimal Kv2.1 C-terminal sequence that can bind syntaxin 1A (STX1A), a far-western assay (Brittain et al., 2011b) was performed on a peptide spot array of seventy-six 15 a.a. sequences derived from Kv2.1, spanning residues 451 to 540 (Rattus norvegicus; Accession # NP_037318.1; (McCord & Aizenman, 2014)) in 1 a.a. overlapping steps (Fig. 1A). STX1A-enriched lysates derived from Chinese Hamster ovary (CHO) cells overexpressing the SNARE protein were used to probe against the bait Kv2.1 peptides. Subsequent immunofluorescence revealed two strongly interacting fragments flanking a region of high STX1A binding, highlighted in red and blue in Figs. 1A and 1B. These two fragments contain an overlapping 9 a.a. sequence, HLSPNKWKW from N- to C-terminus, corresponding to rat Kv2.1 a.a. residues 478-486. Of note, this exact sequence is present in mouse Kv2.1, corresponding to a.a. 482-490 (Mus musculus; Accession # NP_032446.2). This sequence likely represents the minimal Kv2.1 C-terminus (C1a) STX1A-binding sequence (C1aB). Addition of the HIV TAT cell-permeable domain to the N-terminus of C1aB yielded TAT-C1aB: YGRKKRRQRRRHLSPNKWKW (Fig. 1C). A second set of membranes were used to confirm a displacement of the spotted peptides to STX1A by TAT-C1aB (100 uM, n=4; Figs 1A, 1B). A BLAST search of C1aB revealed no identical sequence in any other mammalian protein, with only an analogously similar (77%), but not identical, sequence in the Kv2.1 cognate Kv2.2 (HLSPSRWKW, Rattus norvegicus and Mus musculus; Accession #'s NP_446452.2 and NP_001091998.1, respectively), a channel that has not yet been implicated in apoptotic processes, possibly as it lacks a p38 target site analogous to Kv2.1 S800 and flanking sequences. Randomizing the C1aB domain of the Kv2.1-derived, STX1A-binding peptide yielded

a scrambled control (TAT-SC; YGRKKRRQRRRNLKWSHPKW). BLAST search of the scrambled C1aB sequence resulted in no identifiable mammalian proteins. A diagram summarizing our overall experimental approach is illustrated in Figure 2, where we hypothesize that the isolated STX1A-binding sequence in TAT-C1aB competes for and prevents the increase of functional Kv2.1 channels on the plasma membrane during apoptosis and is thus neuroprotective.

2.3.2 TAT-C1aB suppresses apoptotic Kv2.1-mediated K+ currents and provides neuroprotection from "slow" excitotoxicity in vitro without influencing NMDA-evoked Ca2+ responses

Previously, we demonstrated that p38 MAPK phosphorylates Kv2.1 at serine residue S800 to induce the pro-apoptotic increase in K+ currents (Redman et al., 2007). A point mutation of the serine to a negatively charged a.a. (E or D) at this position results in apoptotic-like enhanced currents in the CHO cell expression system, provided that tyrosine residue Y124 remains intact (Redman et al., 2007; Redman et al., 2009; He et al., 2015). It is noteworthy that CHO cells do not express any endogenous voltage-gated K+ channels (Yu & Kerchner, 1998), but contain all relevant signaling components that lead to pro-apoptotic trafficking of Kv2.1 (Pal et al., 2003; Aras & Aizenman, 2005). This offers an advantageous preparation to evaluate the effects of the peptide, as it focuses on the STX1A binding-mediated insertion process itself, in the absence of potentially confounding signaling events and other apoptosis-related processes. We observed that overnight exposure to 10 μM TAT-C1aB beginning immediately following the transfection protocol significantly prevented Kv2.1(S800E)-mediated enhanced currents. In fact, current densities in TAT-C1aB treated, Kv2.1(S800E)-expressing CHO cells were not different from those

observed in CHO cells expressing wildtype (WT) Kv2.1 (Fig. 3A). Importantly, the identical TAT-C1aB treatment did not reduce the current density of WT Kv2.1 channels, indicating that normal channel trafficking was not affected by the peptide. Moreover, the control, scrambled peptide TAT-SC (10 μM) had no measurable effects on the current density of either Kv2.1 construct (Fig. 3A). Although these results strongly suggest that TAT-C1aB prevents apoptotic trafficking of Kv2.1, a non-equivocal demonstration of this process will require single particle tracking of fluorescently labeled channels with techniques such as total internal reflection microscopy (TIRF).

As TAT-C1aB could effectively prevent enhanced, pro-apoptotic Kv2.1 current, we next evaluated whether the peptide would be neuroprotective in an in vitro neuronal system. Embryonically-derived rat cortical cultures were treated with 100 μM DL-threo-beta-benzyloxyaspartate (TBOA) at 25-29 days in vitro (DIV), in the absence or the presence of 0.3, or 1 μM of either TAT-C1aB or TAT-SC. TBOA, like other glutamate transporter blockers, elicits slow NMDA receptor-mediated excitotoxicity in neuronal cultures (Blitzblau et al., 1996; Wang et al., 1998). We opted for this cell toxicity model as it has long been established that relatively mild exposure to NMDA receptor agonists, over long periods of time, can induce apoptotic injury (Bonfoco et al., 1995; Leist & Nicotera, 1998). Moreover, apoptotic excitotoxic stimuli can elicit K+ current increases (Yao et al., 2009), and NMDA receptor activation has been closely associated with ischemic stroke injury (Meldrum et al., 1987; Aarts et al., 2002). Within 24 h, TBOA incubation led to the appearance of dendritic and membrane blebs. Critically, the presence of 1 μM TAT-C1aB seemed to be sufficient to ameliorate the TBOA-mediated toxicity, as visualized via prior transfection of the neurons with eGFP (Fig. 3B). To quantify the degree of cellular damage induced by TBOA and neuroprotection via TAT-C1aB, a lactate dehydrogenase (LDH) viability assay was performed 24 h after TBOA treatment. The release of long-lived cytosolic

proteins, such as LDH, is indicative of compromised cellular integrity (Koh & Choi, 1987; Aras et al., 2001). In corroboration with our qualitative assessment, we found that TAT-C1aB treatment significantly decreased TBOA-induced injury in cortical cultures. In contrast, TAT-SC afforded no neuroprotection (Fig. 3C).

Finally, we evaluated whether TAT-C1aB could directly influence NMDA-evoked Ca2+ responses. Intracellular Ca2+ recordings were performed as described earlier (Aizenman et al., 1990; Reynolds et al., 1990) in neurons that had been exposed to 1 µM of either TAT-C1aB or TAT-SC overnight (~18 h), until just immediately prior to recordings. Fura-2 measurements revealed that initial Ca2+ responses to 30 µM NMDA + 10 µM glycine, as well as delayed calcium dysregulation profiles (Brittain et al., 2012b) were not significantly different between both groups of cells (50 cells per coverslip; n=3 coverslips per group. Total 150 cells per condition; Fig. 4). These data strongly suggest that the neuroprotective actions of the peptide occur well downstream from NMDA receptor activation, as predicted by our model (Shah & Aizenman, 2014) and by the observed delayed enhancement of apoptotic potassium currents following injury (~3 h) described in prior work (McLaughlin et al., 2001).

2.3.3 TAT-C1aB provides neuroprotection in vivo

Once we established that TAT-C1aB was effective in both inhibiting pro-apoptotic Kv2.1-mediated currents and providing neuroprotection in vitro, we evaluated the in vivo efficacy of TAT-C1aB using a transient ischemic stroke model. First however, we investigated whether intraperitoneal (i.p.) administration of TAT-C1aB in mice reached the CNS vasculature within a therapeutically relevant timeframe. For this purpose, a fluorescein (FitC) fluorophore was conjugated to the C-terminus of TAT-C1aB for live in vivo 2-photon imaging in young adult

C57BL/6J male mice (24-29g; n=3). A single i.p. injection of TAT-C1aB-FitC (6 nmol/g) was administered after a stable imaging position had been reached at 100-200 μm depth from the cortical surface through a craniotomy window over the temporal cortex. A rapid rise in FitC fluorescence throughout cerebral vessel structures was observed within 10 minutes of the i.p. injection (Fig. 5A). Vessel fluorescence intensity continued to increase and peaked at 30 minutes after the injection (Fig. 5B).

Further, we confirmed CNS penetration by the TAT peptide using low power fluorescence microscopy. After complete saline transcardial perfusion, animals previously injected with TAT-C1aB-FitC (6 nmol/g) were found to present increased fluorescent signal throughout the brain, when compared to animals injected with the non-fluorescent TAT-C1aB (Fig. 5C). These findings are in line with previous characterization of the CNS penetrance of other TAT-linked peptides (Schwarze et al., 1999; Stalmans et al., 2015). Because other TAT-linked peptides have been shown to positively influence CNS neurons in various animal models of ischemic stroke (Kilic et al., 2006; Brittain et al., 2011a; Cook et al., 2012; Zou et al., 2013), and based on our own observations here, we concluded that TAT-C1aB can reach its intended target in a therapeutically realistic fashion following an i.p. injection. Our observations, in fact, directly confirm that a TAT-linked peptide can rapidly be detected within the brain vasculature and brain parenchyma following a peripherally i.p.-administered injection.

In addendum to the original publication, lower panels of Fig. 5C shows that without the conjugation of the TAT domain, FitC cannot by itself enter the brain parenchyma.

The Longa method of transient middle-cerebral artery occlusion (MCAO) (Longa et al., 1989) was used in young adult C57BL/6J mice (Jackson, ages 8-10 wks, male, 24-29g; n=67 for entire study) to evaluate TAT-C1aB's neuroprotective efficacy. Successful induction of the

MCAO procedure was first validated in a small cohort of animals (n=3) by monitoring changes of cerebral blood perfusion using a Laser Doppler Camera before, during, and after 50 min of MCAO. We found that compared with the pre-MCAO baseline (Fig. 6A), the procedure reliably reduced ipsilateral Doppler signal intensity by 50%, as compared to the contralateral, non-infarcted side (Fig. 6B). Removal of the suture for blood reperfusion achieved partial recovery of the cerebral blood flow after 15 min (Figs. 6C, 6D).

The half-life for TAT-conjugated peptides is cargo-dependent and has been found to range from 1 h to as high as 18 h (Krosl et al., 2003; Bach et al., 2012; Wang et al., 2016). Our 2-photon data indicated that the FitC-tagged TAT-C1aB remained detectable above baseline in the CNS vasculature for at least 2 h after i.p. injection (Fig. 5B), suggesting a turnover rate within the range of comparable compounds. In vitro, the pro-apoptotic channel insertion process is known to take place by 3 h following an acute injury (Pal et al., 2006), while neuronal delayed rectifier currents have been observed to remain elevated 24 h after MCAO (Wu et al., 2015). Based on all of this information, we designed our experimental protocol to consist of two separate i.p. peptide injections, 1 and 6 h following the initiation of reperfusion (6 nmol/g per injection; Fig. 7A). Remarkably, in TAT-C1aB treated animals (n=7), 2,3,5-triphenyltetrazolium chloride (TTC) staining at 24 h after reperfusion revealed a 40% decrease in total brain infarct ratio compared to that of the TAT-SC (n=8) or saline-treated (n=10) animals (Figs. 7B, 7C). Analysis of individual 2 mm coronal sections revealed that the reduction in infarct ratio provided by TAT-C1aB treatment was most prominent in the central infarct area (Fig. 7D). Of note, a ~13% increase in MCAO-induced ipsilateral swelling was observed in all animal groups, regardless of the presence or absence of the peptide treatments. That is, ipsilateral swelling was nearly identical in all three

treatment groups (saline: 112.9 ± 1.7%, n=10; TAT-SC: 114.0 ± 3.5%, n=8; TAT-C1aB: 115.2 ± 2.2%, n=7; One-way ANOVA p=0.7811).

We next evaluated the extent of neurological deficit amelioration provided by TAT-C1aB's in vivo neuroprotection. In preliminary studies, animals treated with 50 min MCAO had an overall survival rate of 38.5% by 2 weeks (TAT-C1aB 42.9% n=3/7; TAT-SC 33.3%, n=2/6; Fisher's exact test, NS), making it difficult to adequately assess behavioral deficits over time. By reducing the ischemia time to 40 min, the survival rate at 2 weeks was improved (TAT-C1aB 92.3%, n=12/13; TAT-SC 76.9%, n=10/13; Fisher's exact test, NS). We thus evaluated the neurological score of animals exposed to 40 min MCAO and treated with either TAT-C1aB or TAT-SC, as described above (6 nmol/g, at 1 and 6 h following reperfusion), on an 8-points neurological deficit scale over 14 days (see Methods) (Xia et al., 2006). Consistent with the neuroprotection profile afforded by TAT-C1aB, a significant treatment group effect was observed in TAT-C1aB treated animals, which had an overall improved (lower) neurological deficits score when compared to TAT-SC treated mice (Fig. 7E). Notably, relatively similar numbers of animals (4/13 for TAT-C1aB; 3/12 for TAT-SC) exhibited seizure-like behavior following MCAO. These in vivo results suggest that the degree of neuroprotection provided by TAT-C1aB is functionally significant.

In addendum to the results of the original publication, we evaluated delayed injection times of TAT-C1aB at 3 and 6 hr. The results found that the treatment remained effective in reducing infarct stroke volume (Fig. 8).

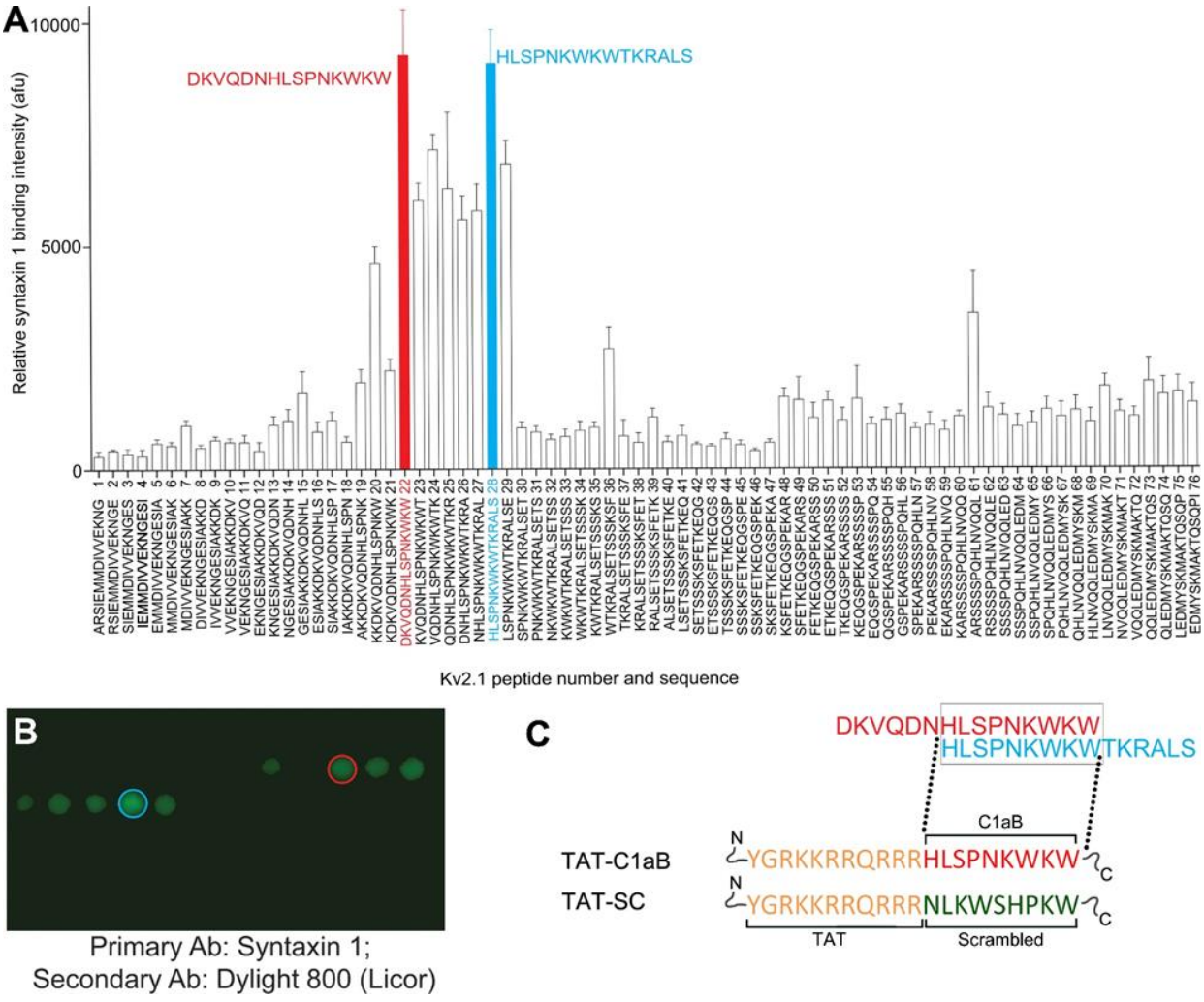

Figure 1. Generation of a Kv2.1-derived, STX1A-binding peptide sequence.

A. Far-western assay of the proximal Kv2.1 C-terminus (C1a) region using 15 a.a. segments spanning residues Kv2.1 451-540, in overlapping one a.a. steps. Two peptides, highlighted in blue and red, flanked a region of high STX1A-binding. Error bars indicate mean ± SEM of signal intensity in 4 independent assays in the absence and presence (black bars) of 100 μM of the TAT-containing derived STX1A-binding peptide described in (C) below. **B.** Representative peptide spot-array of the far-western experiment. **C.** Final sequences of the peptides used in the this study are shown. Orange sequence represents the cell-permeable HIV trans-activator of transcription

domain (TAT). Red sequence represents the STX1A-binding domain derived from Kv2.1. Green sequence represents a scrambled control based on the C1aB sequence.

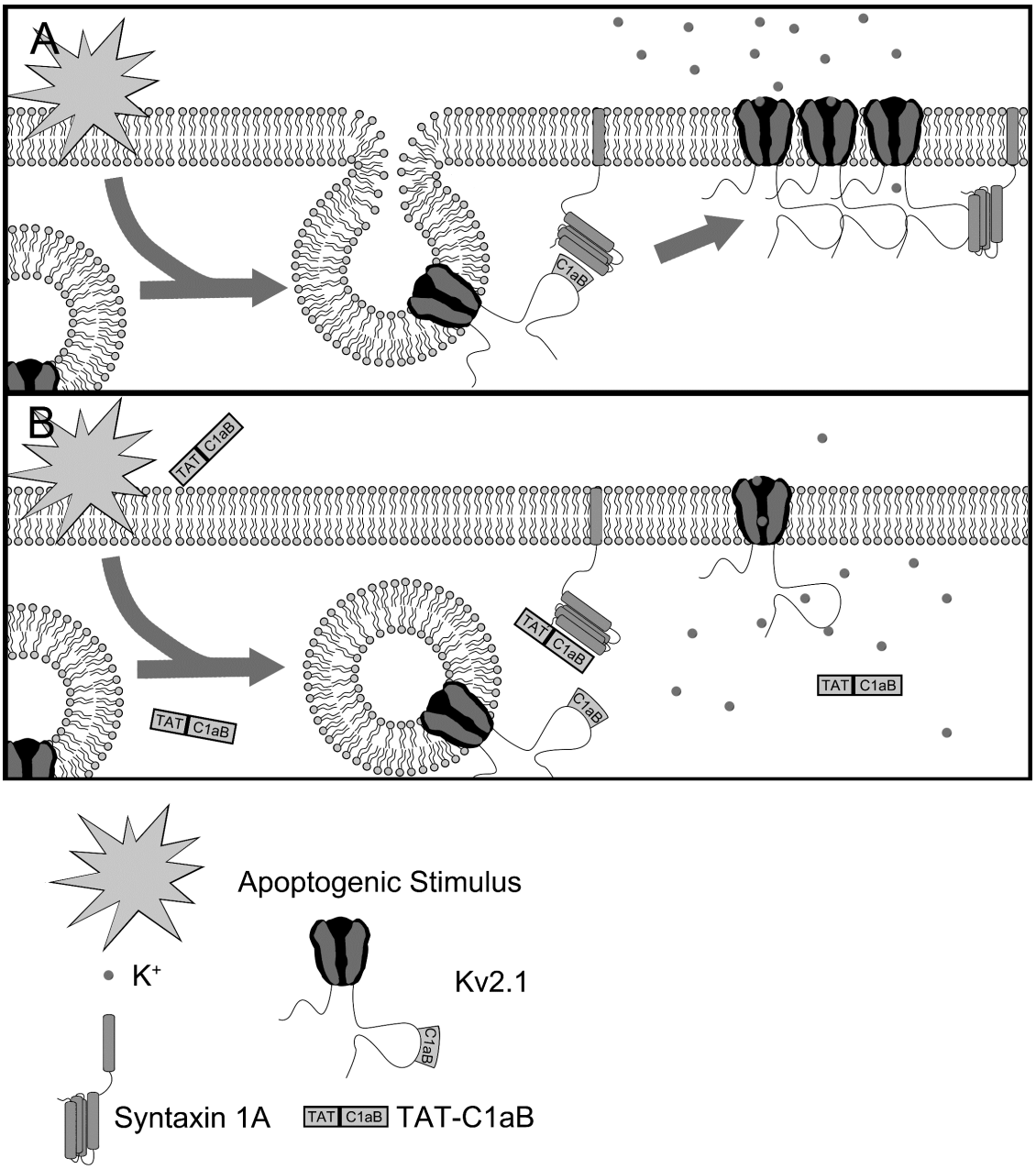

Figure 2. An illustration of the enhancement of Kv2.1 surface expression during neuronal apoptosis model and the protective mechanism of TAT-C1aB.

A. In an untreated neuron facing lethal injury, the increased interaction between Kv2.1 and the SNARE protein STX1A through the Kv2.1 C1aB domain promotes channel incorporation into the plasma membrane (Pal *et al.*, 2006). This enhances K^+ efflux and enables apoptosis. **B.** A cell-permeable peptide (TAT-C1aB) is created to contain the Kv2.1-derived STX1A-binding domain

C1aB. By competitively binding the Kv2.1-binding site on STX1A, TAT-C1aB provides neuroprotection by attenuating the enhancement of pro-apoptotic K^+ efflux.

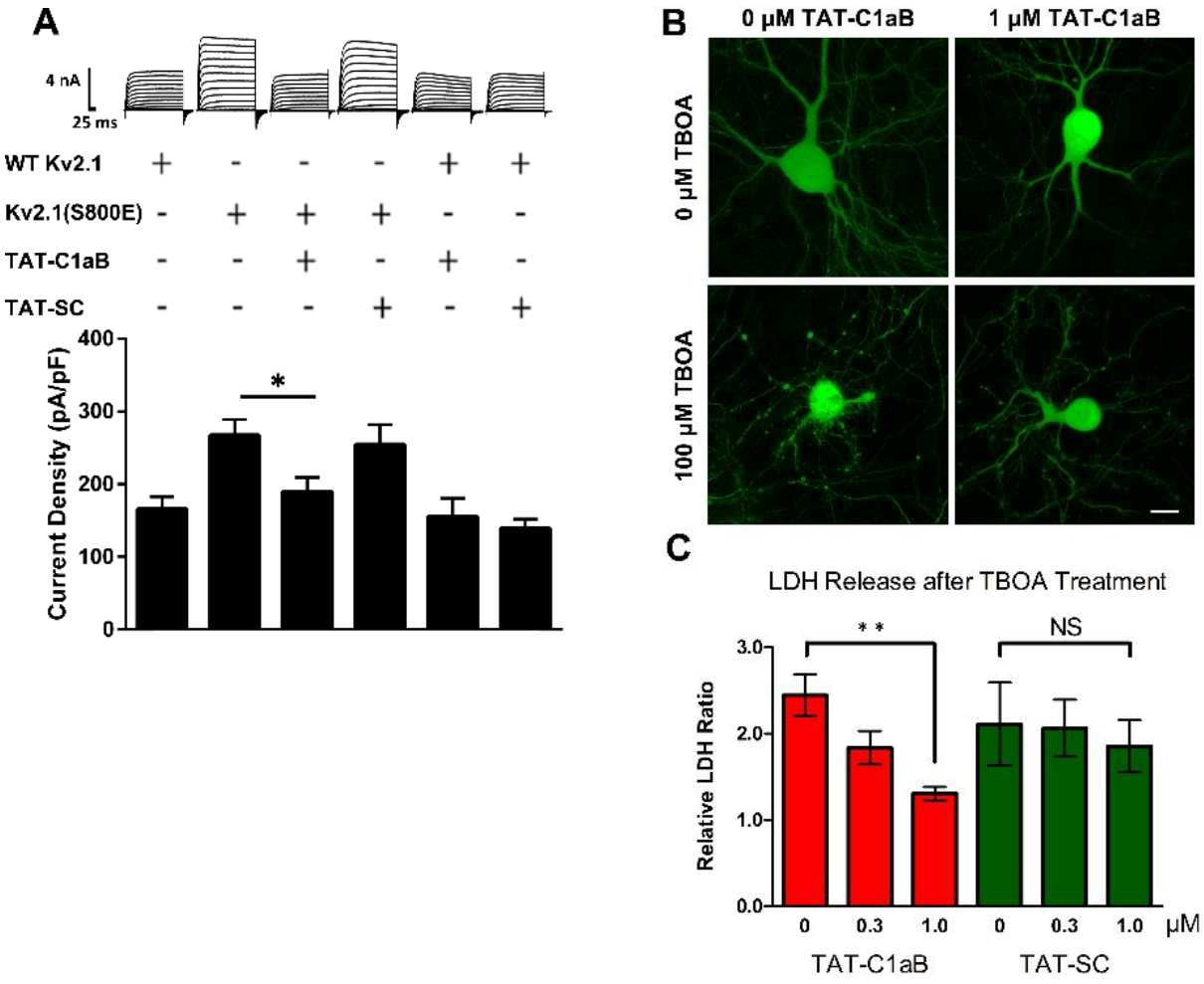

Figure 3. TAT-C1aB prevents enhanced currents mediated by Kv2.1(S800E) and ameliorates TBOA-induced neuronal damage in vitro.

A. Representative whole-cell K^+ current traces and pooled means ± SEM of current densities recorded from CHO cells expressing WT Kv2.1 treated with vehicle (n = 11), 10 µM TAT-C1aB (n = 12), or 10 µM TAT-SC (n = 11) and CHO cells expressing Kv2.1(S800E) treated with vehicle (n = 11), 10 µM TAT-C1aB (n = 11), or 10 µM TAT-SC (n = 11). Overnight TAT-C1aB incubation significantly blocked the enhanced currents present in Kv2.1(S800E)-expressing cells (current density at +30 mV, vehicle vs TAT-C1aB: 267.2 ± 22.0 pA/pF vs 189.5 ± 19.6 Mean ± SEM; ANOVA/Dunnett, *p<0.05). Scale bar denotes 4nA/25ms. **B**. 100 µM TBOA treatment induces toxicity in GFP-expressing rat cortical neurons in vitro (28-32 DIV), but not in the presence of 1

μM TAT-C1aB. Scale bar denotes 10 μm. **C.** Lactate dehydrogenase (LDH) release, as an index of cell toxicity, was measured 24 h following TBOA treatment in 28-32 DIV rat cortical neuronal cultures. Co-incubation of 1 μM TAT-C1aB mitigated cellular damage of TBOA-treated neurons as indicated by decreased LDH release (1.31 ± 0.077 vs 2.45 ± 0.24 Mean ± SEM normalized colorimetric ratio; ANOVA/Dunnett, **$p<0.01$; n = 4 independent experiments, each performed in quadruplicate). Co-incubation with TAT-SC had no protective effects (n = 6 independent experiments, each performed in quadruplicate).

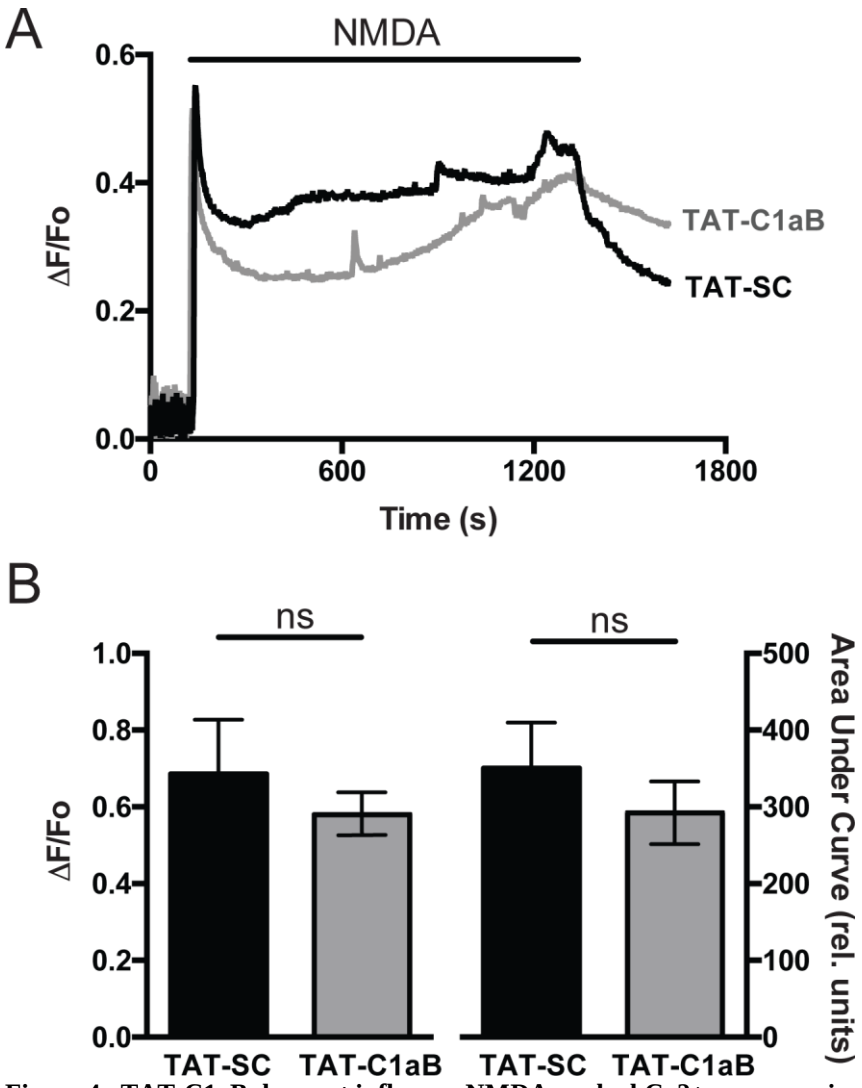

Figure 4. TAT-C1aB does not influence NMDA-evoked Ca2+ responses in cortical neurons in vitro.

A. Representative Ca^{2+} transient traces illustrating the average response of 50 rat cortical neurons from a single coverslip previously exposed to either (1 µM; 18 h) TAT-SC (black) or TAT-C1aB (gray). NMDA (30µM + 10µM glycine) was applied for 20 min following a 2 min baseline recording, and later washed for 5 min. **B.** Pooled means ± SEM (n=50 cells/coverslip; 3 coverslips per condition) show there is no significant difference in ΔF/Fo (0.69 ± 0.14 vs 0.58 ± 0.06; t-test, $p>0.05$) or area under the curve for the first 15 min of NMDA application (350.2 ± 59.6 vs 292.1 ± 41.1; t-test, $p>0.05$) between both peptide treatments.

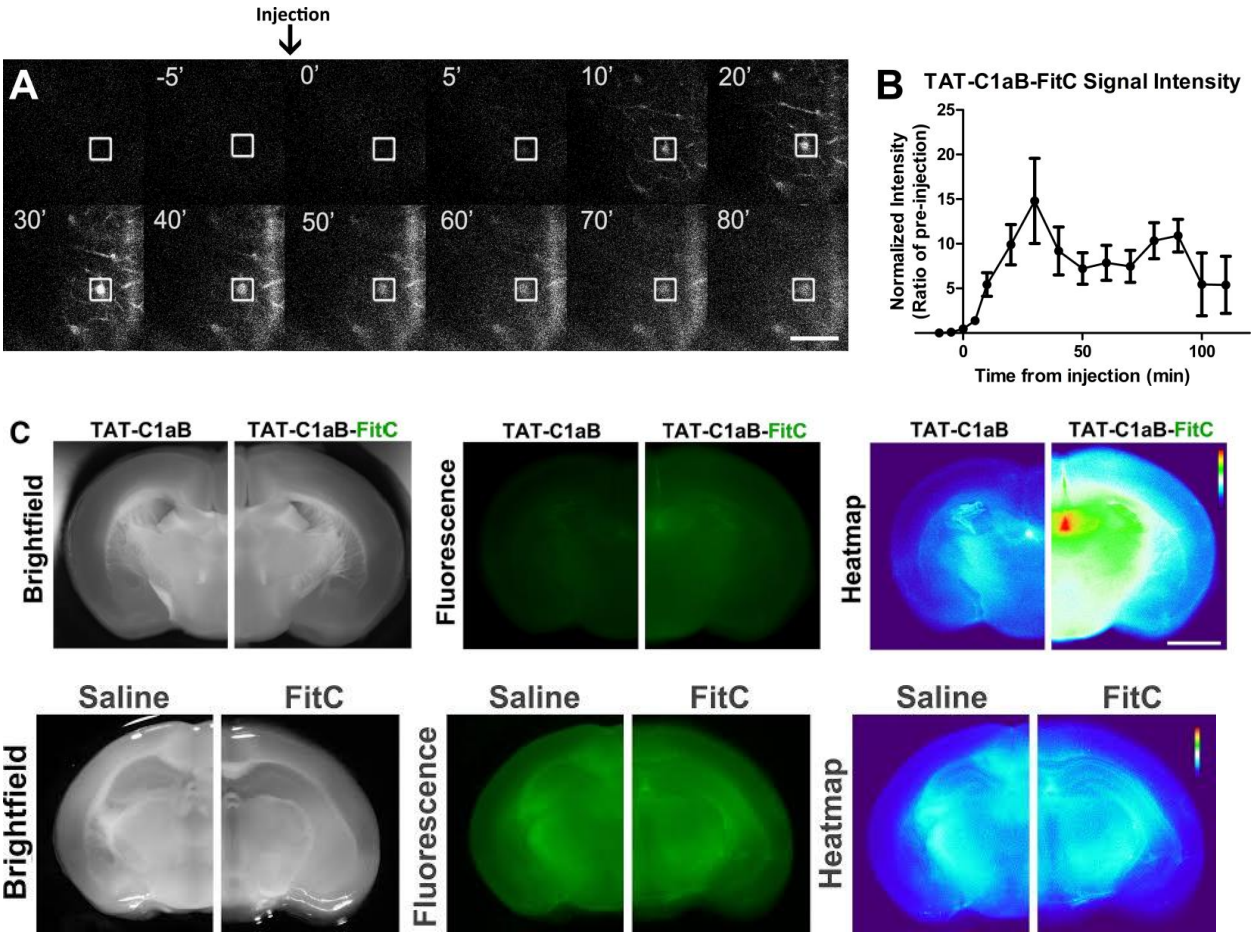

Figure 5. Intraperitoneal TAT-C1aB administration reaches the brain vasculature.

A. A representative montage of the *in vivo* two-photon imaging of FitC-tagged TAT-C1aB (TAT-C1aB-FitC) fluorescent signals through a cranial window. TAT-C1aB-FitC was injected i.p. at 0 min (6 nmol/g). An example region of interest (ROI; blood vessel) evaluated for fluorescence intensity over time is denoted by white square. Scale bar indicates 50 μm. **B**. Quantification of the 2-photon imaging data. FitC fluorescence intensity was normalized to the pre-injection baseline. Error bars indicate SEM of mean signal intensity at the ROIs such as that shown in prior panels (n = 3). **C**. Injection of TAT-C1aB-FitC (6 nmol/g; i.p.), but not TAT-C1aB, increased fluorescence intensity throughout the brain nervous tissue at 1 h after injection. Animals were thoroughly, transcardially perfused before brain sections (2 mm) were obtained. Shown are, from left to right,

bright field images, fluorescence images, and heat maps generated from the fluorescent images. Note the higher signals present in section obtained from TAT-C1aB-FitC-labelled brains (n = 3). Scale bar indicates 2 mm. In addition, lower section is unpublished data showing that without the conjugation of the TAT domain, FitC by itself cannot enter the brain parenchyma.

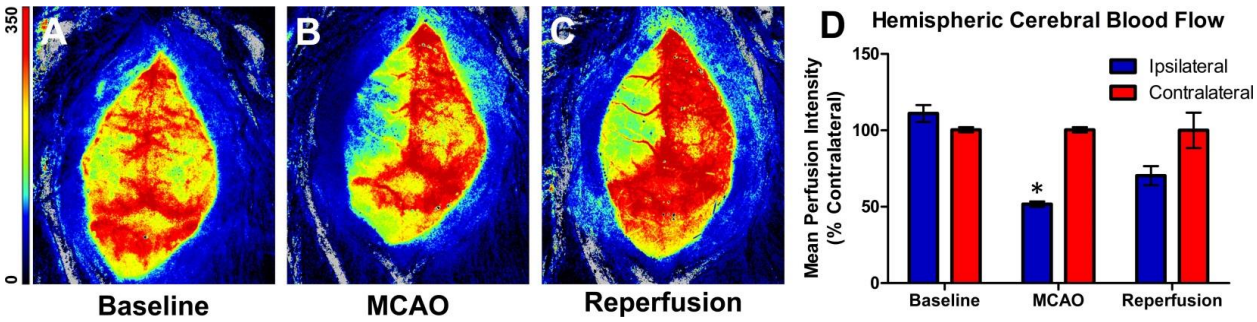

Figure 6. In vivo validation of MCAO model.

A-C. Laser sparkle Doppler images through the skull of an anesthetized mouse undergoing MCAO treatment. Images were taken at roughly 40 min pre (A), 15 min into MCAO (B), and 15 min post MCAO (C). Scale bar indicates relative signal intensity. **D.** Quantification of the mean Doppler signal intensity at each time point. A 50% decrease in Doppler signal intensity was observed during MCAO. Perfusion was partially recovered after suture was withdrawn. Bar graph indicates mean ± SEM of % perfusion vs contralateral of each time point (n = 3; Two-way ANOVA, Sidak's multiple comparison, *** $p<0.001$, *$p<0.05$).

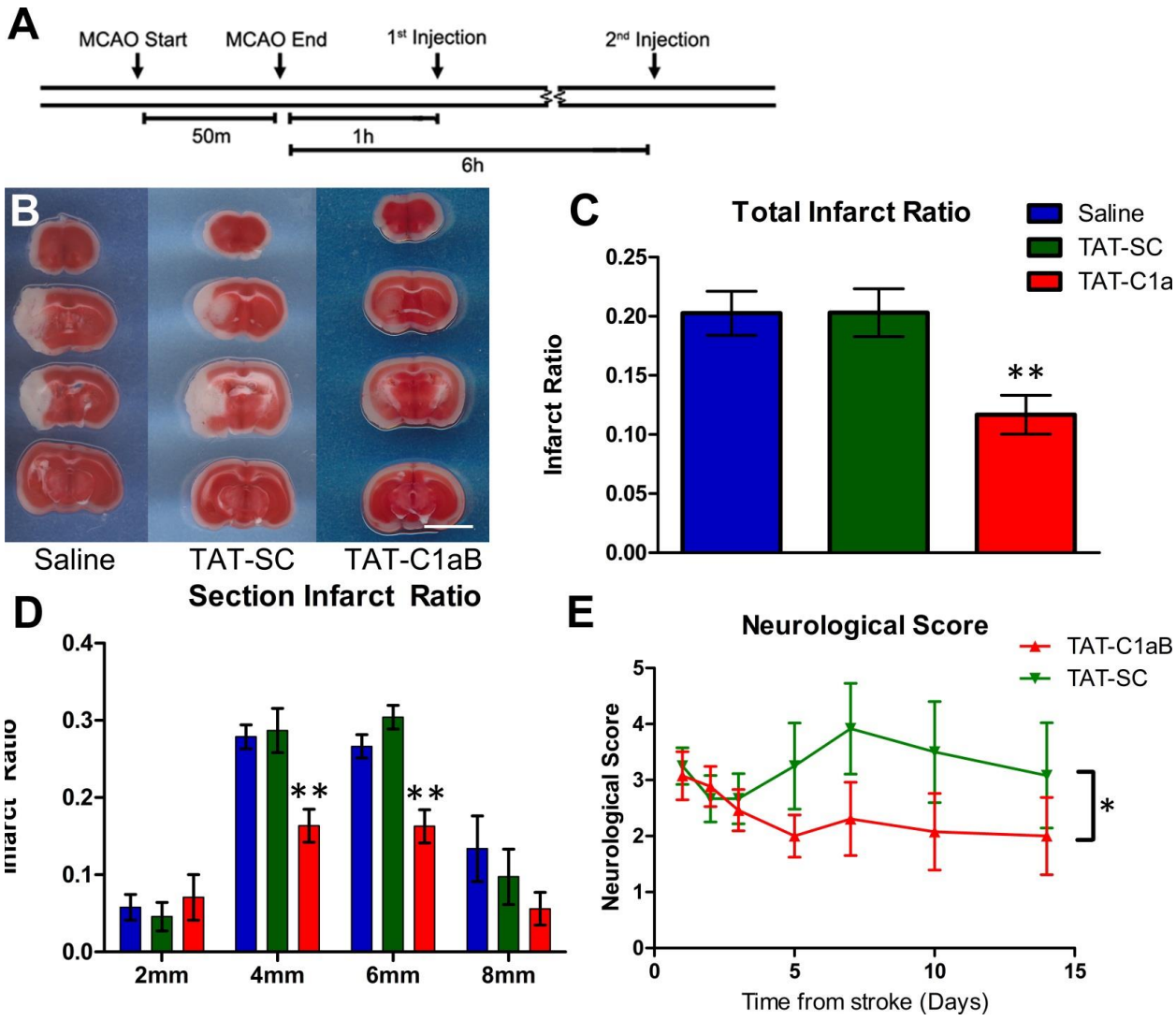

Figure 7. TAT-C1aB ameliorates ischemic stroke damage and improves neurological deficits in mice after MCAO.

A. Timeline of the experiment, note TAT-C1aB was injected twice (i.p.) at 1 and 6 h following the initiation of reperfusion. **B**. Representative images of brain sections after TTC staining at 24 h after 50 min of MCAO injury. Injections of TAT-C1aB (i.p., 6 nmol/g, at 1+6 h reperfusion) seemed to drastically reduce infarct size. Scale bar indicates 5 mm. **C**. Quantification of total infarct ratio is shown (infarct ratio is defined as infarcted area/total area). The total infarct ratio of TAT-C1aB animals (n = 7) was significantly decreased compared with that of either saline (n =

10) or TAT-SC (n = 8) treated animals (0.12 ± 0.02 vs 0.20 ± 0.02 and 0.20 ± 0.02 mean ± SEM; ANOVA/Dunnett, **p < 0.01) at 24 h reperfusion. **D.** The majority of the neuroprotective actions of TAT-C1aB were located within the core infarct area. The infarct ratio at 4 mm (0.16 ± 0.02) and 6 mm (0.16 ± 0.02) coronal section of TAT-C1aB treated animals was significantly reduced compared to that of either vehicle (0.28 ± 0.02; 0.27 ± 0.03) and TAT-SC treated animals (0.29 ± 0.03; 0.30 ± 0.02; ANOVA/Dunnett, **p<0.01). **E.** Evaluation of neurological scores of mice following for 14 days following a 40 min MCAO using an 8-point neurological scoring system (see Methods). TAT-C1aB treated animals (n = 13) exhibited a significant improvement in overall neurological outcome when compared with the TAT-SC treated animals (n = 13; two-way ANOVA, *p = 0.0174). Error bars indicate mean ± SEM of neurological score. Please note that treatments were randomized for all *in vivo* studies. Investigators performing surgeries, injection, and image or behavioral analyses were all blinded to the treatment group assignments.

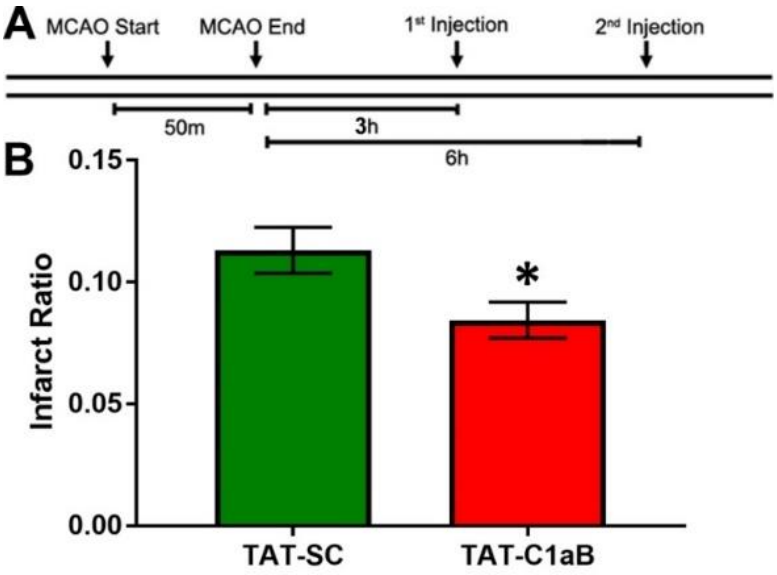

Figure 8. TAT-C1aB significantly reduced infarct ratio after transient stroke with a delayed treatment regimen.

A. Diagram of the experimental scheme in evaluating delayed TAT-C1aB treatment. Mice (24-26g) received a delayed initial dose of TAT-C1aB or TAT-Scramble treatment (6 nmol/g) at 3h after 50m of transient ischemic stroke. The second dose was applied identically as previously at 6h. **B**. TAT-C1aB significantly reduced the infarct ratio of mice brain after ischemic stroke compared with a scrambled control peptide (0.084±0.007 vs 0.11±0.009, n=8 and 7 respectively; *p=0.031, two-tailed t-test)

2.4 Discussion

Ischemic stroke is a leading cause of death worldwide (Thrift et al., 2016). Stroke survivors are often afflicted with permanent physical disabilities due to the loss of central neurons. While acute stroke causes almost immediate necrotic cell death in the ischemic core, programmed neuronal apoptosis in the penumbral region occurs for hours and can continue for several days (Bretón & Rodríguez, 2012). Unfortunately, over the past three decades, essentially all successful stroke treatments observed in preclinical studies have failed to demonstrate any therapeutic benefits in subsequent human trials (Kikuchi et al., 2014; Tymianski, 2014). Only recently, the excitotoxicity-ameliorating NA-1 (TAT-NR2B9c) has shown efficacy in a phase II clinical trial (Evaluating Neuroprotection in Aneurysm Coiling Therapy - ENACT), representing a potential novel approach to ischemic stroke treatment that is not a thrombolytic agent, and which, of relevance to the present study, is also a TAT-linked agent directed at interfering with an ion channel-associated lethal cascade (Hill et al., 2012). Nonetheless, no FDA approved stroke treatment yet exist that is intrinsically neuroprotective against delayed cell death (Tymianski, 2013). The results presented here suggest that the inhibition of the apoptotic-specific functions of Kv2.1 is a potential novel approach to address this medical shortcoming.

Recent findings have indirectly implicated the possible involvement of Kv2.1 antagonism as the underlying mechanism in other modes of neuroprotection. For instance, the FDA-approved anticonvulsant and KCNQ (Kv7) channel opener retigabine was shown to provide neuroprotection in an MCAO rodent model, an effect that was initially proposed to be mediated via regulation of neuronal excitability (Bierbower et al., 2015). Interestingly however, retigabine was also recently shown to inhibit Kv2.1 currents via a poorly reversible, open channel block mechanism, which could account for its neuroprotective actions (Stas et al., 2016). A similar mechanistic convergence

may also be present in an alternate model of Kv2.1-mediated neuronal apoptosis. Mutation of Kv2.1 N-terminal cysteine residue C73A to an alanine prevents cysteine-targeted oxidation of the channel, a step suggested to also be intimately linked to neuronal injury (Sesti, 2016; Yu et al., 2016). Rodents carrying this mutation were found to show some protection in a model of traumatic brain injury (Yu et al., 2016), an injurious process with many parallel molecular cell death cascades to those observed in ischemic stroke (Quillinan et al., 2016). Interestingly, we have found that the C73A mutation also effectively prevents p38 phosphorylation of serine residue S800 and the associated K+ current elevation (He et al., 2015), thereby linking the oxidative and the membrane insertion processes of the channel during cell death cascades. Regardless, these observations offer support to the notion of suppressing enhanced Kv2.1 current after lethal injury as a potentially important and novel neuroprotective approach.

The minimal STX1A binding domain within the Kv2.1 C-terminus is seemingly unique to this channel as we were unable to identify any other proteins containing this specific sequence via a BLAST search, except, as noted earlier, for a sequence within Kv2.2 containing 7 of the 9 a.a. found in Kv2.1 C1aB. In an overexpression system, Kv2.2 has indeed been shown to interact with STX1A, albeit in a manner different from that observed for Kv2.1 (Wolf-Goldberg et al., 2006). Specifically, Kv2.1/STX1A interactions are dramatically influenced by the presence of the additional SNARE protein SNAP-25, while this is not the case for Kv2.2 (Michaelevski et al., 2003; Wolf-Goldberg et al., 2006). We have previously found that enzymatic cleavage of either STX1A or SNAP-25 alone is sufficient to eliminate pro-apoptotic trafficking of Kv2.1 (Pal et al., 2006), strongly suggesting that a formation of the STX1A/SNAP-25 SNARE complex is necessary for the observed enhanced currents. It is entirely possible that STX1A can indeed bind and influence Kv2.2 function in neurons, but given the various factors noted here, as well a lack of a

p38 phosphorylation site in Kv2.2 that is analogous to S800 in Kv2.1, we believe that the effects of our peptide reported in our study are mostly, if not perhaps exclusively, mediated through a Kv2.1-directed mechanism.

As Kv2.1 is only expressed in the CNS in neurons (Murakoshi & Trimmer, 1999; Speca et al., 2014), TAT-C1aB may represent a unique and direct approach of suppressing cell death programs associated with neuronal enhanced K+ currents. Although traditional Kv blockers, such as tetraethylammonium and clofilium, have been shown to ameliorate ischemic damage (Wei et al., 2003), these drugs are also associated with increased vulnerability to epileptic seizures and ventricular tachycardia (Graham, 1950; Fueta & Avoli, 1993; Batey & Coker, 2002). These off-target effects make these molecules less than optimal candidates for stroke treatment. In contrast, we have observed no effects of TAT-C1aB on baseline currents, very similar to our previously reported actions of C1a overexpression and neuroprotection, both specifically targeting Kv2.1/STX1A interactions during apoptotic injury (McCord et al., 2014). In agreement with these findings, no increase in seizure-like behavior was observed in TAT-C1aB animals after ischemic stroke. The lack of reduction in post-stroke cerebral swelling also ruled out indirect protective mechanisms that could accompany ion flow manipulation in endothelial cells. Altogether, these data strongly suggest that TAT-C1aB targets a unique property of Kv2.1 that is intimately linked to a cell death process, and, importantly, it does not influence upstream processes such as NMDA receptor mediated Ca2+ responses. Along with the growing body of evidence indicating the significant involvement of pro-apoptotic Kv2.1 functions in many other neurodegenerative conditions (McCord & Aizenman, 2014; Shah & Aizenman, 2014; Yu et al., 2016), our observations may foreshadow the development of a new generation of highly robust neuroprotectants for human neurological conditions.

2.5 Materials and Methods

Peptide spot array and far-western assay. Far-western protein binding affinity assays were performed as previously described (Brittain *et al.*, 2011b). Peptide spot arrays (15 mers) spanning the proximal C-terminus residues 472-522 of rat Kv2.1 were constructed using the SPOTS-synthesis method. Standard 9-fluorenylmethoxy carbonyl (Fmoc) chemistry was used to synthesize the peptides and spot them onto nitrocellulose membranes pre-derivatized with a polyethylene glycerol spacer (Intavis AG). Fmoc protected and activated amino acids were spotted in 20-30 arrays on 150 mm by 100 mm membranes using an Intavis MultiPep robot. The nitrocellulose membrane containing the immobilized peptides was soaked in *N*-cyclohexyl-3-aminopropanesulfonic acid (CAPS) buffer (10 mM CAPS, pH 11.0 with 20% vol/vol methanol) for 30 min, washed once with Tris-buffered 0.1% Tween 20 (TBST), and then blocked for 1 h at RT with gentle shaking in TBST containing 5% (mass/vol) non-fat milk and then incubated with enriched STX1A protein for 1 h at RT with gentle shaking. Next, the membrane was incubated in primary antibody for STX1A (Millipore Cat# AB5820-50UL, RRID: AB_2216165) for 2 h at RT with gentle shaking, followed by washing with TBST. Finally, the membrane was incubated in secondary antibody (goat anti-rabbit DyLight 800, Cat# 355571, Thermofisher) for 45 min, washed for 30 min in TBST and visualized by infrared fluorescence (Li-Cor). Four independent peptide spot arrays were utilized in this study. A second set of membranes (n=4) was treated as above, but also in the presence of the identified peptide C1aB which had been coupled to TAT (TAT-C1aB; 100 uM; See Fig. 1). Peptides were synthesized at >95% purity (theoretical molecular weight 2737.20 g/mol; GenScript), and were prepared in small aliquots with ultrapure water.

Electrophysiology. Whole-cell patch clamp experiments were carried out on CHO cells transfected with either WT Kv2.1 or Kv2.1(S800E), together with eGFP-expressing plasmid constructs. The S800E point mutation was performed in a prior study (Redman *et al.*, 2007) and transfection was carried out as previously described (McCord *et al.*, 2014). Briefly, CHO cells were plated on coverslips in 24-well plates at a density of 5.6 x 10^4 cells per well. Cells were treated for 3-4 h in serum-free medium with a total of 1.2 μL lipofectamine (Invitrogen) and 0.28 μg DNA per well. Following transfection, cells were incubated with vehicle, 10 μM TAT-C1aB, or 10 μM scrambled control (TAT-SC) and maintained in F12 medium containing fetal bovine serum in 37°C and 5% CO_2 for 24 h prior to recording. Current recordings were performed on eGFP-positive CHO cells using the whole-cell patch clamp configuration as described previously (McLaughlin *et al.*, 2001). Borosilicate glass electrodes (3-4 MΩ; 1.5mm diameter; Sutter Instruments) were filled with internal solution composed of (mM): 100 K-Gluconate, 10 KCl, 1 $MgCl_2$, 1 $CaCl_2$, 10 HEPES, 11 EGTA, 2.2 ATP, 0.33 GTP. The internal solution was further adjusted to pH 7.2, and to 280 mOsm with the addition of sucrose. The pH-adjusted (7.2) external solution was composed of the following (mM): 115 NaCl, 2.5 KCl, 2.0 $MgCl_2$, 10 HEPES, 10 D-glucose. Partial compensation (80%) for series resistance was performed for all recordings; currents were filtered at 2 kHz and digitized at 10 kHz (Digidata 1440A; Axon Instruments). Delayed rectifier currents were evoked with a series of 200 ms voltage steps to +80 mV from the holding potential of -80 mV in +10 mV increments. Measurements were performed with an Axopatch 200B amplifier and Clampex. Steady state current analysis was carried out at 180 ms, at the +30 mV voltage step relative to baseline current. Current density (pA/pF) was calculated by normalizing the current amplitude measurement to cell capacitance, an electrical determination of cell size. Recordings were carried out at room temperature (~25°C).

Cortical cultures, LDH Assay and Calcium Measurements. All animal protocols in this study were approved by the Institutional Animal Care and Use Committee of the University of Pittsburgh School of Medicine. Cortical neurons were prepared from embryonic day 16 (E16) rats of either sex as described previously (McCord *et al.*, 2014). Pregnant donor rats (Charles River Laboratories) were euthanized by gradual CO_2 inhalation, an American Veterinary Medical Association approved protocol (Leary *et al.*, 2013). Cortices were dissociated with trypsin, and plated at 670,000 cells per well on glass coverslips in six-well plates as described in (Hartnett *et al.*, 1997). Non-neuronal cell proliferation was inhibited with 1-2 μM cytosine arabinoside. DL-threo-beta-benzyloxaspartate (TBOA; Tocris) excitotoxicity assays were carried out on 28-35 DIV cultures. Coverslips were transferred into 24-well plates containing 10 mM HEPES-supplemented MEM without phenol red. On each individual plate, coverslips were treated with vehicle or 100 μM TBOA and 0, 0.3, or 1 μM of either TAT-C1aB or TAT-SC at 37°C and incubated in 5% CO_2 for 24 h. Following this, external medium was collected for LDH colorimetric measurements using a toxicity kit (Sigma-Aldrich), as previously described (Aras *et al.*, 2001). Each experiment contained 4 replicates of 6 conditions, including 3 control and 3 TBOA treatment groups; peptide treatment groups (TAT-C1aB, TAT-SC) were evaluated in separate experiments. Cell toxicity was quantified as the LDH ratio of TBOA-treated over no TBOA control values within each experiment. For direct visualization of individual neurons in a similar set of assays, eGFP protein transfection was carried out using Lipofectamine 2000 (Invitrogen) as previously described (McCord *et al.*, 2014). Cells were imaged at 60x using an A-1 confocal microscope (Nikon).

Intracellular Ca^{2+} measurements were performed essentially as previously described (Aizenman *et al.*, 1990; Reynolds *et al.*, 1990) on the same cortical culture preparations as above, but with 20 DIV cells plated on MatTek glass bottom 35 mm culture dishes. At this developmental

stage, neurons robustly express both GluN2A and GluN2B subunits of the NMDA receptor (Sinor *et al.*, 2000). Prior to recordings, cultures were incubated overnight with 1 μM of either TAT-C1aB or TAT-SC. These treatments were removed just prior to the Ca^{2+} measurements. For recordings, neurons were incubated with the fluorescent Ca^{2+} indicator Fura-2 AM ester (5 μM; Invitrogen) with 0.02% Pluronic F-127 (Invitrogen) for 1 h at 37°C. Culture dishes were then mounted on an inverted microscope stage (Olympus) and continuously perfused with a 10 mM HEPES buffered normal salt solution. Perfusion rate (5 mL/min) was controlled with a gravity flow and a rapid-switching local perfusion system (Warner Instruments). Firmly attached, refractile cells were identified as regions of interest (50 cells/coverslip; 3 coverslips per condition). A ratio of fluorescence emission (F) at 510 nm in response to excitations at 340 and 380 nm was acquired at 1 Hz (Lambda DG-4 and 10-B SmartShutter; Sutter Instruments) via camera (ORCA-ER; Hamamatsu Corporation) and saved to a computer using HCImage (Hamamatsu Corporation). Baseline Ca^{2+} signals were recorded for 2 min prior to a 20 min application of NMDA (30 μM + 10 μM glycine) followed by a 5 min washout period. Peak increases in intracellular calcium concentration were measured by calculating $\Delta F/Fo$, (ΔF=peak fluorescence, Fo=average signal across 2 min baseline period). The area under the response for the first 15 min of NMDA application was also calculated.

Fluorescently-labeled peptide brain imaging. For 2-photon imaging of TAT-C1aB-FitC in cortical vasculature, a cranial window was opened over the temporal lobe area in head-fixed young adult mice under isoflurane anesthesia (induction: 3% in oxygen, maintenance: 1.5% in oxygen; Butler Schein). Mode-locked infrared laser light (940 nm, 100-200 mW intensity at the back focal plane of the objective, MaiTai HP, Newport) was delivered through a galvanometer-

based scanning 2-photon microscope (Scientifica) controlled with scanimage (Pologruto *et al.*, 2003), using a 40X, 0.8 NA objective (Olympus). After obtaining a stable imaging location (field of view 145 μm x 145 μm, 100-200 μm deep from the cortical surface), a single i.p. injection of TAT-C1aB-FitC (6 nmol/g) was administered to the animal. We imaged FitC fluorescence emission with a photomultiplier tube (PMT) and a green emission filter (FF03-525/50, Semrock) at 5 to 10 minute intervals for 15 minutes before and two hours after i.p. injection. The laser power and PMT voltage remained constant throughout the imaging session. Quantification of ROI signal intensity was evaluated by Image J analysis software (NIH).

To confirm blood brain barrier permeability of the TAT-linked peptide, mice were thoroughly perfused with ice-cold saline 1 h after i.p. injection of either TAT-C1aB or TAT-C1aB-FitC (6 nmol/g). Brains were quickly removed, sectioned into 2 mm slices and imaged using an Olympus MVX10 microscope with a SPOT RT3 camera. TAT-C1aB and TAT-C1aB-FitC-labelled brains were imaged sequentially with identical camera settings. Generation of the 8-bit fluorescence signal heat map was performed using the ImageJ plugin HeatMap Histogram (http://www.samuelpean.com/heatmap-from-stack/).

***In vivo* cerebral blood flow measurements**. Cerebral blood flow was monitored using a two-dimensional laser speckle contrast analysis system (PeriCam PSI High Resolution with PIMSoft; Perimed). Anesthesia was induced by 3%, and maintained at 1.5% isoflurane (Butler Schein) in 3:1 NO:O_2 gas mixture using a vaporizer (General Anesthetic Service). Throughout the experimental procedure, rectal temperature was maintained between 36.5 and 37.0°C using a feedback-controlled heating system (PhysioSuite). The skull of the animal is secured in a stereotactic frame (David Kopf Instruments). A midline incision was made in the scalp and the skull surface was cleaned with sterile normal saline. At 40 min prior to MCAO, 15 min into

MCAO, and 15 min after reperfusion, blood perfusion images were taken with a charged-coupled device camera placed 10 cm above the skull. Raw speckle images were taken in a 1.6 cm x 1.4 cm field at 19 frames/second, 57 frames averaging, with the resolution of 0.02 mm. Five consecutive images at each time point per animal were averaged for analysis using oval-shaped regions of interest (ROI) covering the frontal and parietal bone plates of the ipsi- and contra-lateral sides. Percent signal intensity was calculated by comparing the ipsilateral side mean signal intensity to that of the contralateral side at each time point.

MCAO procedure. Each cohort of young adult mice (ages 8-10 wks, male, 24-29g; Jackson Laboratory) were randomized to each group to account for possible confounding factors in the experimental order and body weight on the day of the surgery. However, as body weight did not vary that much we were able to use the same model/thickness of single-use silicon-coated sutures for all animals (# 602212PK10; Doccol Corporation). The suture was advanced from the junction of the external and the common carotid artery into the internal carotid artery for ~9 mm or until resistance was felt. The suture was secured in this position for the duration of the ischemia time (40/50 min). Mice were anesthetized with isoflurane and maintained at physiological body temperature as described above. Animals were only anesthetized during the surgery. Researchers performing MCAO (C-Y.Y), drug injections (C-Y.Y.), neurological assessment (A.M.B.), and quantitative analysis of the infarct size (E.A.) were all blinded to the treatment groups. Treatments (saline, TAT-C1aB or TAT-SC) had been previously randomized by an additional experimenter (K.A.H., A.M.B.).

Infarct Ratio Measurements. For quantification of the infarct area, whole brains were extracted from each animal and dissected into 2 mm sections before being stained with 2,3,5-triphenyltetrazolium (TTC; Sigma-Aldrich) with the optimal staining protocol specifications

described previously (Joshi *et al.*, 2004): 0.05% TTC in PBS, at 37°C, for 30 min. Brain slices were scanned after TTC staining and the infract ratio was measured as the total or section infarct area/total area. Infarct size was measured through Image J analysis software. Percent swelling was calculated as (Ipsilateral volume/Contra lateral volume) x 100%.

Neurological Testing. Neurological deficits were assessed on days 1, 2, 3, 5, 7, 10, and 14 following MCAO surgery. Mice were evaluated by a blinded experimenter on an 8-point scale as described previously (Xia *et al.*, 2006), adapted for left side MCAO. Briefly, 0 = no neurological deficit; 1 = right forelimb flexion when suspended the tail or failure to extend left forepaw fully; 2 = right shoulder adduction when suspended by tail; 3 = reduced resistance to lateral push towards the right; 4 = spontaneous movement in all directions with circling to the right exhibited only if pulled by tail; 5 = circle or walk spontaneously only to the right; 6 = walk only when stimulated; 7 = no response to stimulation; 8 = stroke-related death.

3.0 Defining the Kv2.1-syntaxin molecular interaction identifies a novel class of small molecule neuroprotectants

3.1 Section Summary

The neuronal cell death-promoting loss of cytoplasmic K^+ following injury is mediated by an increase of Kv2.1 potassium channels in the plasma membrane. This phenomenon relies on Kv2.1 binding to syntaxin 1A via 9 amino acids within the channel intrinsically disordered C-terminus. Preventing this interaction with a cell and blood brain barrier-permeant peptide is neuroprotective in an *in vivo* stroke model. Here, a rational approach was applied to define the key molecular interactions between syntaxin and Kv2.1, some of which are shared with Mammalian UNCoordinated-18 (munc18). Armed with this information, we discovered the first small molecule Kv2.1-syntaxin binding inhibitor (cpd5) that improves cortical neuron survival by suppressing the SNARE-dependent enhancement of Kv2.1-mediated currents following excitotoxic injury. We validated that cpd5 selectively displaces Kv2.1 syntaxin-binding peptides and, at higher concentrations, munc18, without affecting either synaptic or neuronal intrinsic properties in brain tissue slices at neuroprotective concentrations. Collectively, our findings reveal insights into the role of syntaxin in neuronal cell death and validate an important, novel target for neuroprotection.

Significance Statement. Enhanced Kv2.1-syntaxin interaction precedes the neuronal cell death-promoting loss of cytosolic K^+ in many neurodegenerative conditions. The work here characterizes the interaction of the disordered C-terminus of Kv2.1 at a molecular level and further translates these findings to discover a first-in-class small molecule with neuroprotective properties.

In doing so, we demonstrated a rational drug discovery workflow that can elucidate protein-protein interactions involving highly unstructured domains.

3.2 Introduction

Therapeutic options to prevent, halt, or ameliorate neurodegenerative disorders remain critical areas of unmet medical need in spite of more than three decades of aggressive research efforts (Gribkoff & Kaczmarek, 2017; Editorial, 2018). Central to this challenge is the fact that many neurological diseases are driven by proteins with highly flexible and unstructured domains that bind multiple partners, making both their mechanistic characterization and their pharmacological targeting exceedingly difficult (Uversky, 2015). Indeed, these intrinsically disordered unstructured domains are quite common amongst various disease-associated membrane-bound receptors and ion channels, especially in their regulatory cytoplasmic regions (Kjaergaard & Kragelund, 2017). One such protein is the delayed rectifier potassium channel Kv2.1, which enables a well-characterized neuronal cell death cascade through its cytoplasmic C-terminus domain (Shah & Aizenman, 2014). In the current study, we focus on a key interactor of the Kv2.1 C-terminus, namely syntaxin 1A (syntaxin), to further unveil the molecular mechanisms involved in Kv2.1-dependent neurodegeneration and to pursue a novel translational strategy.

Following an injurious stimulus, Kv2.1-mediated regulation of intracellular K^+ is a critical convergent factor in neuronal cell death programs. At normal physiological concentrations, cytoplasmic K^+ suppresses the catalytic activity of several proteases and nucleases linked to cellular pathology (Hughes & Cidlowski, 1999). Enhanced K^+ efflux in injured neurons, however, facilitates rapid execution of cell death cascades (Yu *et al.*, 1997; Yu, 2003). Kv2.1 mediates this

cell death-promoting cytoplasmic K^+ loss in a number of neuronal subtypes including cortical neurons (Pal *et al.*, 2003), hippocampal pyramidal neurons (Chi & Xu, 2000; Wu *et al.*, 2015), midbrain dopaminergic neurons (Redman *et al.*, 2006), and cerebellar granule cells (Jiao *et al.*, 2007). The Kv2.1-dependent cell death pathway is normally initiated by the oxidative liberation of zinc from intracellular metal-binding proteins (Aizenman *et al.*, 2000), leading to the sequential phosphorylation of Kv2.1 residues Y124 and S800 by Src and p38 kinases, respectively (Redman *et al.*, 2007; Redman *et al.*, 2009; He *et al.*, 2015). The dual phosphorylation of the channel enhances its interaction with syntaxin and increases its surface expression, inducing the subsequent loss of intracellular K^+ (Pal *et al.*, 2003; Pal *et al.*, 2006; Redman *et al.*, 2006; McCord & Aizenman, 2013; Shah & Aizenman, 2014).

The Kv2.1 domain responsible for the interaction with syntaxin is located within the intrinsically disordered Kv2.1 proximal cytosolic C-terminal, originally termed C1a by Gaisano, Lotan, and co-workers (Leung *et al.*, 2003; Singer-Lahat *et al.*, 2007; Singer-Lahat *et al.*, 2008). Overexpression of a fragment containing residues 441-522 within the C1a region (Kv2.1 rat sequence; NCBI accession # NP_037318.1) is sufficient to inhibit the injury-induced plasma membrane insertion of Kv2.1 channels in neurons and provide neuroprotection *in vitro* (McCord *et al.*, 2014). Recently, we further narrowed down the amino acid sequence within C1a to 9 residues, namely H_1LSPNKWKW$_9$ (C1aB; from N- to C-terminus, corresponding to Kv2.1 residues 478-486 in rat, and 482-490 in mouse and humans; Accession #s NP_032446.2 and NP_004966.1, respectively). Most importantly, blocking the interaction between Kv2.1 and syntaxin using a blood-brain-barrier permeable conjugated peptide (TAT-C1aB) effectively ameliorates acute neuronal ischemic injury, limiting infarct damage and improving neurological function *in vivo* (Yeh *et al.*, 2017).

The chemical disruption of protein-protein interactions involving intrinsically disordered regions such as the Kv2.1 C-terminus is an unique challenge for pharmaceutical intervention, as these domains not only undergo structural rearrangements upon binding but also involve selectively promiscuous sites that regulate multiple interactions (Pabon & Camacho, 2017). This task is further hindered by the fact that the syntaxin site for Kv2.1 binding has not, heretofore, been resolved. To address these challenges, we developed a rational approach that combines molecular modeling, biophysics, and cell-based experimental validations. This approach led us to elucidate the molecular actors essential to the Kv2.1-syntaxin interaction, predicting it to exist within the complex binding site previously resolved for the co-crystal structure between syntaxin and Mammalian UNCoordinated 18 (munc18), a critical component of exocytotic processes (Toonen & Verhage, 2007). We then began the translation of these results with a virtual screening of small molecule libraries with the goal of inhibiting the Kv2.1-syntaxin interaction while minimally interfering with munc18 function. This process led to the identification of a first-in-class protein-protein inhibitor and lead compound that can prevent neuronal injury. These findings reveal mechanistic insights of syntaxin's role in cell death functions and validate a novel target for the development of neuroprotective therapeutics.

3.3 Results

3.3.1 Structural modeling of Kv2.1 C1aB H_1LSPNKWKW$_9$ peptide and its interactions with syntaxin

Syntaxin binding to the C1a region of Kv2.1 is largely restricted to within a nine amino acid sequence of the channel we previously defined as C1aB (H_1LSPNKWKW$_9$). We had observed a rapid drop-off in syntaxin binding when C-terminal C1aB residues are removed in a large avidity panel of Kv2.1 C1a-derived 15-mer peptides (Yeh *et al.*, 2017), alerting us to the possibility that the essential interactions of the syntaxin binding domain could be further refined. We thus carried out molecular dynamics simulations of Kv2.1-derived peptides containing partial or complete C1aB sequences to analyze the stability of these peptides. Figures 9A and 9B show both a representative snapshot and the conformational ensembles entailed by the C1aB K6W7 sequence motif for four different peptides. Two of the strongest syntaxin-binding peptides (Yeh *et al.*, 2017) (pep-22 and pep-28) consistently show a fully solvent-exposed W7 residue with the preceding K6 in the opposite trans direction. In contrast, the two weakest syntaxin-binding peptides (pep-20 and pep-21) show the increasing occlusion of W7 by interactions with K6 side chain upon deletion of either the K8W9 residues or just the W9 from the corresponding C1aB sequence. This is evident in the increasing probability of K6 to be in the interfering *cis* positions when the two anchoring residues are removed in the weakly binding peptides (Fig. 9B). The observed stability of the free W7 in strongly binding peptides suggests that this residue plays a critical role in the recognition of syntaxin, whereas deletion of W9 could have an impact in binding affinity by inducing the occlusion of W7 but, as suggested by our previous work (Yeh *et al.*, 2017), the shorter peptide would still able to bind the SNARE protein to some extent.

3.3.2 The Kv2.1 C1aB W7 syntaxin-binding structural motif is shared with munc18 W28

The co-crystal structure of the closed form of syntaxin and Mammalian UNCoordinated 18 (munc18) (PDB code 4JEH (Toonen & Verhage, 2007; Burkhardt et al., 2008)), a known modulator of synaptic transmission that is essential for the proper assembly of syntaxin with other SNARE components (Jiao et al., 2018), is stabilized by multiple hydrogen bonds and non-polar interactions encompassing both the syntaxin regulatory Habc and core SNARE H3 domains. This includes a specificity determinant aromatic stacking between munc18 W28 and syntaxin F34, on the first helix of the Habc domain (Fig. 10A). Structural similarities between our simulated C1a peptides (Fig. 9A) and the corresponding motif in munc18 bound to syntaxin (Fig. 9C), which also has an adjacent lysine residue (K29), led us to perform an unbiased docking of a C1aB peptide on syntaxin's binding surface with munc18 (PDB 4JEH). Using the software SMINA (Koes et al., 2013) with default settings, we obtained the C1aB docked pose shown in Fig. 10B.

3.3.3 Experimental validation of C1aB/syntaxin interactions

All the intermolecular interactions in our C1aB/syntaxin binding model (see detailed view in Fig. 10D) are not only chemically favorable but are also strikingly consistent with an alanine scan mutagenesis of individual C1aB amino acids in a syntaxin-binding peptide array assay (Fig. 9D). In particular: (i) W7 stacking interaction with syntaxin F34 is eliminated in W7A, but nonpolar contacts remain; (ii) W9 hydrophobic contacts with syntaxin I115 are absent in W9A, thereby significantly decreasing binding affinity; (iii) C1aB K6 backbone, whose side chain is opposite to W7, interacts via hydrogen bonds with Q119, a property retained in K6A; (iv) L2 is

buried in a hydrophobic pocket formed by syntaxin's L123, K126 and T122, and, thus, the hydrophobic side chain present in L2A may somewhat decrease binding affinity; finally, (v) C1a H1 hydrogen bonds with T122 and D231 are expected to be replaced in H1A, with D231 bonding to the free amine group in the N-terminus of the peptide.

It is noteworthy that interactions equivalent to those seen in our C1aB model are also observed in the munc18 and syntaxin co-crystal (Fig. 10C), further supporting the accuracy of our proposed model. Specifically, and as shown in detailed contacts of munc18 and syntaxin in Fig. 10C, (i) munc18 W28 stacking with syntaxin F34, with the nearby K29 pointing in the opposite direction, is analogous to the arrangement of C1aB W7, (ii) munc18 T56 and I57 contact syntaxin I115, analogous to the interactions of C1aB W9; (iii) the crystal water in the munc18 binding interface, fully coordinated by syntaxin Q119, T122, R41, together with the munc18 M51 backbone, is reshaped into a non-polar pocket in syntaxin, burying C1aB L2; and, finally, (iv) munc18 T48 hydrogen bond with syntaxin D231 is mimicked by C1aB H1. Taken together, unbiased docking of C1aB peptide fully rationalizes the alanine scanning, where W7 aromatic stacking with syntaxin's F34 and the burial of L2 in a non-polar pocket are the specificity determinant interactions of Kv2.1 C1aB with syntaxin. Notably, deletion of either of these residues in our C1a-derived 15-mer peptides obliterate binding (Yeh et al., 2017) (see, also, Fig. 13).

3.3.4 Virtual screening of Kv2.1/syntaxin inhibitors identifies six small molecule candidates

Leveraging the aforementioned structural insights, we performed a small molecule virtual screening with the goal of inhibiting C1aB protein-protein interaction with syntaxin. To do this, we designed pharmacophore models and use the search engine ZINCPharmer (Koes & Camacho, 2012) to screen 26+ million commercially available compounds present in the ZINC database

(Irwin & Shoichet, 2005). Models were designed to include a ring-stacking interaction with F34 and also match different combinations of hydrogen bonds formed by crystal water 315 in PDB 4JEH with syntaxin's Q119, T122 and R41 (Fig. 10A, 10C). After the primary screening based on these pharmacophores, compounds matching our design underwent an all atom optimization (Ye et al., 2016), resulting in the six molecules shown in Fig. 11A that were selected for in vitro experimental testing. Fig. 15A, 15B shows the list and chemical structures of these selected compounds, abbreviated as cpd1 to cpd6.

3.3.5 Cell-based screening of small molecule cpd5 reveals neuroprotective properties

To determine whether cpd1-6 could recapitulate the previously described biological effects of C1a and TAT-C1aB (McCord et al., 2014; Yeh et al., 2017), we evaluated them in vitro first for intrinsic toxicity and then for neuroprotective actions in rat cultured cortical neurons. We found that cpd1 did not readily dissolve at a reasonable concentration using a variety of solvents. We also observed that cpd2 was at times neurotoxic after 24 hr incubation at 10 μM (Fig. 15C), quantified as a significant increase in extracellular lactate dehydrogenase (LDH) above baseline (relative toxicity), a sign of cellular damage (Aras et al., 2008). Therefore, cp1 and cpd2 were excluded from further studies. The remaining four compounds were not neurotoxic at concentrations as high as 10 μM (Fig. 15C, 15D). We next examined whether these molecules could provide neuroprotection against overnight applications of threo-beta-Benzyloxyaspartate (TBOA; 75 μM), a non-selective glutamate reuptake inhibitor (Shimamoto et al., 1998). TBOA induces relatively slow (overnight) NMDA receptor-mediated excitotoxicity characterized by Kv2.1-dependent cell death in our cultures (Yeh et al., 2017; Justice et al., 2018). We found that pre-treatment (1 hr) and co-incubation with 10 μM cpd5 (3-[3-(1,3-benzothiazol-2-yl)phenyl]-1-

[(3,4-dimethoxyphenyl)methyl]urea; molport-009-741-732) significantly diminished TBOA toxicity, an effect nearly identical to the actions of 1 μM TAT-C1aB treatment (Fig. 12A, 12B). In phase contrast imaging, we observed that TBOA treatment reduces the number of phase-bright, healthy neurons, which was ameliorated with the co-treatment of cpd5 (Fig. 12A left). To better visualize this result, we transfected neurons with eGFP prior to treatment and confirmed that TBOA treatment causes significant cellular damage, which is ameliorated in cells co-treated with cpd5 (Fig. 12A right). In contrast to cpd5, cpds 3,4 and 6 did not afford any measurable neuroprotection and thus were also excluded from further studies (Fig. 15E).

The docked pose of cpd5 with syntaxin, shown in Fig. 11A, 11B, recapitulates all the interactions that we found to be essential for C1aB binding to syntaxin. Namely, it shows an optimal stacking with F34 through the benzothiazole ring, hydrophobic contact between the benzene ring and V37, hydrogen bonds with A41, N119, and T122 all established by the munc18 crystal water and essential for C1aB L2 binding to syntaxin, and the interaction of the veratrole group and K126. This fully rationalizes cpd5 as potentially effective in disrupting the Kv2.1/syntaxin interaction. Mechanistically, dispersing somatodendritic Kv2.1 clusters has also been shown to be a viable approach to prevent the increase of death-inducing K+ currents (Justice et al., 2017). To rule out that cpd5 is providing neuroprotection by declustering Kv2.1, we transfected neurons with Kv2.1-eGFP and evaluated their clustering status after 24 hr exactly as previously described (Justice et al., 2017). We found no significant effect of 24 hr 10 μM cpd5 treatment on Kv2.1 clusters (Fig. 15F). This finding is consistent with the previously observed lack of declustering properties of Kv2.1 C1a over-expression in cortical neurons (Justice et al., 2017), strongly suggesting that inhibiting Kv2.1/syntaxin interaction subdues the translocation of new Kv2.1 channels to the membrane.

3.3.6 Cpd5 suppresses cell death-enabling K^+ currents

The hallmark of Kv2.1-facilitated neuronal cell death is the accompanying large increase in delayed rectifier K^+ currents as the result of syntaxin-dependent *de novo* Kv2.1 channel insertion in the plasma membrane (Pal *et al.*, 2006). We previously showed plasmid-mediated overexpression of C1a or the use of the TAT-C1aB peptide prevents the Kv2.1-mediated current surge (McCord *et al.*, 2014; Yeh *et al.*, 2017). To determine whether cpd5 achieves similar inhibition of current enhancement, we carried out whole cell patch clamp recordings of rat cortical neurons *in vitro* after co-incubation with TBOA (50 μM for 2 hr followed by a 2 hr wash period), a treatment that we have shown to cause the canonical Kv2.1 current increase (Justice *et al.*, 2018). In strong agreement with our neuroprotection assays, we found that cpd5 (10 μM) pre-loading (1 hr) and co-treatment with TBOA effectively suppressed the post-injury enhancement of delayed rectifier K^+ currents in neurons to levels comparable to uninjured neurons (Fig. 12C striped red bar). Importantly, we found no significant effects of cpd5 incubation alone on basal K^+ currents (Fig. 12C red bar), strongly suggesting that the pre-existing membrane-bound channels and the normal trafficking of the channel during the 5 hours total duration of cpd5 incubation are unaffected by the drug. This is consistent with previous findings in cells expressing the C1a fragment or treated with TAT-C1aB (McCord *et al.*, 2014; Yeh *et al.*, 2017). Most significantly, the inhibition of the injury-enhanced currents, a syntaxin-dependent process (Pal *et al.*, 2006), strongly points to an on-target action of cpd5.

Because NMDA receptors mediate the neurotoxicity elicited by glutamate reuptake inhibitors (Blitzblau *et al.*, 1996), we evaluated whether cpd5 inhibited NMDA-evoked Ca^{2+} response, a major component of acute excitotoxicity (Choi, 1987; Sattler & Tymianski, 2001). We thus performed Fura-2 ratiometric Ca^{2+} imaging in cultured neurons during NMDA (30 μM with

10 μM glycine) exposure, noting a lack of any effect of concurrently-administrated cpd5 (10 μM) on NMDA-evoked Ca^{2+} responses (Fig. 12D). This strongly indicates that the aforementioned neuroprotective actions of cpd5 likely did not occur as a result of direct interference with the upstream components of the excitotoxic cascade. Rather, these findings are evidence that cpd5, like TAT-C1aB, provide neuroprotection against TBOA-induced excitotoxicity specifically by preventing the expression of enhanced Kv2.1-mediated K^+ currents.

3.3.7 Cpd5 is a first-in-class inhibitor of Kv2.1 binding to syntaxin

The docked model of cpd5 shown in Fig. 11B predicts cpd5 to strongly compete with essential interactions of C1aB and syntaxin. In addition, since munc18 binds to both the core SNARE domain and the N-terminal region of the closed conformation syntaxin (Fig. 10A) (Misura *et al.*, 2000), we expected cpd5 to displace C1aB more effectively than displacing munc18. To confirm this prediction, we first performed a peptide array binding assay and observed that cpd5 (100 μM) significantly reduced binding between syntaxin and all of the previously identified (Yeh *et al.*, 2017) Kv2.1 C1a-derived syntaxin-binding peptides (Fig. 13). Of note, inhibition occurred for all the peptides that contained the predicted stacking interaction between C1aB W7 and syntaxin F34, as well as C1aB L2. We also gauge the specificity of cpd5 by noting that it had a negligible effect on any of the remaining non-specific or weak reads. To evaluate the potency of cpd5, we measured concentration-dependent inhibition of syntaxin binding to peptides 22 to 28, which contain the full C1aB sequence, obtaining a fitted IC_{50} of 5.5 μM with a maximum effectiveness of up to ~75% binding displacement by 100 μM Cpd5 (Fig. 13 Inset, fitted curve of averaged data). Higher concentrations of Cpd5 could not be tested due to solubility issues. Next, we performed a co-immunoprecipitation assay of syntaxin and munc18 in transfected HEK293

cells incubated in various concentrations of cpd5. Consistent with our prediction, we found that cpd5, at both 30 and 100 μM, robustly disrupts binding between munc18 and syntaxin (Fig. 16A); the specificity of the antibodies used in this experiment was also confirmed (Fig. 16B). Of note, munc18 was not displaced by cpd5 at the neuroprotective concentration of 10 μM, which, as evident above, can displace C1aB-containing peptides from syntaxin. Together, these results demonstrate that the observed neuroprotective actions of cpd5 are likely due to the inhibition of the C1a region of Kv2.1 binding to syntaxin.

3.3.8 Cpd5 does not alter either synaptic or intrinsic properties of neurons

Loss of munc18 function blocks neurotransmitter release, causing munc18$^{-/-}$ animals to suffer paralysis and rapid global neurodegeneration after birth (Verhage *et al.*, 2000; Weimer *et al.*, 2003). Despite cpd5's overlapping syntaxin binding site with that of munc18, we did not find it to be neurotoxic *in vitro* at concentrations as high as 30 μM (Fig. 15D). However, it remained necessary to evaluate the possibility of cpd5 causing non-specific effects on neuronal synaptic and intrinsic properties. For this purpose, we evaluated the effects of 10 μM cpd5 on the synaptic and intrinsic properties of two distinct populations of projection neurons in the mouse auditory cortex: the layer 2/3 corticocallosal neurons projecting to the contralateral auditory cortex and the layer 5B corticocollicular neurons projecting to the ipsilateral inferior colliculus (Joshi *et al.*, 2015; Joshi *et al.*, 2016). In addition to being guided by anatomical landmarks such as the rhinal fissure and the hippocampus anatomy to locate the auditory cortex, we injected green retrograde fluorospheres in the contralateral cortex and red retrograde fluorospheres in the ipsilateral inferior colliculus to label the layer 2/3 corticocallosal and layer 5B corticocollicular neuronal populations respectively (Fig. 14A Left). We have previously confirmed that retrogradedly labeled layer 2/3 corticocallosal

and layer 5B corticocollicular neurons in this manner consistently overlay with the functionally localized auditory cortex (Joshi *et al.*, 2015; Joshi *et al.*, 2016). Local stimulations to layer 2/3 were used to evoke EPSCs in retrogradely labeled layer 2/3 corticocallosal neurons (Fig. 14A Right). Application of cpd5 (10 μM) caused no significant differences in the amplitude of AMPAR-mediated excitatory post-synaptic currents evoked in these cells (Fig. 14B-D). Next, we examined the effects of cpd5 (10 μM) on the intrinsic properties of labeled layer 5B corticocollicular neurons (Fig. 17A). Cpd5 did not have any effect on resting membrane potential (Fig. 17B), input resistance (Fig. 17C), and HCN channel-mediated (I_h) sag potential (Fig. 17D). Action potential threshold (Fig. 17E), width (Fig. 17F), and firing rates (Fig. 17G) were also unchanged by the cpd5 treatment. These results demonstrate that cpd5 does not affect either the synaptic properties of layer 2/3 corticocallosal neurons or the intrinsic properties of layer 5B corticocollicular neurons in the mouse auditory cortex, consistent with the fact that the drug does not disrupt munc18/syntaxin binding at minimal neuroprotective concentrations.

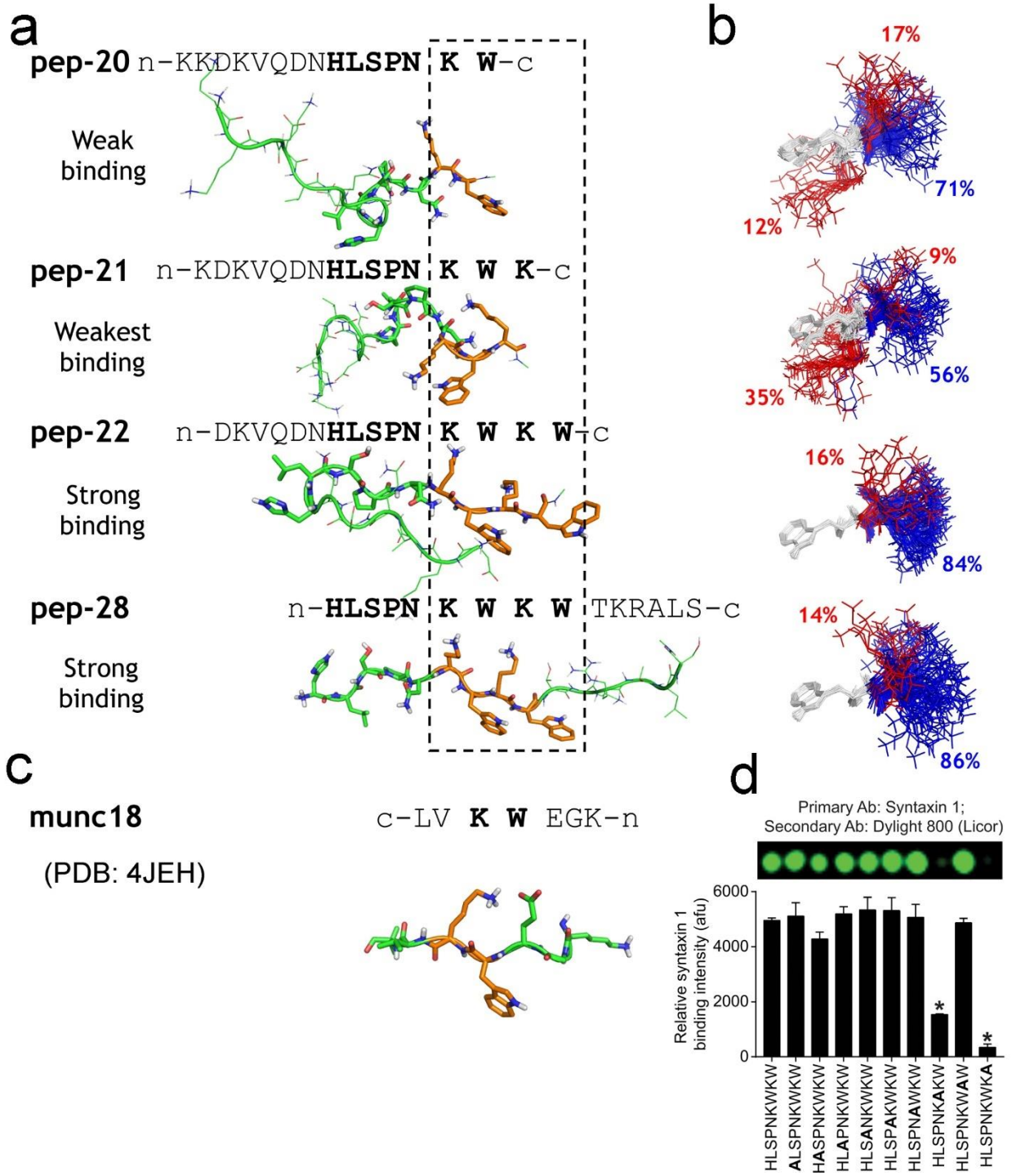

Figure 9. Structural analysis and validation of Kv2.1 syntaxin-binding peptides.

A, Representative molecular dynamics snapshots of four Kv2.1-derived peptides labeled with their relative binding strength (Yeh *et al.*, 2017). From first row down, Kv2.1 peptides sequences

containing up to: W7 (pep-20), K8 (pep-21), and the entire C1aB region (pep-22, pep-28). **B,** Assembly of 100 snapshots of K6W7 from the corresponding peptides sampled every 4 ns after 100 ns of equilibration. Snapshots were aligned on W7 (grey) with K6 sampling both possibly interfering cis (red) and non-interfering trans (blue) conformations. The W7s of the strong binding peptides (pep-22 and pep-28) were solvent exposed and ready to make contacts with interacting surfaces. This is disrupted in peptides (pep-20 and pep-21) with direct contacts between K6 and W7 side chains. **C,** A similar structural motif as C1aB is observed in munc18 W28K29 when bound to syntaxin (PDB 4JEH). **D,** Peptide array binding assay of the C1aB sequences with sequential alanine substitutions, one residue at a time. Tryptophan to alanine-substituted peptides had significantly less syntaxin binding than the parent peptide (*$p<0.05$; ANOVA/Dunnett). Results indicate mean ± SEM of fluorescent signal intensity in 4 independent assays.

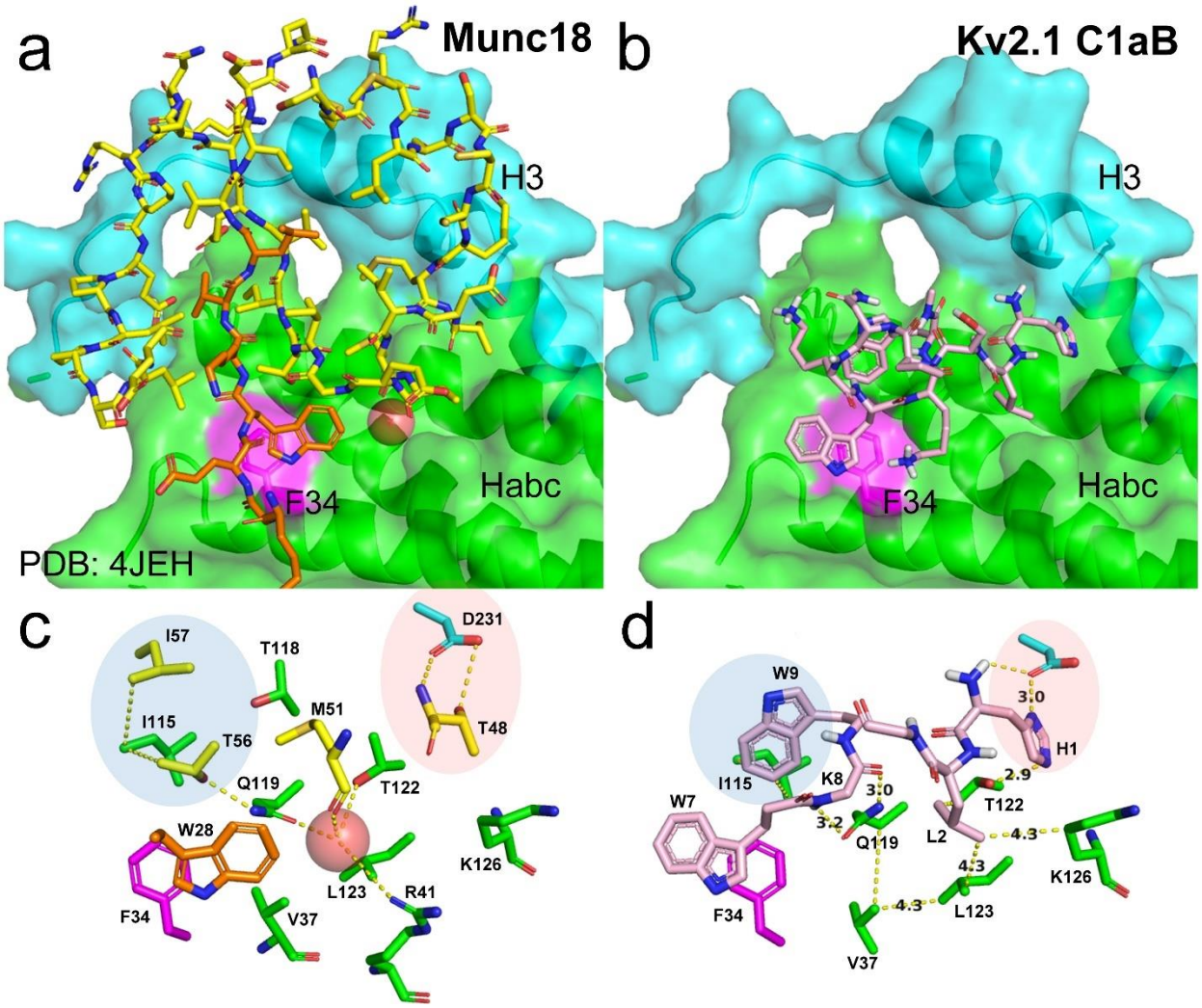

Figure 10. Docked C1aB peptide recapitulates interactions of munc18/syntaxin co-crystal.

Closed form of syntaxin from munc18 co-crystal (PDB 4JEH) is shown in green and cyan (surface/sticks) corresponding to the Habc and the H3 domains, respectively. Syntaxin F34 is shown in magenta to emphasize specific aromatic stacking interaction in all panels. **A,** Partial view of munc18/syntaxin co-crystal. Orange sticks show same munc18 peptide as in Fig. 9C, other munc18 residues making favorable interactions are shown in yellow sticks. Red sphere highlights fully coordinated crystal water. **B,** Unbiased docking model of C1aB/syntaxin. **C,** Highlighted intermolecular interactions of munc18/syntaxin that are recapitulated in **D,** detailed view of interactions between docked pose of C1aB and syntaxin. Specifically, munc18 W28 aromatic

stacking is mimicked by C1aB W7; hydrophobic interactions between munc18 I57 and T56 and syntaxin I115 are mirrored by C1aB W9 (blue shade); hydrogen bond between munc18 T48 and syntaxin D231 is reproduced by H1 in C1aB (red shade). Syntaxin is identical in all the structures with the exception of Q119 and T122 sidechains in C1aB/syntaxin, which, in the absence of the crystal water, rotate slightly to satisfy its hydrogen bonds and methyl group interactions.

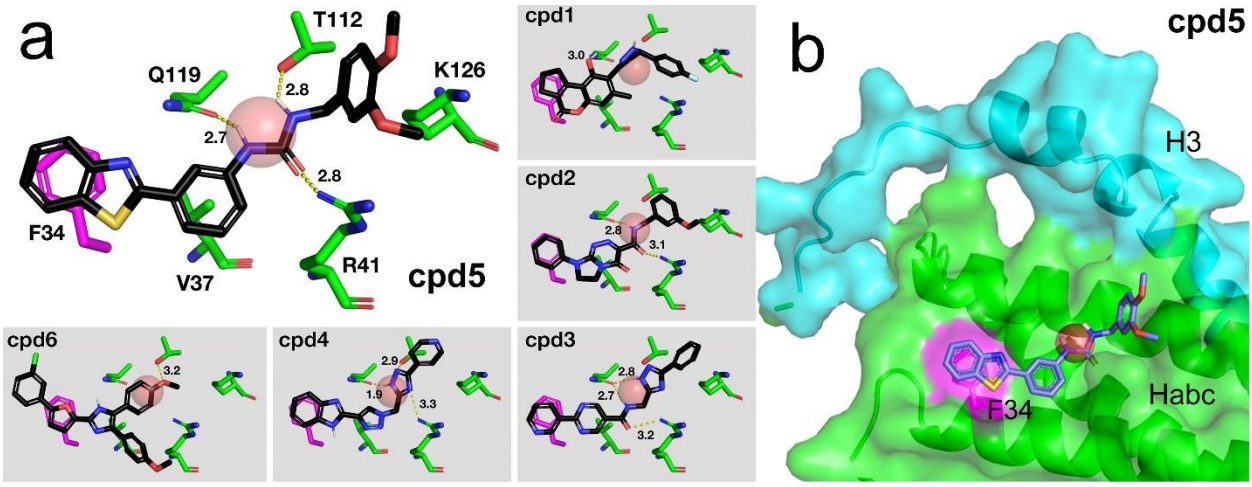

Figure 11. Virtual screening discovered six compounds (cpd1-6) that potentially recapitulates munc18/C1aB interactions with syntaxin.

A, Interactions between cpd1-6 and syntaxin. For cpd5 specifically, benzothiazole ring forms stacking interaction with F34, with urea moeity fully recapitulating hydrogen bonds formed by crystal water in munc18 (red sphere). Water molecule is shown as a guide to highlight the overlap with the urea moeity of cpd5. **B,** Docking model of cpd5/syntaxin.

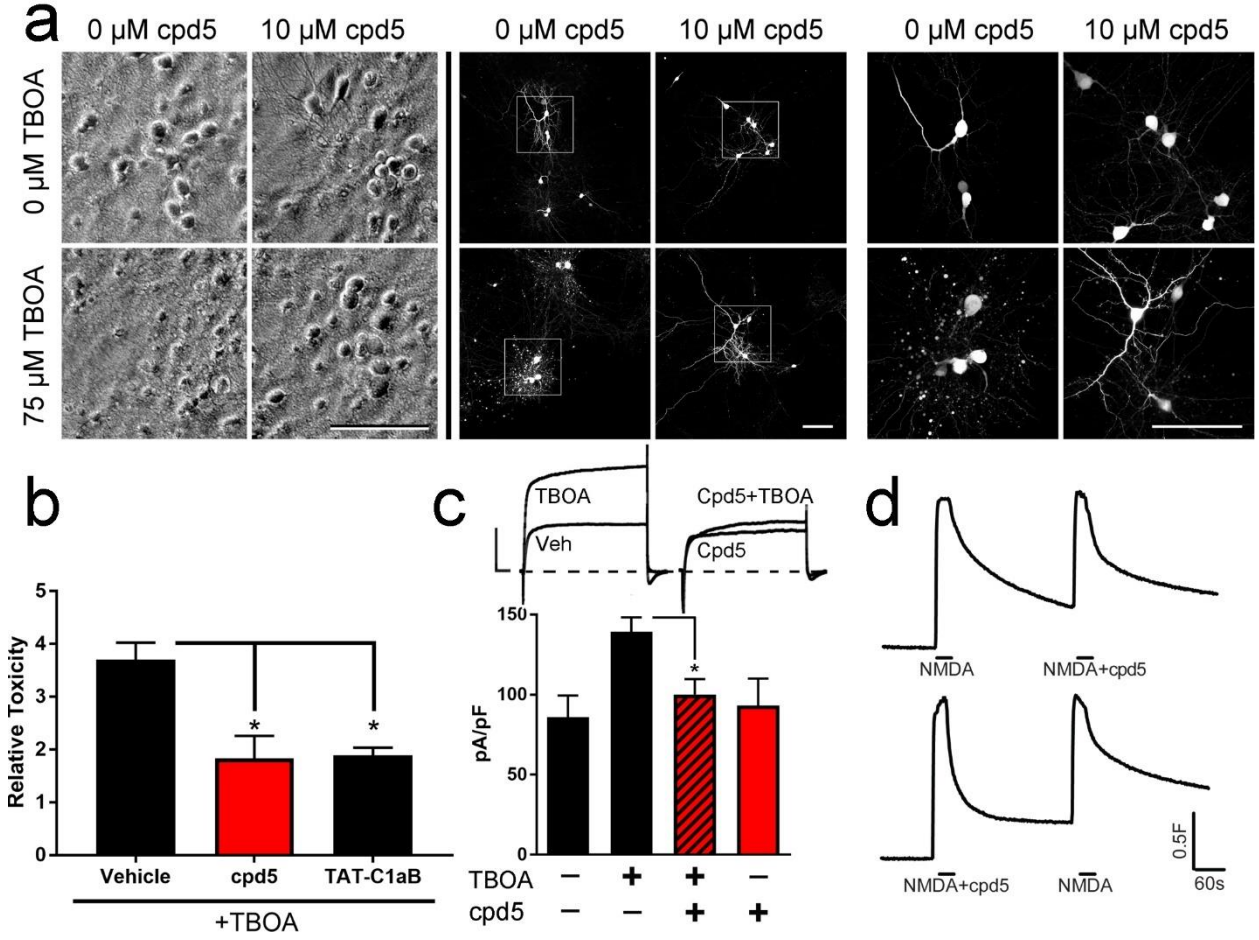

Figure 12. Cpd5 suppresses death-inducing Kv2.1 current and is a neuroprotective agent.

A, Representative figures of the neuronal culture treated with TBOA, with and without cpd5 pre- and co-incubation. Phase-bright cells represent neurons. In subsequent panels, neurons transfected with eGFP plasmid after identical treatment as described. Scale bar denotes 100 μm in all panels. **B,** Incubation of cortical culture neurons with 10 μM cpd5 was found to be highly neuroprotective against 75 μM TBOA-induced excitoxicity. This protective effect was comparable with its peptide counterpart, TAT-C1aB (1 μM). (Vehicle vs cpd5 vs TAT-C1aB relative toxicity mean ± SEM: 3.70 ± 0.33 vs 1.84 ± 0.42 vs 1.89 ± 0.15; *p<0.05; Kruskal-Wallis non-parametric ANOVA; n = 3-8). Relative toxicity is defined as $LDH_{TBOA+cpd5}/LDH_{cpd5}$ **C,** Representative current traces (top) and plots of the evoked delayed rectifier currents at +30 mV. The 50 μM TBOA-evoked increase

in delayed rectifier current was significantly suppressed by the presence of 10 μM cpd5 (DMSO vs TBOA vs cpd5+TBOA: 85.92 ± 13.53 vs 139.28 ± 9.05 vs 100.12 ± 9.61 pA/pF; One-way ANOVA/Dunnett, *p<0.05). Scale bar indicates 1000 pA and 20 ms; n = 10-12. **D,** Cpd5 (10 μM) did not inhibit NMDA-induced Ca^{2+} responses in cultured cortical neurons (% Control ± SEM, F-peak treated 101.26 ± 1.47, AUC treated 104.67 ± 1.98, *p>0.05; t-test). Responses shown are the average of 40 Fura-2 loaded cells in 2 separate coverslips. Four coverslips were utilized for our analysis, representing about 160 cells.

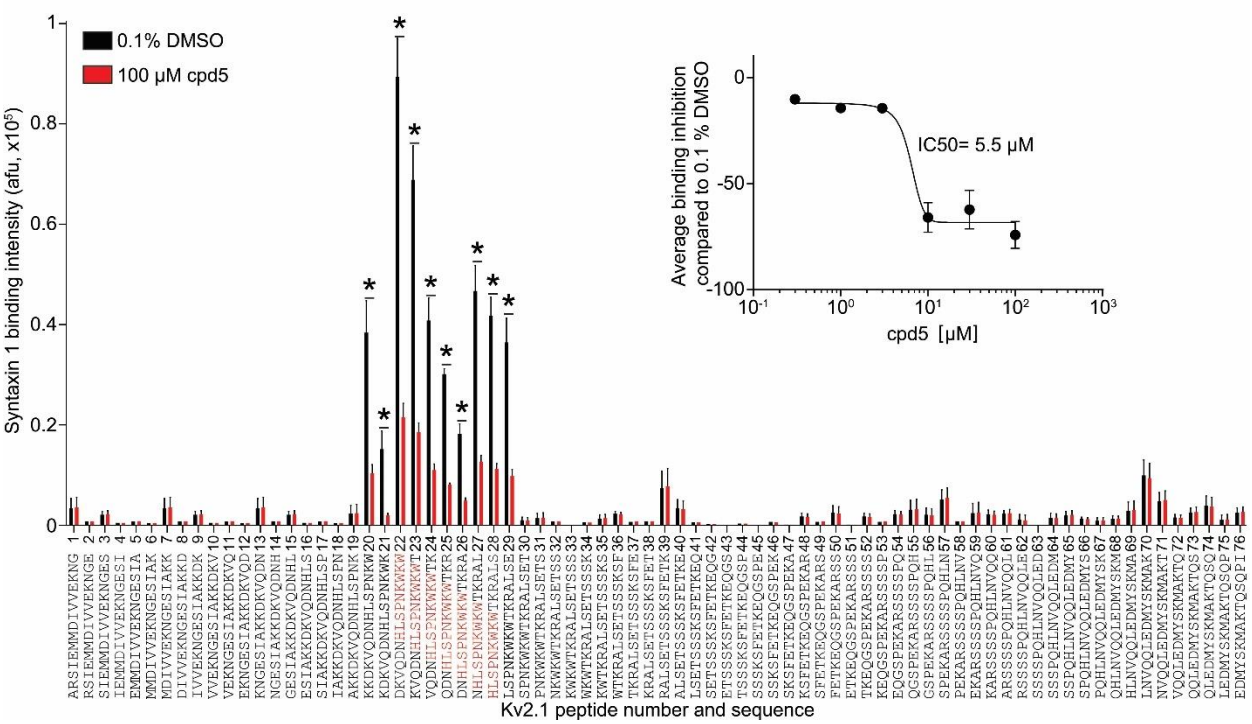

Figure 13. Cpd5 competitively binds syntaxin against C1aB-containing Kv2.1 peptides.

Peptide array binding assay of the proximal Kv2.1 C-terminus (C1a) region using 15 a. a. segments spanning residues Kv2.1 451–540, in overlapping 1 a. a. steps. Bar graph shows the summary (n = 4) of syntaxin binding intensity in the presence of 100 µM cpd5 or 0.1 % DMSO as vehicle control. The C1a binding sequence is highlighted in red. *p<0.05, non-parametric Mann-Whitney for each peptide. **Inset,** Average concentration-dependent effect of cpd5 on syntaxin binding to the peptides 22-28 (containing the full C1aB domain; n=4 for each peptide) of the peptide array. Percent inhibition of syntaxin binding compared to 0.1 % DMSO is plotted for various concentrations of cpd5. The fitted sigmoid curve to the pooled, averaged data is shown in red. The data were fitted in GraphPad Prism with a log (inhibitor) vs normalized pooled response with a variable slope curve, yielding an IC_{50} of 5.5 µM. Data are expressed as mean ± SEM of the indicated values.

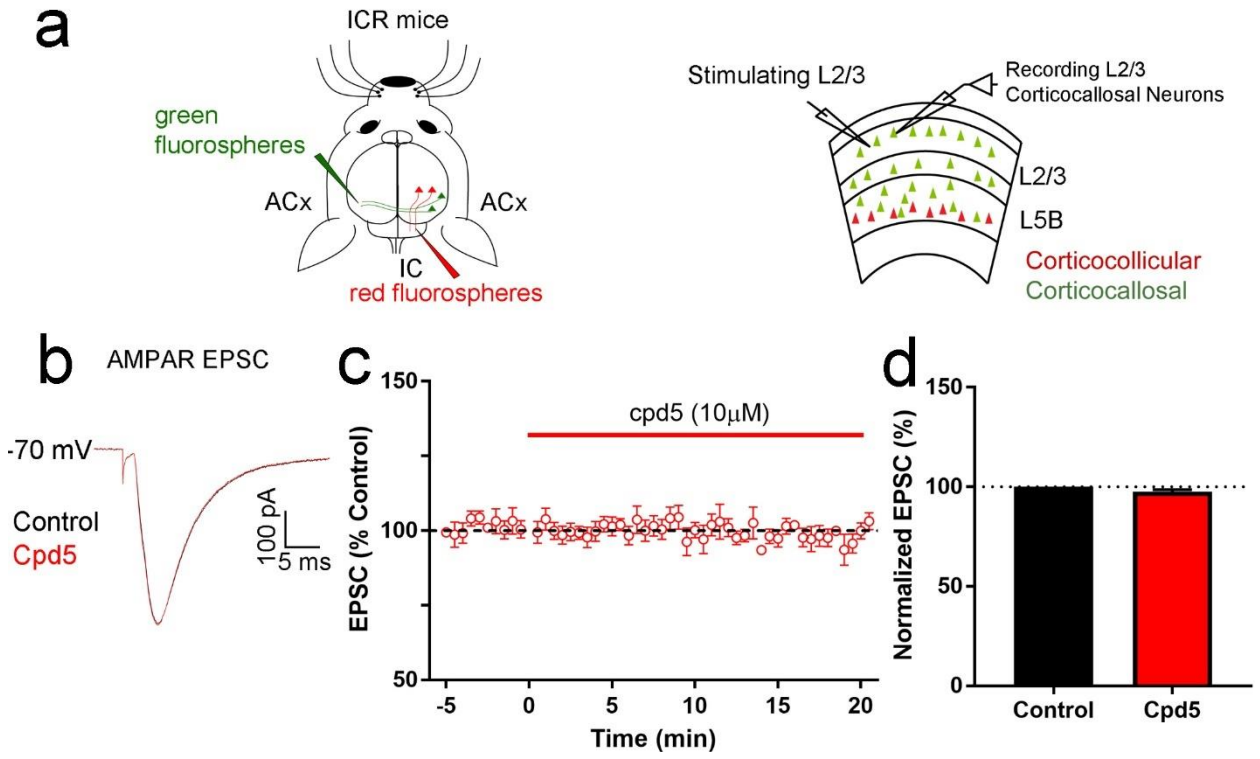

Figure 14. Cpd5 (10 μM) does not affect evoked AMPAR EPSCs in layer 2/3 corticocallosal neurons in the mouse auditory cortex.

A, Left: Schematic of stereotaxic injections for labeling of corticocollicular and corticocallosal neurons with different flourospheres to identify select neurons in the auditory cortex for acute slice electrophysiology. Right: Schematic illustrating slice electrophysiology experiment involving electrical stimulation of auditory cortex layer 2/3 while recording from adjacent labeled corticocallosal neurons. **B,** Representative traces of a layer 2/3 corticocallosal neuron AMPAR EPSCs evoked by electrical stimulation of adjacent layer 2/3 sites while incubated in control (black) and in 10 μM cpd5 (red). **C,** Time course of the average amplitude of AMPAR EPSCs before and after cpd5 treatment. **D,** Average effect of cpd5 (red) on layer 2/3 corticocallosal neuron AMPAR EPSCs amplitudes, normalized to control (control vs. cpd5: 97.6 ± 0.9%, p = 0.153, paired t-test, n = 4 cells from 4 mice).

a

Common Name	Abbreviation	Molport	IUPAC
STK71814	cpd1	004-858-802	8-[5-(4-fluorophenyl)-4,5-dihydro-1H-pyrazol-3-yl]-9-hydroxy-7-methyl-1H,2H,3H,4H-cyclopenta[c]chromen-4-one
F24820058	cpd2	003-124-884	N-[(3-methoxyphenyl)methyl]-4-oxo-8-phenyl-4H,6H,7H,8H-imidazo[2,1-c][1,2,4]triazine-3-carboxamide
52850683	cpd3	028-585-673	N-[(3-phenyl-1H-1,2,4-triazol-5-yl)methyl]-2-(pyridin-3-yl)pyrimidine-5-carboxamide
21447796	cpd4	023-316-923	2-(1-{[3-(pyridin-4-yl)-1H-1,2,4-triazol-5-yl]methyl}-1H-1,2,3-triazol-4-yl)-1H-1,3-benzodiazole
F5772-8410	cpd5	009-741-732	3-[3-(1,3-benzothiazol-2-yl)phenyl]-1-[(3,4-dimethoxyphenyl)methyl]urea
neurodazine	cpd6	009-019-497	2-[5-(3-chlorophenyl)furan-2-yl]-4,5-bis(4-methoxyphenyl)-1H-imidazole

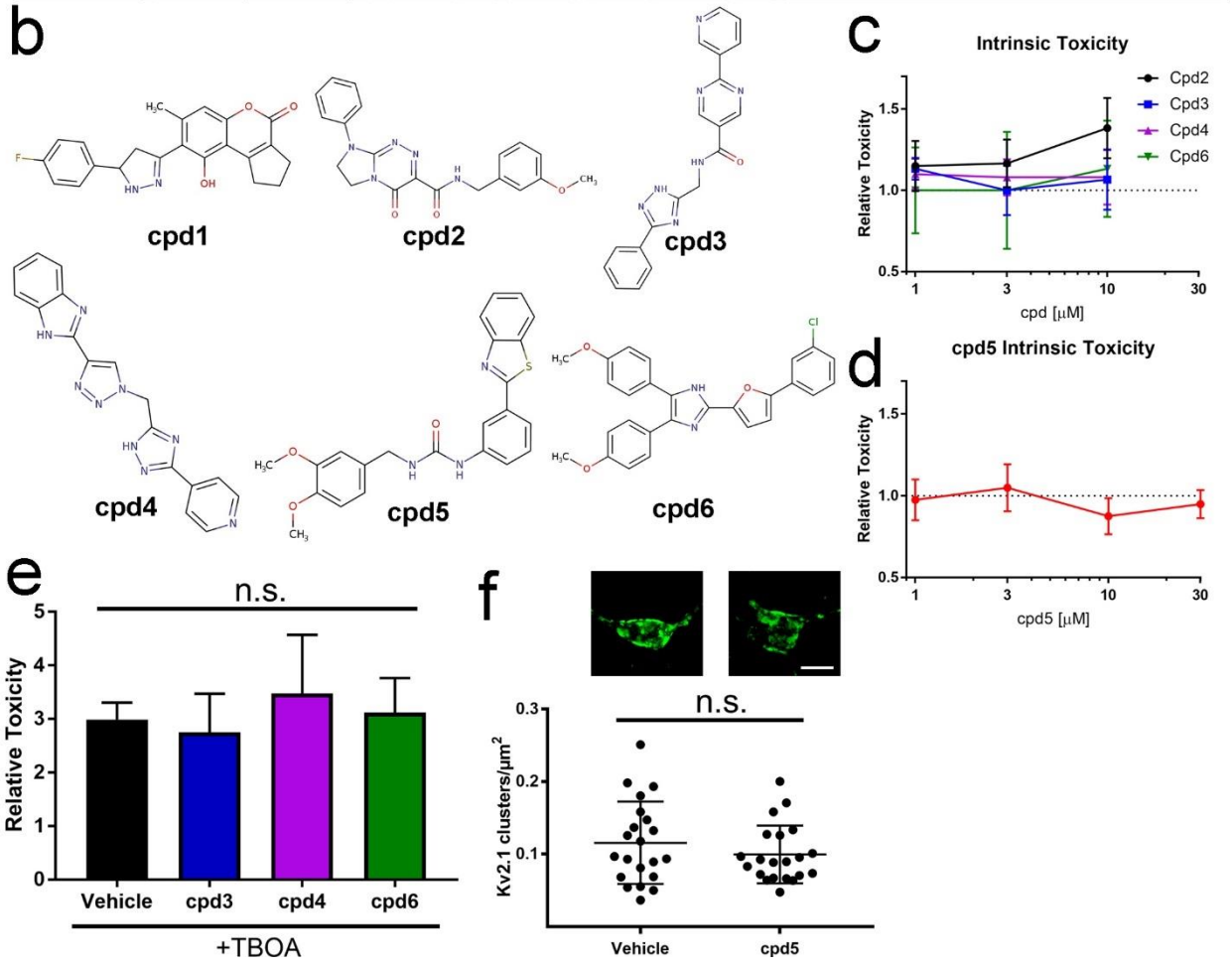

Figure 15. Small molecules discovered in virtual screening.

A, Full name and abbreviations of the six compounds selected for study after ZINCPharmer virtual screening and all-atom optimization based on the discussed pharmacophores. **B,** Chemical structure of the compounds selected for testing. Images adapted from Molport. **C,** LDH toxicity assay screening of four small molecules evaluated for innate toxicity to primary rat cortical neuron cultures. Relative toxicity is defined as $LDH_{Treatment}/LDH_{Veh}$ **D,** LDH toxicity assay screening of the lead compound cpd5 in primary cortical neuron cultures found no innate toxicity of up to 30

μM for 24 hr. **E,** Incubation of cortical culture neurons with 10 μM cpd3, cpd4, or cpd6 provided no neuroprotection against 75 μM TBOA-induced excitoxicity (Vehicle vs cpd3 vs cpd4 vs cpd6 relative toxicity mean ± SEM: 2.99 ± 0.32 vs 2.75 ± 0.72 vs 3.48 ± 1.1 vs 3.12 ± 0.65; Kruskal-Wallis non-parametric ANOVA; n=3-9). Relative toxicity here is defined as $LDH_{TBOA+cpd}/LDH_{cpd}$. **F,** Cpd5 does not decluster Kv2.1. Cortical culture neurons were transfected with Kv2.1-eGFP and incubated in 10 μM cpd5 for 24 hr. No declustering effects were observed. Mean clusters per μm^2 ± SEM: Veh 0.12 ± 0.01, Cpd5 0.10 ± 0.01; n=21 cells. Unpaired t-test. Scale indicates 10 μm.

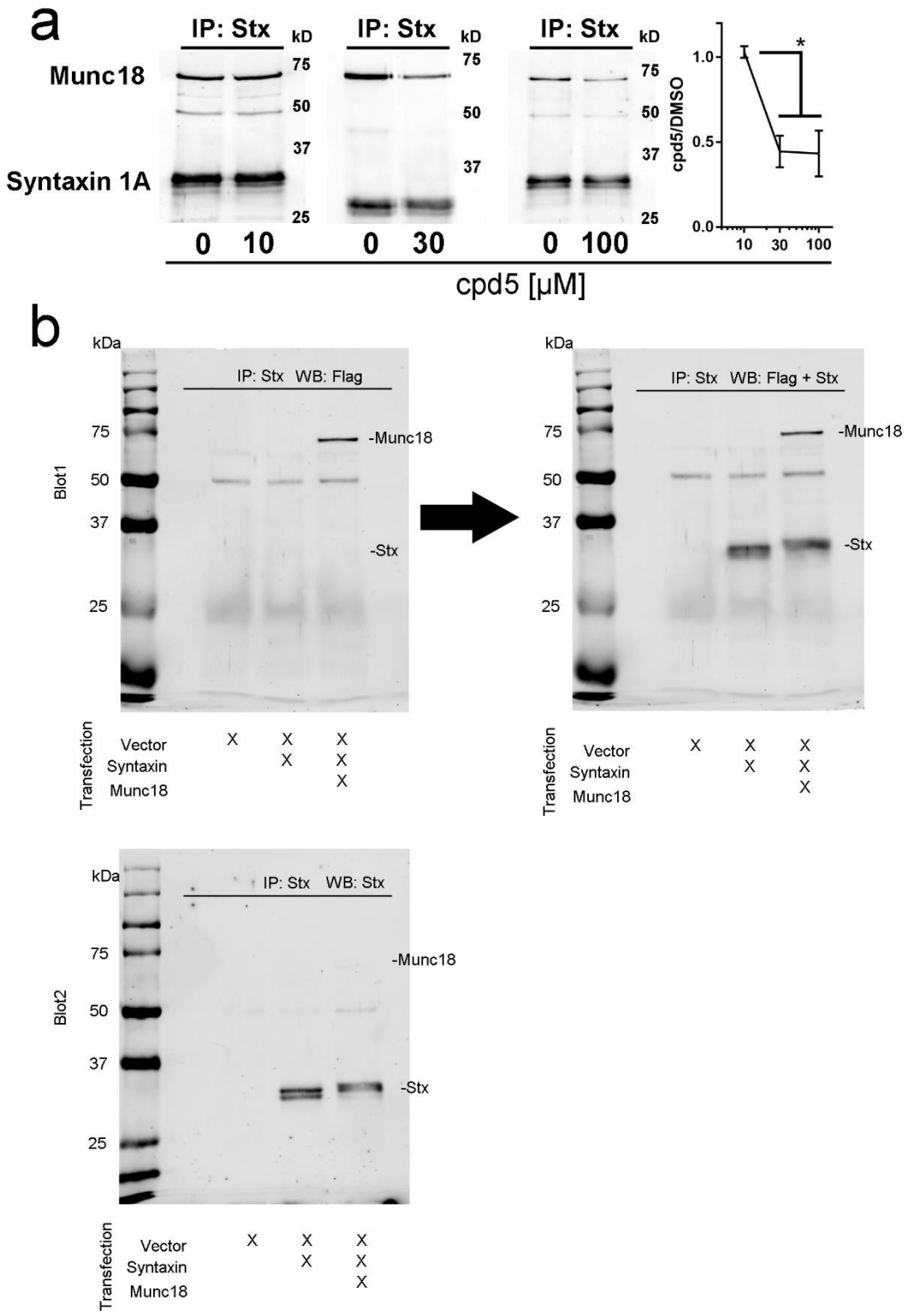

Figure 16. Cpd5 disrupts munc18/syntaxin binding at high concentrations.

A, A graphical summary of co-immunoprecipitation experiments using HEK293 cells transfected with munc18 and syntaxin in the presence of 10, 30, or 100 μM cpd5. Cells incubated in either 30 or 100 μM cpd5 showed a significant displacement of munc18 from syntaxin. Cpd5 at the concentration that we have observed neuroprotection (10 μM) did not displace munc18 from syntaxin. One representative blot from each concentration is presented above. (From 10 to 100 μM: 1.032 ± 0.034, 0.4459 ± 0.09367, 0.4339 ± 0.135, cpd5/DMSO mean ± SEM; *$p<0.05$, Tukey's multiple comparisons, n=3 each). **B,** Evaluation of antibodies used in the co-IP experiments. We evaluated antibody specificity varying the transfection composition and probed with individual antibodies. **Top**: We confirmed the 68 kDa band to be munc18 and the 33 kDa band to be syntaxin 1A by observing that they do not appear in samples without prior transfection with appropriate plasmids in HEK cells. The munc18 antibody does not detect the syntaxin band. In the first blot, munc18 was probed first, followed by syntaxin. **Bottom**: In a separate run of the same sample, we confirmed the specificity of the syntaxin antibody by probing with the syntaxin antibody only, observing relatively lack of signal at the MW for munc18. The co-transfection of munc18 with syntaxin appears to induce a formation of a higher molecular weight syntaxin species. Bands at 50 and 25 kDa are the heavy and light chain of the pulldown antibody, respectively.

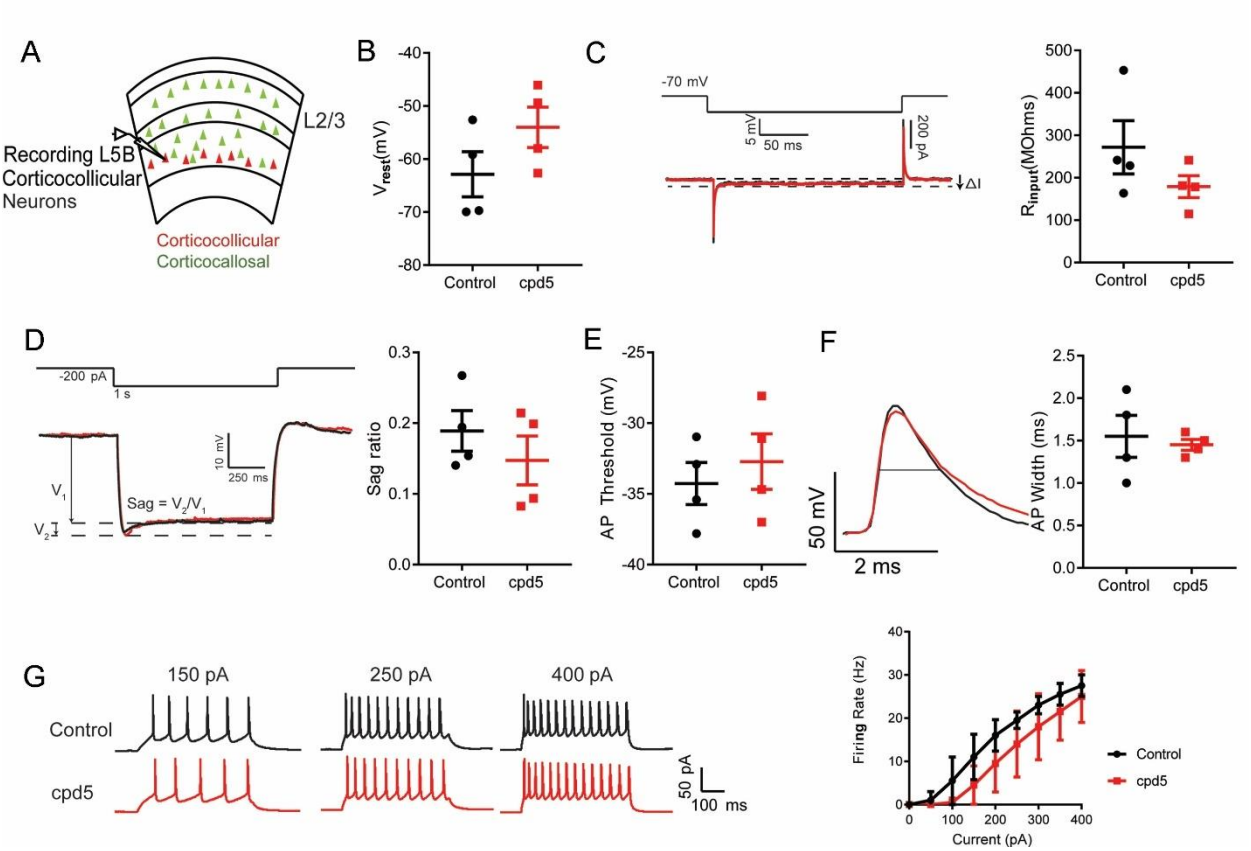

Figure 17. Cpd5 does not affect intrinsic electrical properties of layer 5B corticocollicular neurons in the mouse auditory cortex.

A, Schematic illustrating slice electrophysiology experiment evaluating the intrinsic properties of L5B corticocollicular neurons after retrograde labeling as shown in Fig. 14A Left. **B-D,** An evaluation of subthreshold intrinsic properties found a lack of significant effect of cpd5 incubation on (B) resting membrane potential, (C) input resistance, or (D) sag ratio (V_2/V_1). **E-G,** An evaluation of evoked properties also found no significant effect of cpd5 incubation on (E) action potential threshold, (F) width, or (G) firing rate. Available representative traces are provided for each experiment. Each neuron is evaluated before and after 10 min incubation in 10 μM cpd5 (Paired t-test; for firing rates, 2-way ANOVA; n=4 cells from 4 mice).

3.4 Discussion

The interaction between the intrinsically disordered proximal C-terminus of the delayed rectifier Kv2.1 (C1a) and the SNARE protein syntaxin was first characterized nearly 15 years ago by Gaisano, Lotan, and co-workers (Leung *et al.*, 2003; Singer-Lahat *et al.*, 2007; Singer-Lahat *et al.*, 2008). Recent work in our laboratory narrowed down the involved Kv2.1 C1a region to 50 amino acids (McCord *et al.*, 2014), and then to the 9 amino acids sequence termed C1aB (Yeh *et al.*, 2017). Preventing the interaction between Kv2.1 and syntaxin by either overexpressing C1a or using the cell-permeant TAT-C1aB peptide are effective neuroprotective strategies in both *in vitro* and *in vivo* models of acute neuronal injury (McCord *et al.*, 2014; Yeh *et al.*, 2017). Here, we report the discovery of a first-in-class neuroprotective small molecule inhibitor (cpd5) of the protein-protein interaction between syntaxin and Kv2.1. Using molecular dynamics simulations of intrinsically disordered peptides containing the Kv2.1 syntaxin-binding sequence C1aB (HLSPNKW$_7$KW) and docking, we predicted the aromatic residue W7 to be a critical binding motif to syntaxin (Fig. 9). This prediction was validated by alanine scanning of individual C1aB residues and competitive binding assays of C1a-derived peptides that demonstrated inhibition of only those peptides containing W7 (Fig. 9D, 13). Furthermore, we predicted C1aB to bind on the rim of the munc18's interactions with syntaxin (Fig. 10A, 10B), suggesting that munc18 should form a much tighter complex with the closed conformation of syntaxin than C1a.

Most importantly, we demonstrate the Kv2.1/syntaxin binding as a highly promising target for eliciting neuroprotection that does not appear to have any detrimental effects in the neuronal cell types examined. Notably, cpd5 at 10 μM is neuroprotective, effectively displacing Kv2.1 C1aB peptides from syntaxin without affecting the binding between munc18 and syntaxin, which we show to only occur at much higher concentrations (Fig. 16A). Indeed, the mechanism of action

predicted for cpd5 shows that besides the aromatic interaction with syntaxin F34, cpd5 competes for direct intermolecular hydrogen bonds and non-polar contacts formed by C1aB with syntaxin, whereas only the water-mediated interactions are significantly disrupted in the munc18-syntaxin binding (Fig. 10C, 10D, 11A). Further, the loss of the entire syntaxin N-terminal Habc globular domain, which includes the F34 residue, does not impede vesicle fusion induced by munc18 (Shen *et al.*, 2010), indicating that exogenous competition at the F34 binding site is not immediately deleterious to SNARE functions.

We have never observed the suppression of basal Kv2.1 current when targeting syntaxin. Cpd5 neither suppressed Kv2.1 current below its control levels nor increased cortical neuron excitability, which is consistent with our previous observations with C1a and TAT-C1aB (McCord *et al.*, 2014; Yeh *et al.*, 2017). This suggests distinct trafficking mechanisms between basal and death-promoting Kv2.1 channel populations. The death-promoting Kv2.1 population has been shown to be inserted *de novo* after lethal insults (Pal *et al.*, 2006), and requires the existence of non-conducting Kv2.1 surface clusters that act as general protein trafficking hubs when in contact with the endoplasmic reticulum (Fox *et al.*, 2015; Justice *et al.*, 2017). On the other hand, the basal Kv2.1 population does not appear to require the interaction with syntaxin, as botulinum neurotoxin-mediated loss of syntaxin and SNAP-25 function only suppresses the expression of the pro-death Kv2.1 currents (Pal *et al.*, 2006). These findings strongly support the idea that basal Kv2.1 maintenance is largely syntaxin-independent and is unaffected by our neuroprotective strategy of targeting a putatively dedicated cell death pathway. The fact that Kv2.1 can be selectively transported for distinct functions was recently reinforced by a study showing that phosphoregulation of a Kv2.1 target sequence motif (a. a. 720-745) can lead to Golgi-independent trafficking of the channel to the axon initial segment (Jensen *et al.*, 2017). In the same vein, we

propose that injury-dependent phosphorylation of Kv2.1 Y124 and S800 (Redman *et al.*, 2009) drives pro-death trafficking of Kv2.1 to the membrane via the syntaxin-dependent process described here.

Kv2.1 serves several non-conducting functions through its large cytosolic domains. Most prominently, Kv2.1 directly interacts with members of the SNARE complex, SNAP-25 and VAMP2 (MacDonald et al., 2002; Lvov et al., 2008), in addition to syntaxin, to facilitate exocytosis and vesicle fusion in several cell types. In neuroendocrine cells, the Kv2.1-syntaxin interaction has been shown to facilitate exocytosis of dense core vesicles independent of Kv2.1's ion channel functions (Singer-Lahat et al., 2008). In pancreatic β cells, the Kv2.1-syntaxin interaction modulates the release of insulin. Namely, clustered Kv2.1 domains in secretory β cells are known to facilitate insulin granule release through the selective binding of Kv2.1 C1a (a.a. 411-522) and C1b (a.a. 523-621) to syntaxin 1A and syntaxin 3, respectively, eliciting the secretion of distinct granules populations (Zhu et al., 2013; Greitzer-Antes et al., 2018). Interestingly, syntaxin 3 has a significantly reduced affinity to C1a. The aligned amino acids sequence of syntaxin 1A and syntaxin 3 revealed a number of distinctions in the immediate residues near the central phenylalanine identified in this study (aligning syntaxin 1A's F34 to syntaxin 3's F36; UniProt alignment: Q16623 STX1A_HUMAN, Q13277 STX3_HUMAN). Specifically, in syntaxin 1A, the amino acids glutamic acid-glutamine-valine (EQV) follows the phenylalanine, while in syntaxin 3, it is serine-glutamic acid-isoleucine (SEI). More studies will be necessary to evaluate how these amino acids sequence distinctions lead to differences in binding preference. Recently, Kv2.1 has been found to associate with the endoplasmic reticulum proteins VAPA and VAPB to form distinct channel clusters at contact points between the plasma membrane and the endoplasmic reticulum (Johnson et al., 2018; Kirmiz et al., 2018). These clusters have been shown

to be necessary for the trafficking of the death-promoting population of Kv2.1 (Justice et al., 2017), suggesting that the interaction between Kv2.1 and the VAP proteins may be involved in cell death processes.

With the discovery of cpd5 as a first-in-class neuroprotective agent, we demonstrate a translational workflow that utilizes structural modeling to guide the resolution of protein-protein interactions involving poorly characterized disordered domains, leading to both mechanistic insights and the identification of an effective new drug. To this end, the approach of temporarily disrupting a protein-protein interaction for neuroprotection is a recently proven successful translational venture, as seen with the TAT-NR2B9c peptide, a currently phase III treatment for acute ischemic stroke that ameliorates excitotoxicity by displacing NMDA receptor function from nitric oxide production (Ballarin & Tymianski, 2018). While we have shown that disrupting the Kv2.1/syntaxin interaction is also efficacious in a mouse model of acute ischemic stroke (Yeh *et al.*, 2017), there is an increasing indication of Kv2.1 involvement in even broader contexts of neurodegenerative conditions, including chronic and progressive neurologic disorders (McCord & Aizenman, 2014; Shah & Aizenman, 2014; Chao *et al.*, 2018; Yu *et al.*, 2018). This reflects the fact that oxidative stress is a major component of most neurodegenerative conditions (Liu *et al.*, 2017) and is known to drive the Kv2.1-mediated cell death pathway (Aizenman *et al.*, 2000). As such, cpd5 is not only a first in class neuroprotective molecule, it represents an important step in realizing the therapeutic potentials of targeting Kv2.1 in neurodegenerative disorders.

3.5 Materials & Methods

Statement of access. Experimental data, models, and analysis presented here are available upon request to the corresponding authors.

Molecular dynamics modeling. All initial structures of the 9-mer Kv2.1-derived peptides were built using PyMOL 1.7 (Schrodinger, 2010). The C-terminus of the peptides were N-methylated. The molecular dynamics (MD) simulations were run with pmemd.cuda (Götz *et al.*, 2012) from AMBER14 (Case *et al.*, 2014) using AMBER ff12SB force field. We used the tLEaP module from AMBER14 to center each individual peptide on an octahedral TIP3P water box(Jorgensen *et al.*, 1983) with a 15 Å distance from the protein surface to the box edges and closeness parameter of 0.75 Å. The system was neutralized by adding the appropriate number of Cl^- ions. In the first energy minimization step, the solute was fixed and we performed two rounds of solvent relaxation through 2,500 cycles of steepest descent followed by 2,500 cycles of conjugate gradient minimization. After minimization, we performed a 50 ps constant volume simulation to raise the temperature of the system to 300 K. Temperature scaling was achieved using the Langevin thermostat (Loncharich *et al.*, 1992) with a collision frequency of 1.0 ps^{-1}. We then ran a 50 ps constant pressure simulation at 300 K using the same temperature scaling scheme. Pressure was maintained at 1 bar (0.987 atm) using periodic boundary conditions with isotropic position scaling and the Berendsen thermostat (Berendsen *et al.*, 1984) with a pressure relaxation time of 2.0 ps. Both the temperature and pressure equilibration MDs used an integration timestep of 2 fs, and coordinates were written to file every 250 steps. Solute heavy atoms were fixed using a harmonic restraint weight of 500.0 kcal/mol·A^2, and bonds involving hydrogens were constrained at constant length using the SHAKE algorithm (Ryckaert *et al.*, 1977). The non-bonded interaction cutoff was 8 Å. Initial velocities were generated randomly from a Maxwell distribution at 300 K.

All production runs were with only the backbone of this C-terminal residue constrained for 200 ns. All following up calculations used the trajectories after 50 ns.

Virtual Screening using ZINCPharmer. The structure of the syntaxin is obtained from PDB 4JEH. Several pharmacophores models were built based on the munc18/syntaxin interactions using ZINCPharmer (Koes & Camacho, 2012). An aromatic sphere was placed close to F34 as pi-pi stacking of the aromatic rings. A hydrogen acceptor sphere was placed to match Q119. A hydrogen donor sphere was placed to match Q119 and D231. A hydrophobic sphere was placed in the F34-V37-L123 hydrophobic pocket. One aromatic and one hydrophobic sphere were placed between the R41 and K126 to match the pi-pi stacking and backbone interactions respectively. The number of primary hints of compounds was 39,892. These structures were then submitted to SMINA (Koes *et al.*, 2013) for structural minimization, and the conformations with RMSD larger than 1.5 Å were removed. A final list of six compounds were then utilized for further experimental testing. Compounds were purchased from Molport.

Cortical cultures, LDH assay, and calcium measurements. All animal protocols described here and below were approved by the Institutional Animal Care and Use Committee of the University of Pittsburgh School of Medicine. Cortical neurons were prepared from embryonic day 16-17 rats of either sex as described previously (McCord *et al.*, 2014). Pregnant donor rats (Charles River Laboratories) were killed by gradual CO_2 inhalation, an American Veterinary Medical Association approved protocol (Leary et al., 2013). Cortices were dissociated with trypsin, and plated at 670,000 cells per well on poly-L-ornithine glass coverslips in six-well plates as described previously (Hartnett *et al.*, 1997). Non-neuronal cell proliferation was inhibited with 1–2 µM cytosine arabinoside at 15 days in vitro (DIV). All cortical culture experiments shown here were performed on 18-25 DIV cultures.

DL-threo-β-benzyloxaspartate (TBOA; Tocris Bioscience) excitotoxicity assays were performed on cortical culture coverslips transferred into 24-well plates containing 10 mM HEPES, 0.01 % bovine serum albumin (BSA)-supplemented MEM without phenol red (MHB). On each individual plate, coverslips were treated with vehicle control or 75 µM TBOA in wells that had been preincubated for 1 hr with either 10 µM of the indicated treatment or vehicle at 37°C,5% CO_2 for 24 hr. Following this exposure, external medium was collected for LDH colorimetric measurements using a toxicity kit (Sigma-Aldrich), as previously described (Aras *et al.*, 2008). Each experiment contained three replicates of four conditions (with/without TBOA, with/without treatment). Relative toxicity was quantified as the LDH ratio of TBOA-treated over vehicle control values within each experiment. For visualization of the cell cultures, coverslips were imaged at 20x using a QCapture camera system.

Intracellular Ca^{2+} measurements were performed essentially as previously described (Aizenman *et al.*, 1990) on the same cortical culture preparations as above, but with 20 DIV cells plated on MatTek glass-bottom 35 mm culture dishes. At this developmental stage, neurons robustly express both GluN2A and GluN2B subunits of the NMDA receptor (Sinor *et al.*, 2000). Neurons were incubated with the fluorescent Ca^{2+} indicator Fura-2 AM ester (5 µM; Invitrogen) with 0.02% Pluronic F-127 (Invitrogen) for 1 h at 37°C. Culture dishes were then mounted on an inverted microscope stage (Olympus) and continuously perfused with a 10 mM HEPES-buffered normal salt solution. Perfusion rate (5 ml/min) was controlled with a gravity flow and a rapid-switching local perfusion system (Warner Instruments). Firmly attached refractile cells were identified as regions of interest (ROIs; 4 coverslips, ~40 cells/coverslip). A ratio of fluorescence emission (*F*) at 510 nm in response to excitations at 340 and 380nm was acquired at 1Hz (Lambda DG-4 and 10-B SmartShutter, Sutter Instruments) via camera (ORCA-ER, Hamamatsu) and saved

to a computer using HCImage (Hamamatsu). Baseline Ca^{2+} signals were recorded for 2 min before the first application of NMDA (30 μM plus 10 μM glycine) with or without 10 μM cpd5 (Cat# MolPort-009-741-732, Molport). The second exposure to NMDA is given 4 minutes later. Peak increases in intracellular calcium concentration were measured by calculating *F*/*F*o (*F*, peak fluorescence; *F*o, average signal across 2 min baseline period). The area under the response for the first 15 min of NMDA application was also calculated.

Confocal imaging. For live imaging, neurons were transfected using Lipofectamine-2000 with plasmids expressing eGFP. Twenty-four hours later neurons were treated with TBOA (75 μM) alone or in combination with 10 μM cpd5. Cells were visualized 24 hours later on a Nikon A1+ confocal microscope. An additional group of cells were transfected with eGFP-tagged Kv2.1 and 24 hours later exposed to vehicle or 10 μM cpd5 overnight. For imaging, five–ten optical sections (0.5 μm) were acquired to generate a maximum intensity projection image that was analyzed for channel cluster counts and surface area using Nikon Instruments Elements Advanced Research software as described previously (Justice *et al.*, 2017). This experiment was repeated 3 separate times and images were obtained from 21 independent fields per condition.

Peptide spot array and binding assay. Peptide array protein-binding affinity assays were performed as previously described (Brittain *et al.*, 2011b; Wilson *et al.*, 2011; Brittain *et al.*, 2012a; Wilson *et al.*, 2012; Moutal *et al.*, 2017; Yeh *et al.*, 2017; Francois-Moutal *et al.*, 2018). Peptide spot arrays (15 mers) spanning the proximal C-terminus residues 451–540 of rat Kv2.1 were constructed using the Spots-synthesis method. Standard 9-fluorenylmethoxy carbonyl (Fmoc) chemistry was used to synthesize the peptides and spot them onto nitrocellulose membranes prederivatized with a polyethylene glycerol spacer (Intavis). Fmoc protected and activated amino acids were spotted in quadruplicates on 20–30 arrays on 75 by 25 mm membranes using an Intavis

MultiPep robot. The nitrocellulose membrane containing the immobilized peptides were rehydrated in Tris-buffered 0.1% Tween 20 (TBST) for 10 min, and then blocked for 1 h at room temperature (RT) with gentle shaking in TBST containing 5% (w/v) nonfat dry milk and then incubated with enriched STX1A protein containing the indicated concentrations of cpd5 for 1 h at RT with gentle shaking. Next, the membrane was incubated in primary antibody for syntaxin 1A (Millipore, catalog #AB5820-50UL, RRID:AB_2216165) for 2h at RT with gentle shaking, followed by washing with TBST. Finally, the membrane was incubated in secondary antibody (goat anti-rabbit DyLight 800, catalog #355571, Thermo Fisher Scientific) for 45 min, washed for 3 times 5 min in TBST, and visualized by infrared fluorescence (Li-Cor). Similar procedures were followed for the alanine scan study with 9-mers.

Cortical culture electrophysiology. Whole-cell patch-clamp experiments were performed on rat cortical culture neurons prepared as described in the LDH toxicity experiments. The TBOA treatment was reduced in severity in this experiment to limit extensive cell injury that would prevent adequate patch clamp recordings. Prior to recording, coverslips were treated with 50 μM TBOA in MHB for 2 hr. The treatment was terminated with 3x MHB washes and by transferring the coverslip to a separate well containing MHB to rest for 2 hr prior to electrophysiology recordings and to allow for the expression of enhanced currents. For cpd5-treated groups, cells were pre-incubated for 1 hr in 10 μM cpd5 prior to the addition of TBOA. Cpd5 was also present during the TBOA and the post-TBOA incubation phases.

Recordings were carried out using 1.5 mm diameter borosilicate glass electrodes (Sutter Instruments) made from a horizontal pipette puller at approximately 6 MΩ. The internal solution contained (in mM): 100 K-gluconate, 10 KCl, 1 $MgCl_2$, 1 $CaCl_2$, 10 HEPES, 11 EGTA, 2.2 ATP, 0.33 GTP. The internal solution was further adjusted to pH 7.2 and to 280 mOsm with the addition

of sucrose. The pH adjusted (7.2) external solution was composed of the following (in mM): 115 NaCl, 2.5 KCl, 2.0 $MgCl_2$, 10 HEPES, 10 D-glucose, and 0.25 µM TTX. Once whole-cell configuration has been achieved, delayed rectifier currents were evoked with 185 ms voltage steps from a holding potential of -80 mV to +80 mV in +10 mV increments. Recordings were filtered at 2 kHz and digitized at 10kHz (Digidata 1440A, Molecular Devices). Series resistance was compensated at 80% for all recordings. Analysis of current density was carried out at the +30 mV voltage step, taking the mean value of the steady-state current between 150 and 175 ms over the whole-cell capacitance (~10 pF). Space clamp is not generally an issue, as Kv2.1 is primarily expressed in the soma and very proximal neurites. Moreover, we quantified our results at +30 mV, where currents are normally not much larger than 2 nA after TBOA. Normality of the data was confirmed via Shapiro-Wilk test.

Stereotaxic injections for electrophysiology. Male or female ICR mice P21-30 (Jackson Laboratory) were anesthetized with 3% isoflurane (1.5% maintenance) and placed on the stereotaxic frame (Kopf). Core body temperature was maintained at ~37 °C with a heating pad and eyes were protected with ophthalmic ointment. Lidocaine (1 %) was injected under the scalp and an incision was made into the skin at the midline to expose the skull. To retrogradely label corticocallosal neurons and corticocollicular neurons in the auditory cortex, the contralateral auditory cortex (PLV -4, +4, +1 mm bregma) and the ipsilateral inferior colliculus (PLV -1, +1, -0.75 mm lambda) respectively were injected with retrograde tracer beads (Lumafluor) through a small craniotomy. A volume of ~0.12 µl fluorospheres was pressure injected (25 psi, 10 ms duration) from capillary pipettes (Drummond Scientific) with a Picospritzer (Parker–Hannifin). After injection, the pipette was held in the brain for 2 min before slowly withdrawing. The scalp of the mouse was closed with cyanoacrylate adhesive. Mice were injected with the non-steroidal

anti-inflammatory drug carprofen at 5 mg/kg (Henry Schein Animal Health) for 24 hours prior to and 48 hours after surgery. Mice were monitored for signs of postoperative stress and pain.

Slice electrophysiology. Slice electrophysiology experiments were performed in mice at least 2 days after fluorospheres injections. Following anesthesia with isoflurane, mice were immediately decapitated. Brains were rapidly removed and coronal slices (300 μm) containing the auditory cortex were prepared in a cutting solution at 1 ^{o}C using a Vibratome (VT1200 S; Leica). For evoked EPSC recordings, the cutting solution, pH 7.4, ~300 mOsm, contained the following (in mM): 2.5 KCl, 1.25 NaH_2PO_4, 25 $NaHCO_3$, 0.5 $CaCl_2$, 7 $MgCl_2$, 7 Glucose, 205 sucrose, 1.3 ascorbic acid, and 3 sodium pyruvate (bubbled with 95% O_2/5% CO_2). For evaluation of corticocollicular neuron electrical properties, the cutting solution, pH ~7.4, contained the following (in mM): 135 NMDG, 1 KCl, 1.2 KH_2PO_4, 1.5 $MgCl_2$, 1.5 $CaCl_2$, 20 $NaHCO_3$, 10 D-Glucose. The slices were then transferred and incubated at 34°C for 30 min (bubbled with 95% O_2/5% CO_2) prior to recording. The incubating and recording solution contained the following (in mM): 125 NaCl, 2.5 KCl, 1.25 NaH_2PO_4, 25 $NaHCO_3$, 2 $CaCl_2$, 1 $MgCl_2$, 10 D-Glucose, 1.3 ascorbic acid, and 3 sodium pyruvate (bubbled with 95% O_2/5% CO_2). Slices were stored at room temperature until the time of recording. The flow rate of the ACSF was ~1.5 ml/min, and its temperature was maintained at 34°C using an in-line heating system (Warner). Both slice electrophysiology experiments were carried out using MultiClamp-700B amplifier equipped with Digidata-1440A A/D converter and Clampex (Molecular Devices). Data were sampled at 10 kHz and Bessel filtered at 4 kHz. Pipette capacitance was compensated and series resistance for recordings was lower than 15 MΩ and measured throughout the experiments. Recordings were excluded from further analysis if the series resistance changed by more than 15% compared to the baseline period.

To evoke AMPAR EPSCs, auditory cortex layer 2/3 neurons were stimulated locally with an Isoflex stimulator (AMPI), through a glass theta electrode containing ACSF, by a single 0.15 ms duration electrical pulse every 30 sec. AMPAR EPSCs were recorded in voltage clamp mode at -70 mV (peak values were averaged over a 0.3 ms time window).

All data for intrinsic properties were acquired and analyzed within the Ephus software package. Series resistance was determined in voltage-clamp mode (command potential set at −70 mV) by giving a −5 mV voltage step. Series resistance was determined by dividing the −5 mV voltage step by the peak current value generated immediately after the step in the command potential R_{input} was calculated in voltage-clamp mode (command potential set to −70 mV) by giving a −5 mV step, which resulted in transient current responses. The difference between baseline and steady-state hyperpolarized current (ΔI) was used to calculate R_{input} using the following formula: $R_{input} = -5\ mV/\Delta I - R_{series}$. The average resting membrane potential (V_m) was calculated by holding the neuron in voltage-follower mode (current clamp, at $I = 0$) ~2 minutes after breaking in and averaging the membrane potential over the next 30 sec. Subthreshold and suprathreshold membrane responses in current clamp were elicited by injecting −200 to +400 pA in 50 pA increments (baseline V_m was maintained at −70 mV, by injecting the required current, if necessary). Sag was measured during the −200 pA current injection, using the formula, $SAG = (V_{min} - V_{steady\text{-}state})/V_{steady\text{-}state}$. The first resulting action potential (AP) at rheobase was analyzed for AP width. AP width was calculated as the full-width at the half-maximum amplitude of the AP.

Both slice electrophysiology experiments utilized borosilicate pipettes (World Precision Instruments) pulled into patch electrodes with 2.5–6 MΩ resistance (Sutter Instruments) and filled with a potassium-based intracellular solution, which was composed of the following (in mM): 128 K-gluconate, 10 HEPES, 4 $MgCl_2$, 4 Na_2ATP, 0.3 Tris-GTP, 10 Tris phosphocreatine, 1 EGTA,

and 3 sodium ascorbate (pH = 7.25, 295 mOsm). Normality of the data collected was confirmed via Shapiro-Wilk test.

Western Blot. Co-immunoprecipitation of munc18 and syntaxin was carried out using PEI transfection of HEK293 cells (American Type Culture Collection) plated and maintained in DMEM medium with 10% FBS and penicillin/streptomycin. Twenty-four hr prior to transfection, HEK293 cells were plated onto 150 mm petri dishes from confluent T75 flasks at the ratio of 2/3 flask per plate. 24 hr after plating, PEI transfection was carried out by mixing 25% munc18 (OriGene RC204873), 25% syntaxin 1A (gift from Raymond A Frizzell, Children's Hospital of Pittsburgh), and 50% pcDNA3 (Invitrogen) plasmids (28 µg total plasmids with 500 µl medium without penicillin/streptomycin, and 110 µl PEI at 1 mg/ml). The PEI was lastly added to the mixture drop-wise to avoid clumping of the DNA precipitates. This transfection reagent was allowed to incubate in room temperature for at least 5 min. The HEK293 medium was replaced with medium without penicillin/streptomycin prior to the addition of the transfection mixture. At 24 hr after transfection, the transfection medium was replaced with regular medium containing either cpd5 or DMSO. The cells were lysed and protein was harvested 24 hr after cpd5/DMSO treatment using 200 µl NP40 buffer (Invitrogen) containing phenylmethylsulfonyl fluoride (PMSF, Sigma-Aldrich) and protease inhibitor cocktail (1/4 tablet, cOmplete Mini, EDTA-free, Sigma-Aldrich). The resulting HEK293 sample was immunoprecipitated using mouse anti-syntaxin 1A antibody (abcam). The western blot was probed using the Biogen system with the same syntaxin 1A antibody and mouse anti-Flag (Sigma-Aldrich) used for the detection of munc18. Quantification of protein pulldown was normalized to the syntaxin signal before comparisons. SDS-PAGE in this study were run in 10% acrylamide. Small variations in band separation were caused by the semi-wet transfer method.

4.0 Injury-dependent expression of HCV protein NS5A ameliorates striatal infarct *in vivo*

4.1 Section Summary

The hepatitis C virus (HCV) protein NS5A prevents the enhancement of death-permitting Kv2.1 potassium current, increasing cell viability in hepatocytes and, ectopically, in neurons. Taking advantage of the injury-dependent release of cytosolic zinc in the Kv2.1-dependent neuronal cell death pathway, we previously utilized the metal regulatory transcription factor 1 (MTF-1)/metal regulatory element (MRE) system to drive the expression of NS5A and provide neuroprotection *in vitro*. Here, we demonstrate that this neuroprotective strategy is also feasible in the mouse brain. We generated serotype 9 adeno-associated virus containing the MRE-driven NS5A construct (AAV9-4xMRE-NS5A.eGFP) and injected it unilaterally into the mouse striatum. The injection of this virus did not elicit any observable abnormal behaviors or liver toxicity after more than 1 month post-injection. When mice were challenged with a transient focal ischemic stroke, strong neuronal NS5A expression was observed within 3 hr in several brain regions ipsilateral to the lesion. Importantly, animals treated with the AAV9-4xMRE-NS5A.GFP virus exhibited reduced striatal infarction when compared to a control, GFP-expressin vector. These results provide *in vivo* confirmation that the MTF-1/MRE expression system can be exploited to elicit injury-dependent expression of specific proteins and that the HCV protein NS5A can be leveraged as a potential neuroprotective agent.

4.2 Introduction

Many essential therapeutic drugs on the market today began their development as naturally occurring compounds. An evolutionary arms race exists in all biological faunas, driving the emergence of highly refined and selective protein-protein interactions. The survival and propagation of the hepatitis C virus (HCV) in host liver hepatocytes is an example of such a mutually competitive relationship between two organisms. Extensive research has aimed to understand the molecular mechanisms underlying HCV persistence and its ability to proliferate, inhibit antiviral mechanisms, and maintain host cell viability. Many of these viral functions involve the direct interactions with the host cell. For example, the expression of several HCV proteins itself requires post-processing by host proteases (Tellinghuisen et al., 2007). The HCV proteins NS2 and NS3/4A were identified as potent inhibitors of host cytokine gene expression to avoid anti-viral functions (Kaukinen et al., 2006). Another highly studied HCV protein that interacts with host cellular functions is the non-structural protein NS5A, which is known to have a direct role in viral replication, virion production, and importantly, the suppression of host cell's ability to commit apoptosis (He et al., 2006; Mankouri et al., 2009).

Physiological levels of potassium concentration prohibit the formation of the apoptosome and other cell death program components (Bortner & Cidlowski, 2007). Thus, the depletion of intracellular potassium is a necessary step in the execution of cell death pathways. In hepatocytes and many neuronal subtypes, Kv2.1 is the main mediator of this potassium loss. Experimental evidence has shown that NS5A prevents the enhancement of Kv2.1 currents during cell death and improves host cell survivability (Mankouri et al., 2009; Norris et al., 2012). This is achieved by the inhibition of kinases responsible for two Kv2.1 phosphorylation events that promote the channel's cell death functions. Specifically, NS5A inhibits the pro-death phosphorylation of Kv2.1

Y124 by Src Kinase (Norris et al., 2012) and Kv2.1 S800 by p38 MAPK kinase by inhibiting its upstream activator, mixed linage kinase 3 (Mankouri et al., 2009; Amako et al., 2013). In both neurons and hepatocytes, the expression NS5A is protective against lethal oxidative stress (Mankouri et al., 2009; Norris et al., 2012; Amako et al., 2013), mirroring extensive studies that show blocking potassium efflux directly or inhibiting upstream components of the Kv2.1-dependent cell death pathway is cytoprotective (Yu, 2003; Shah & Aizenman, 2014).

Oxidative stress is a significant component of cell death in many neurodegenerative diseases (Liu et al., 2017). Oxidized metalloproteins lose their ability to bind metals, such as zinc, releasing them into the cytosol (Marreiro et al., 2017). In injured neurons, this rise in cytosolic zinc is the predominant driver of the two aforementioned kinases that phosphorylate Kv2.1 for the expression of the death-permitting potassium current (McCord & Aizenman, 2014). Concurrently, unbound zinc can activate the metal regulatory transcription factor 1 (MTF-1), which translocates to the nucleus, driving the transcription of genes controlled by metal regulatory elements (MRE), such as that of metallothionein (Radtke et al., 1993) and ZnT-1 (Langmade et al., 2000). We previously demonstrated in vitro that 4xMRE can be used to ectopically drive the expression of NS5A during injury, inhibiting the Kv2.1-dependent cell death pathway and provide neuroprotection (Justice et al., 2018). Here, we evaluate the *4xMRE-NS5A* construct in vivo and evaluate the feasibility of this neuroprotective module in the mouse brain with the use of adeno-associated virus serotype 9 (AAV9) as the viral vector.

4.3 Results

4.3.1 *pAAV-4xMRE-NS5A.eGFP* recapitulates the *in vitro* effects of *4xMRE-NS5A.eGFP*

To begin the *in vivo* translation of the *4xMRE-NS5A.GFP* construct, we used traditional restriction enzyme cloning to transfer the gene into a commonly used AAV9 vector (*pAAV9-CMV-eGFP*; John T Gray Addgene ID 32395). The resulting plasmid construct (*pAAV9-4xMRE-NS5A.GFP*; Fig. 18A) is flanked by the AAV2 inverted terminal repeats that allow the selective packaging of the sequence into AAV capsids (Gray & Zolotukhin, 2012). To confirm that *4xMRE-NS5A* retained its neuroprotective properties when flanked by the viral cassettes in this vector, we evaluated it in an *in vitro* model of neuronal cell death as we have done previously with the original plasmid (Justice *et al.*, 2018). Rat cortical culture neurons 28-34 days *in vitro* (DIV) were co-transfected with luciferase and either *pAAV9-4xMRE-NS5A.GFP* or *pcDNA3*. The neurons were then challenged 24 hr after transfection with 60 µM TBOA, a selective glutamate reuptake inhibitor that we have previously shown to induce the death-permitting enhanced Kv2.1-mediated currents and neurotoxicity. Compared to those transfected with a vector plasmid, the neurons transfected with *pAAV9-4xMRE-NS5A.eGFP* exhibited significantly increased luciferase expression, a sign of cellular viability after injury (Aras *et al.*, 2001) (Fig. 18B). This result successfully recapitulates previous findings with the *4xMRE-NS5A.eGFP* plasmid, without the pre-AAV inverted terminal repeats (Justice *et al.*, 2018).

4.3.2 Striatal injection of AAV9-4xMRE-NS5A.eGFP does not alter behavior, liver

Brain ischemia has been shown to both increase the release of cytosolic free zinc in degenerating neurons (Koh *et al.*, 1996) and increase the expression of proteins regulated by MRE, such as metallothionein 1, 2 (Ebadi *et al.*, 1995), and ZnT-1 (Tsuda *et al.*, 1997). For these reasons, we used the mouse middle cerebral artery occlusion (MCAO) model of transient ischemic stroke to evaluate the *in vivo* neuroprotective efficacy of virally-mediated expression of 4xMRE-NS5A.GFP. Because transient ischemic stroke cause infarct predominately covering the striatal regions (Yeh *et al.*, 2017), we injected AAV9-4xMRE-NS5A.eGFP (~$5.30x10^8$ GC) into the striatum (coordinates from bregma: +0.5 AP, -2.1 LM, -3.2 DV) of young adult male mice (~8 wks; C57BL/6J) at the rate of 500 nL per minute. The animals were allowed to rest for 1 week after surgery before any further experiments. First, we evaluated the safety aspects of this virus and determined whether any leak, basal expression of the NS5A protein driven by 4xMRE would have any significant effects on the striatal motor functions of these animals. Throughout 43 days of behavioral testing, we did not detect any significant differences in the body weight of virus-injected animals when compared with that of non-injected controls (Fig. 19A). In a simple accelerating rotorod performance experiment, both the AAV9-4xMRE-NS5A.eGFP and the control groups performed consistently, and no treatment effect was detected (Fig. 19B). In a sensorimotor adhesive removal test, the group injected with the NS5A virus performed comparably to the non-injected controls with the exception of one pre-surgery day and one experiment 35 days after surgery, which returned quickly to normal in the next evaluation (Fig. 19C). We concluded that striatal injection of AAV9-4xMRE-NS5A.eGFP did not cause any detectable sensory motor deficits.

AAV9 is a widespread viral vector that has been reported to have strong affinity to liver hepatocytes when injected systemically through the tail vein (Zincarelli *et al.*, 2008). To assess the feasibility of leveraging a hepatitis virus protein as a transgene, we further performed H&E staining of the liver samples at the end of the above behavioral experiment and consulted an animal pathologist blinded to the experimental groups for evaluation of liver toxicity and for signs of chronic inflammation. No pathological signs of any kind normally associated with a viral infection were observed in the livers of either the virus-injected group or the non-injected control group (Fig. 20A). Mild acute extramedullary hematopoiesis (EMH) were observed in 1-2 animals in both groups of mice, of which, EMH presentation in one virus-injected animal was slightly more pronounced, but still was deemed within normal physiology. No animals exhibited any chronic or pathological symptoms that would indicate a liver-related disease. Further, the liver weight of animals injected with AAV9-4xMRE-NS5A.GFP did not significantly differ compared to non-injected controls (Fig. 20B). In addition, separate groups of animals were injected with the virus as described above and were filmed while free-behaving in a test cage over a period of ~2 months after injection. We observed no abnormal behaviors from animals injected with AAV9-4xMRE-NS5A.eGFP when compared to that of non-injected animals and also animals injected with AAV9.CMV-eGFP (Representative video links at final time point: GFP and NS5A).

4.3.3 Focal ischemic stroke induces the expression of NS5A.eGFP in animals received striatal injection of AAV9-4xMRE-NS5A.eGFP

Three hr prior to sacrifice, the animal group for the sensorimotor testing and the liver toxicity evaluation was treated with 50 min MCAO. Using anti-NS5A antibody (abcam ab13833; FitC secondary antibody Sigma F0257), we found that this ischemic stroke treatment was

sufficient to elicit the expression of NS5A.eGFP in regions surrounding the striatum (Fig. 21). We observed that NS5A was expressed in projection pyramidal neurons in the cortex (Fig. 21B) and other neuronal subtypes in the cortex (Fig. 21C) and in thalamic regions (Fig. 21D). Curiously, AAV9 is also known to transduce astrocytes and oligodendrocytes (Aschauer *et al.*, 2013) but we did not observe any non-neuronal cells expressing detectable amounts of the NS5A protein. Within the striatal area, we have not detected the expression of any NS5A.eGFP.

4.3.4 Preventative treatment of AAV9-4xMRE-NS5A.eGFP reduces striatal infarct

In a separate cohort of animals, mice were injected with either AAV9-4xMRE-NS5A.eGFP or AAV9-CMV-eGFP to the striatum identically as described above. After 3-4 weeks from injection, we subjected these animals to 50 min MCAO and evaluated the striatum 24 hr after ischemic reperfusion. We sectioned and stained the striatum with triphenyltetrazolium chloride (TTC) and evaluated the infarction ratio of only the ipsilateral striatum ($Striatum_{Infarct}/Striatum_{Total}$) with an experimenter blinded to the treatment groups. The results show that the animals injected with AAV9-4xMRE-NS5A.eGFP exhibited significantly reduced striatum infarct ratio compared to that of the animals injected with AAV9-eGFP (Fig. 22).

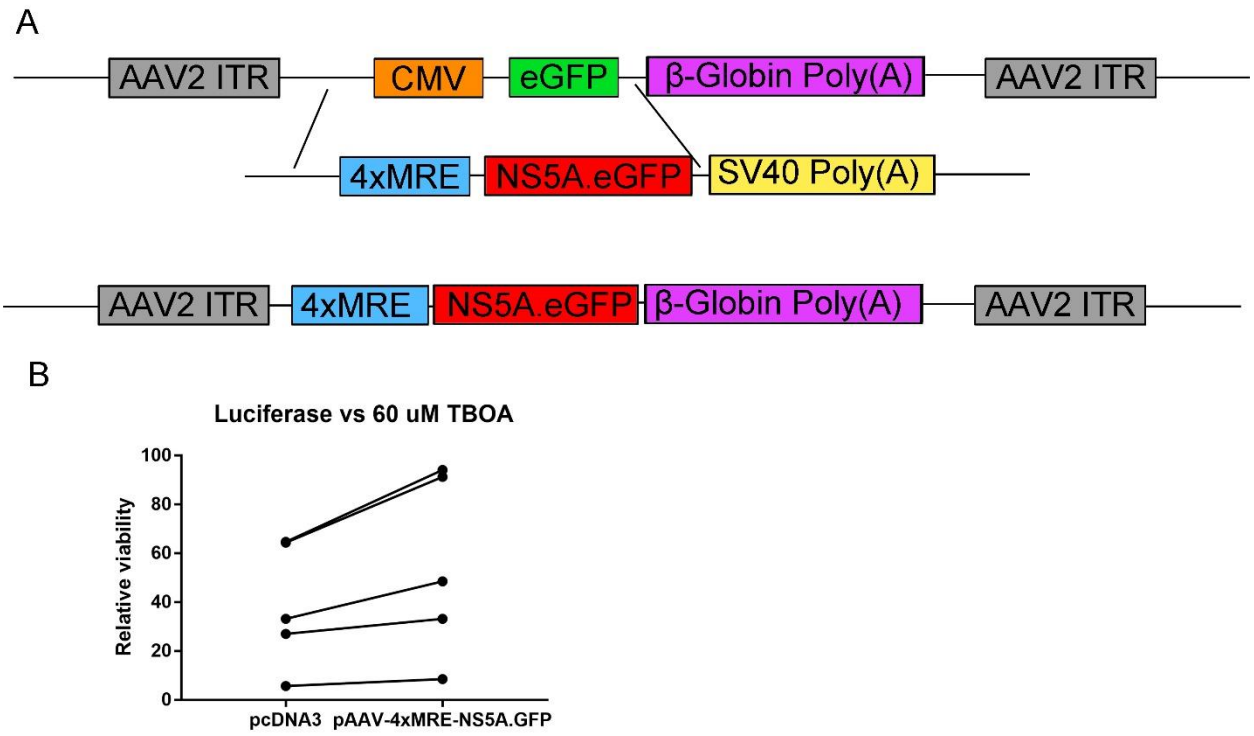

Figure 18. Construction and validation of the *pAAV-4xMRE-NS5A.GFP* plasmid.

A. The pre-viral *pAAV-4xMRE-NS5A.eGFP* plasmid flanked by AAV2 ITRs is generated by traditional restriction enzyme cloning of the *4xMRE-NS5A.eGFP* construct into the widely used *pAAV-CMV-eGFP* vector. **B.** Cortical culture neurons were transfected with luciferase and either *pAAV-4xMRE-NS5A.GFP* or a control plasmid. After 24 hr of 60 uM TBOA incubation, the experimental group transfected with *pAAV-4xMRE-NS5A.GFP* expressed significantly more luciferase, a signal of cellular viability. Mean of differences ± SEM: 16.132 ± 5.32669. n=5. * $p<0.05$; paired t-test.

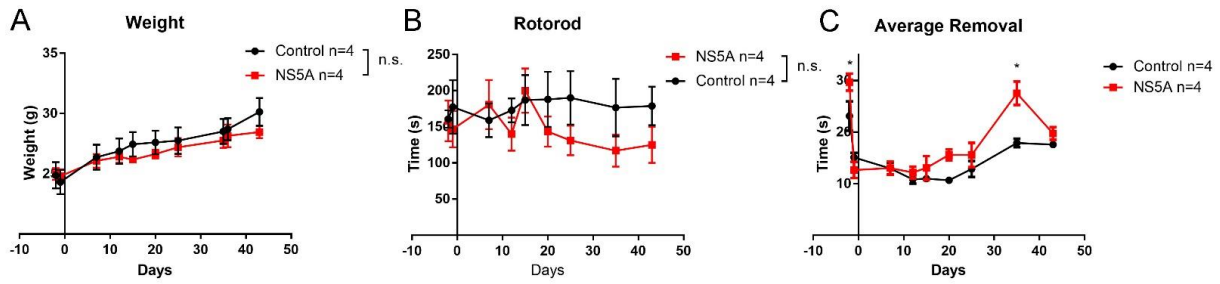

Figure 19. Striatum injection of AAV9-4xMRE-NS5A.eGFP does not cause behavioral deficits.

A. Body weight of animals injected with the experimental virus did not differ from that of the non-injected control group. **B.** Rotorod performance did not differ significantly in animals injected with the AAV9-4xMRE-NS5A.eGFP virus. **C.** Virus-injected animals performed significant worse in the adhesive removal test in two days of the experiments. However, one of the significant days was pre-surgery and the other quickly returned to baseline in the next session. Mean ± SEM are shown for all. N = 4 for all groups. Two-way ANOVA. * $p < 0.05$.

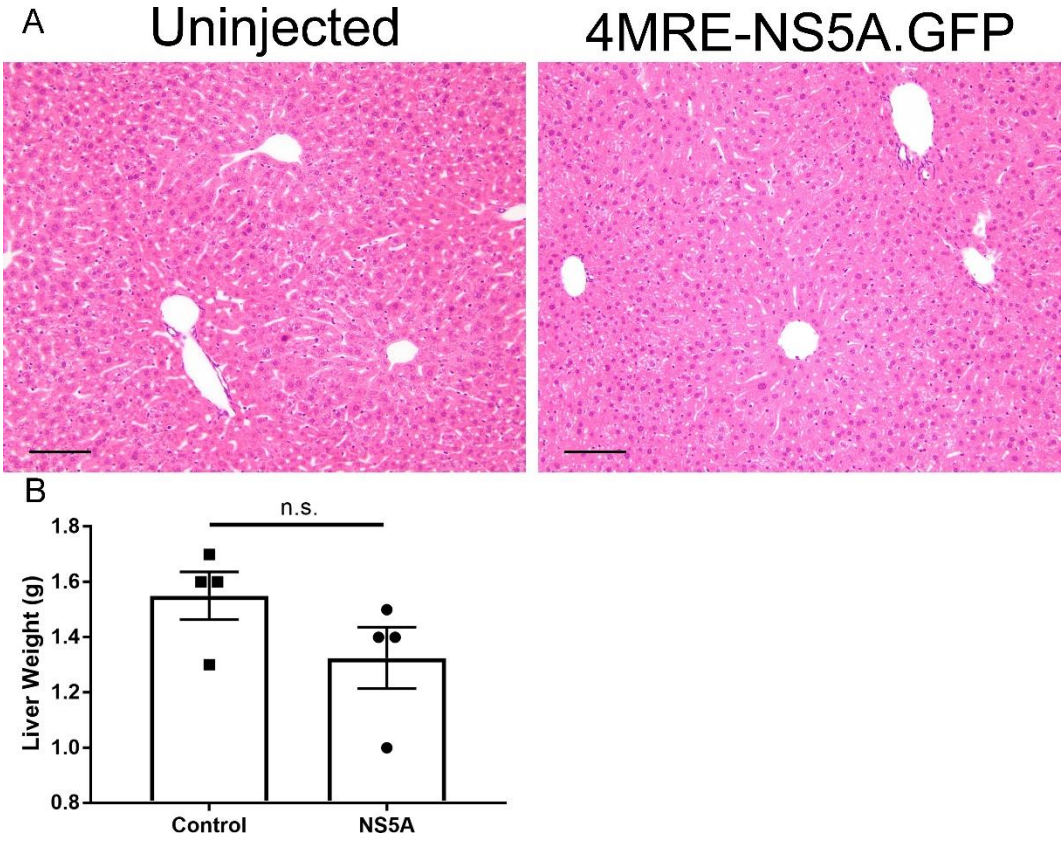

Figure 20. Liver of animals treated with striatal injection of AAV9-4xMRE-NS5A.GFP is not affected.

A. Mice (~4 months of age) received intracerebral injection of AAV9-4xMRE-NS5A.GFP do not show any abnormal liver pathology in H&E stained sections after 5 weeks when compared to non-injected controls. Minor acute extramedullary hematopoiesis was observed in 1-2 animals of both groups. Scale bar = 100 uM. **B.** Wet liver weight of these animals taken immediately after perfusion were not significantly different. Mean ± SEM; Control: 1.55 ± 0.087, NS5A: 1.33 ± 0.11. For both groups, n=4. Unpaired t-test.

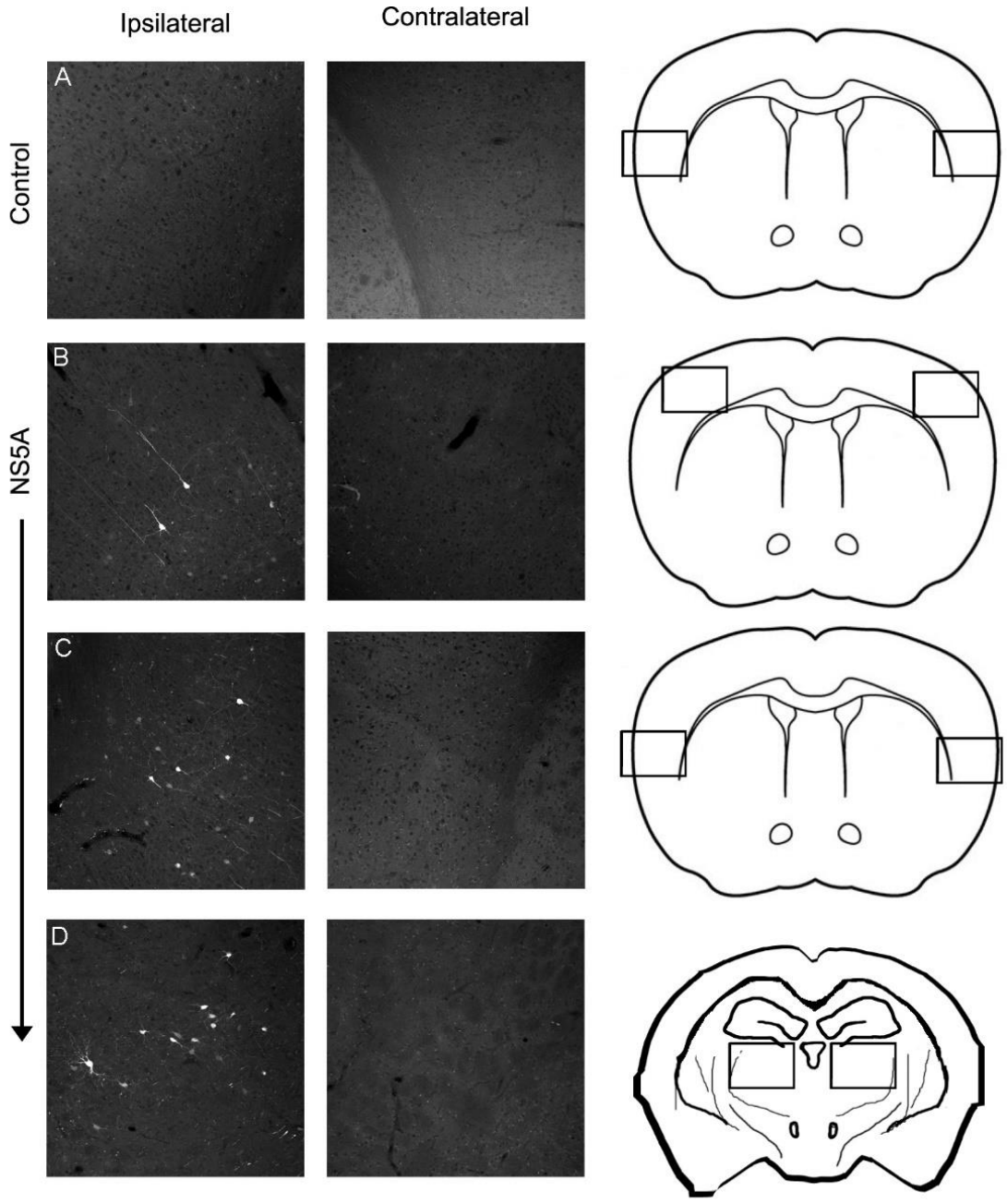

Figure 21. 4xMRE-driven expression of NS5A after focal ischemic stroke.

MCAO (50 min) of mice 5-6 weeks after striatum injection of AAV9-4xMRE-NS5A.GFP induces the expression of NS5A.GFP within 3 hrs. We observed sparsely distributed expression of NS5A.GFP in neurons throughout the ipsilateral side. Expression was observed in cortex layer projection pyramidal neurons (**A**), and locally synapsing neurons in the cortex (**B**) and in the

thalamic regions (**C**). These areas are typically in the ischemic penumbra. Curiously, we did not detect any expression of NS5A.GFP in glia anywhere or in neurons within the ischemic core (striatum). Virus-injected group, n=3.

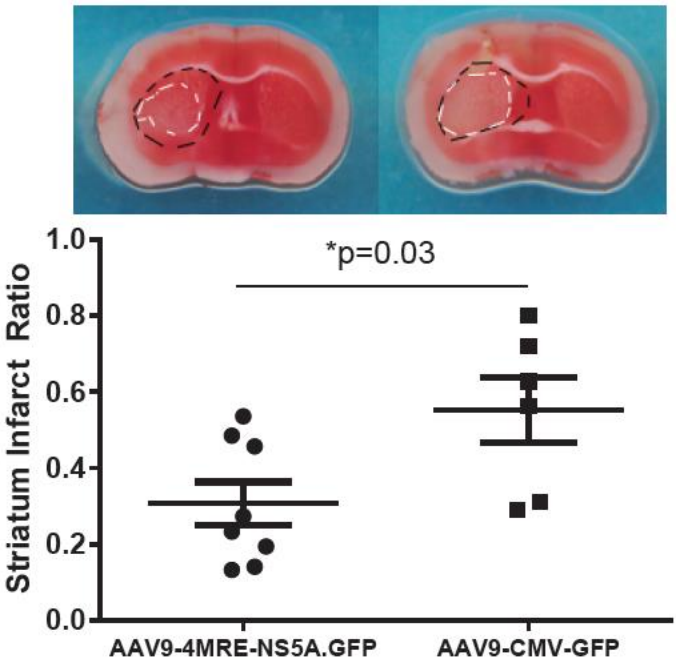

Figure 22. 4xMRE-driven expression of NS5A.eGFP reduces infarct area in focal ischemic stroke.

Blinded evaluation of mice brain injected with the NS5A virus after 50 min MCAO found a significant reduction of infarct volume in the region compared with that of animals injected with AAV9-CMV-GFP. Infarct ratio: $Striatum_{Infarct}/Striatum_{Total}$. Striatum infarct ratio mean ± SEM: NS5A 0.31 ± 0.06, GFP 0.55 ± 0.09; * $p < 0.05$. Unpaired t-test.

4.4 Discussion

The HCV genome is comprised of 9.6 kb of RNA containing a single open reading frame of ~3000 amino acids, flanked by un-translated regions highly conserved between virus genotypes (Tellinghuisen *et al.*, 2007). The translated polyprotein is processed by both host and viral proteases, resulting in 10 individual virus proteins: the structural proteins core, E1, E2, the viroporin p7, and the non-structural proteins NS2, NS3, NS4A, NS4B, NS5A, and NS5B (Tellinghuisen *et al.*, 2007). The structure of NS5A is composed of three domains, with domain 1 as the only domain with a defined tertiary structural. Domain 1 contains coordinated cysteine motifs at the n-terminus that binds 1 atom of zinc that is critical for HCV replication (Ross-Thriepland & Harris, 2015), a disulfide bond towards the C-terminus, and a known phosphorylation site near a lipid droplet motif (Ross-Thriepland & Harris, 2015). In addition, there is evidence that NS5A domain 1 can form highly stable dimers, although the exact conformation has not been determined (Tellinghuisen *et al.*, 2005; Love *et al.*, 2009).

While the precise mechanism of NS5A neuroprotection remains to be confirmed, there are a few proposed mechanisms targeting the Kv2.1-dependent cell death pathway. Initial characterization of NS5A's effects on Kv2.1 in hepatocytes found that NS5A inhibits p38 phosphorylation of Kv2.1 S800, which is a necessary step in the expression of the death-inducing currents (Mankouri *et al.*, 2009). It was later determined that this effect may be the result of direct inhibition of mixed lineage kinase 3 (MLK3) by NS5A, which prevents the activation of p38 kinase (Amako *et al.*, 2013). However, NS5A has also been shown to inhibit the phosphorylation of Kv2.1 channels at the Y124 residue, which is the target of Src kinase (Norris *et al.*, 2012). While NS5A can prevent phosphorylation by Src kinase in general, the non-phosphorylable mutant Kv2.1 S800A does not abolish the inhibition of NS5A on channel current (Norris *et al.*, 2012). The

importance for the Y124 site is further supported by a later study revealing that the Kv2.1 Y124 phosphorylation precedes and facilitates the S800 phosphorylation (He *et al.*, 2015). It is possible that NS5A's inhibition of death-permitting phosphorylation on Kv2.1 is redundant, as it has been proposed that a highly conserved polyproline sequence between domains 2 and 3 of NS5A mediates these effects by binding to a Src homology 3 (SH3) sequence (Macdonald *et al.*, 2004), which is present in both Src and MLK3.

Following the zinc-induced phosphorylation events at Kv2.1, the channel interacts with syntaxin, resulting in enhanced channel insertion (McCord & Aizenman, 2013; McCord *et al.*, 2014). Unlike previous neuroprotective strategies that interfere with the interaction between Kv2.1 and syntaxin directly (McCord *et al.*, 2014; Yeh *et al.*, 2017), NS5A, which acts upstream, also suppresses basal Kv2.1 current (Norris *et al.*, 2012). This likely corresponds with nominal kinase phosphorylation of Y124 and S800 in uninjured neurons. However, with the addition the conditional promoter 4xMRE, this effect on the basal current is abolished (Justice *et al.*, 2018), presumably due to the significant reduced expression of NS5A in healthy neurons where cytosolic zinc remains tightly regulated.

Several research groups, most notably in the field of cardiac arrest, have explored the utilization of conditionally expressed promoters, such as MRE. AAV delivery of DNA constructs driven by hypoxic response element (HRE) was utilized in a mouse ischemic heart model to great success by conditionally expressing angiogenic factors (Su *et al.*, 2002) or heme oxygenase (Pachori *et al.*, 2004). Expression driven by hypoxic response element in myocardium remains elevated for at least 4 hr after ischemia and return to baseline after 8 hr (Prentice *et al.*, 1997). Designer promoters that combined several regulatory elements, so-called chimeric promoters, have been created to achieve even better signal-to-noise ratio between dormant and active states.

An early example combined Egr-1 binding site (EBS), MRE, and 3x hypoxia regulatory element (HRE) to form a promoter composed of EBS-MRE-3xHRE, capable of generating very low basal activity and up to 69 times the expression when stimulated with either metal or hypoxia (Lee *et al.*, 2006). Innovations in cancer studies combine HRE with tumor-specific promoters to achieve great tissue specificity, for instance, the combination of estrogen regulatory element (ERE) and HRE in breast cancers and the combination of nestin promoter and HRE for targeting glioblastoma (Javan & Shahbazi, 2017). While we are the first to employ MRE alone in similar strategies *in vivo*, these studies inspire considerations of leveraging and optimizing the use of MRE in combination with various other regulatory elements and in the context of specific neurodegenerative diseases.

A major challenge in treating neurodegenerative conditions is the ability to provide interventions to patients prior to the significant loss of neurons. This is difficult as the detection of a neurodegenerative disease may only come as symptoms appear, which already signifies significant cell death. While the identification of prodromal disease biomarkers is becoming more sophisticated, effective treatments remain elusive. We believe that the strategy of using an injury-dependent promoter to drive the expression of a neuroprotectant, exemplified by 4xMRE-NS5A, is a very rational approach to a treatment design that can overcome these challenges. Its components are ideal for their roles: MRE relies on zinc for expression, essentially mirroring the Kv2.1-dependent cell death pathway; the protective agent NS5A has evolved to inhibit Kv2.1-dependent cell death; and the AAV vector itself is known to induce stable expression of gene constructs to last for >7 years in patients in the muscle and the liver (Nathwani *et al.*, 2011), and for >10 years in the human brain (Leone *et al.*, 2012). Because the release of intracellular zinc relies on oxidative stress, which is a major component of most neurodegenerative conditions (Liu

et al., 2017), our work here has broad implications and represents an essential step towards an effect gene therapy for neurodegenerative diseases.

5.0 General Discussion

This dissertation focused on targeting the Kv2.1-syntaxin interaction for neuroprotection. This was achieved in several ways. In chapter 2, we followed the proven workflow of determining a minimal binding amino acid sequence in a protein-protein interaction and generating a TAT-linked peptide, namely TAT-C1aB. Administration of TAT-C1aB provided the first evidence that the Kv2.1-syntaxin interaction contributes to neuronal cell death *in vivo*. In chapter 3, we characterized the molecular actors in the binding between C1aB and syntaxin, allowing us to screen for small molecules that recapitulates these actions. In chapter 4, we took a step back and evaluated the *in vivo* potential of the HCV virus protein NS5A, which is a known upstream inhibitor to the Kv2.1-syntaxin interaction. Importantly, this last project geared towards the field of gene therapy, which represents one of the most promising approaches to combat neurodegenerative diseases. In this final discussion, I describe several unresolved questions regarding these topics and suggest paths to clarity wherever possible. Lastly, I propose an addition to the workflow that we have so far leveraged in our studies.

5.1 The Kv2.1-syntaxin interaction

We have repeatedly demonstrated that disrupting the Kv2.1-syntaxin interaction is a viable neuroprotective strategy. Most notably, this is shown *in vivo* with the TAT-C1aB peptide in chapter 2 and with the AAV9-4xMRE-NS5A.eGFP virus in chapter 4. In addition, preliminary data from our collaborators strongly suggest a neuroprotective effect of the 4xMRE-NS5A.eGFP

construct in fly models of chronic/progressive neurogenerative diseases. While these results clearly established Kv2.1-dependent cell death as an important mechanism in neurodegeneration in animal models, whether this mode of cell death exist in human patients is still a lingering question. To support the data presented here that demonstrated treatment efficacy in animal models, an *in vivo* detection method for a biomarker of Kv2.1-dependent cell death should be developed and confirmed with human patient tissues. This final step is necessary to make the connection from the decades of research in underlying mechanisms to clinical relevancy.

A phospho-specific antibody was developed previously (Redman *et al.*, 2007) to detect the phosphorylation of Kv2.1 S800 by p38 (pS800). An increase in phosphorylation of Kv2.1 S800 after an injury *in vivo* would imply an enhanced Kv2.1-syntaxin interaction and provide evidence for our cell death model. Using the Kv2.1 pS800 antibody, I have attempted immunofluorescence staining of the mouse brain as well as western blot of the brain lysate 24 hr after MCAO. In both cases, I was unable to detect a significant difference between the ipsi- and the contra-lateral brain sample. In the immunofluorescence staining experiment, I was unable to produce Kv2.1-specific staining of the brain sections using the Kv2.1 pS800 antibody. Because this antibody is polyclonal, I expect further optimization of the staining protocol may be able to achieve at least weak staining of Kv2.1. Although any immunofluorescence staining with this particular antibody has not been demonstrated either *in vitro* or *in vivo*. In the western blot, the Kv2.1 pS800 band was very light, which is typical, and may have contributed to the inability to detect a difference in band intensity. To increase the concentration of phosphorylated Kv2.1 protein, the ischemic brain samples may be enriched by isolating regions most affected by the MCAO procedure. While these biochemical experiments are so far inconclusive due to technical challenges, overcoming these issues or developing an entirely different biomarker detection technique will allow the direct application of

these procedures to brain samples from human patients of ischemic stroke and of other neurodegenerative diseases. This is an important step in solidifying Kv2.1-dependent cell death as an important mechanism in humans prior to future efficacy studies.

It is possible that TAT-C1aB and cpd5 merely induce localized disruption of the Kv2.1-syntaxin binding to block the enhanced interaction and does not totally displace Kv2.1 from syntaxin. I acknowledge this possibility because the co-immunoprecipitation of Kv2.1 and syntaxin in CHO cells treated with 10 μM TAT-C1aB overnight did not immediately detect an effective decrease in proteins pulldown from either direction. My initial interpretation for this phenomenon is that other members of the SNARE complex, which are known to bind both Kv2.1 and syntaxin, may act as scaffolding intermediates and retain both proteins in contact. Further, the docking model (chapter 3) shows that the C1aB peptide binds to a pocket surrounded by several syntaxin domains, making it likely that Kv2.1 interacts with syntaxin elsewhere. Note that I have only demonstrated the displacement of syntaxin from 15mer, not full-length, Kv2.1 peptides with TAT-C1aB and cpd5 in the cell-free peptide array (chapter 2, 3) (Yeh *et al.*, 2017), which sidesteps the above two suggested scenarios. This is in contrast with previous results of McCord et al., where, in an overexpression system, full length C1a or $C1a_{441-522}$ successfully displaced full-length Kv2.1 from syntaxin in a co-immunoprecipitation experiment (McCord *et al.*, 2014). It is possible that the additional amino acids in the full-length C1a and $C1a_{441-522}$ provide the steric volume necessary to fully unbind Kv2.1 from syntaxin and also disrupt any interactions provided by the other SNARE proteins. It is also likely that higher concentrations of TAT-C1aB is necessary to displace Kv2.1 and syntaxin in the overexpression systems, although 10 μM was the effective concentration to suppress the enhanced current of the pseudo-phosphorylated Kv2.1 S800E in the same overexpression CHO cell system (chapter 2) (Yeh *et al.*, 2017). Nevertheless, full

displacement of Kv2.1 from syntaxin may not be necessary and small molecule-mediated destabilization of the interaction is clearly sufficient to inhibit the expression of the enhanced currents for neuroprotection.

5.2 The role of Kv2.1 somatodendritic clusters

A critical aspect of Kv2.1 not explored in this dissertation is the role of Kv2.1 somatodendritic clusters in cell death. In neurons, Kv2.1 exists in micron-sized cluster that depends on a proximal restriction clustering (PRC) motif (Lim *et al.*, 2000) and acts as protein trafficking hubs through its interactions with the endoplasmic reticulum anchoring proteins VAPA and VAPB (Johnson *et al.*, 2018; Kirmiz *et al.*, 2018). Although, not all Kv2.1 cluster appears to serve the same functions, or at least regulated in the same manner. Phosphoregulation of a Kv2.1 target sequence motif (a. a. 720-745) can lead to Golgi-independent trafficking of the channel to the axon initial segment, which also form clusters that are not dependent on the PRC motif (Jensen *et al.*, 2017). This subcellular localization draws similarities with the microtubule protein tau, which forms aggregates through liquid-liquid phase separation and is highly clustered also at the axon hillock (Wegmann *et al.*, 2018). The connection between Kv2.1 and tau is not yet discovered.

Kv2.1 clusters form in neurons *in vivo,* in primary cultured neurons, as well as in Kv2.1-transfected HEK cells (O'Connell *et al.*, 2006). Despite being the most prominent structural feature of Kv2.1, channels within the clusters have been shown to be a non-conducting population (O'Connell *et al.*, 2010). Interestingly, these clusters are very dynamic structures and can be dispersed quickly when treated with some types of cell death stimulus. Merely 2 min of CO_2 treatment in rats will decluster Kv2.1 channel in hippocampus neurons (Misonou *et al.*, 2005).

Brief excitatory treatment with 10 μM glutamate for 15 min is sufficient to decluster Kv2.1, recovering within 2 hr after the washout of glutamate (Cerda & Trimmer, 2011). The clustering of Kv2.1 was found to be dependent on the phosphorylation of Kv2.1 S603 by cyclin-dependent kinase 5 (Cerda & Trimmer, 2011), which is regulated by cyclin E1 (Shah *et al.*, 2014). Zinc chelation also blocks declustering after ischemia (Aras *et al.*, 2009b). Intriguingly, repeated electrical stimulation causes an increase in the number of Kv2.1 clusters in *Aplysia* bag cell neurons (Zhang *et al.*, 2008). This is difficult to reconcile, as excitatory glutamate treatment readily declusters Kv2.1 in cultured rat hippocampal neurons (Misonou *et al.*, 2004), and direct sciatic nerve stimulation also reduces Kv2.1 clusters in an intact rat motor neuron preparation (Romer *et al.*, 2016). The observations in *Aplysia* bag cell neurons is likely specific to the animal model and I will avoid excessive conjectures.

Kv2.1 clusters appear to play an integral part in the Kv2.1 cell death pathway, but their exact roles are just beginning to be explored. As mentioned, after treatment with several types of insults, Kv2.1 channels quickly decluster. However, a sublethal injury that does not kill the neurons can also decluster the channel. This treatment, commonly referred to as preconditioning, provides increased resistance and viability against later injuries that are typically deadly. This neuroprotection can be achieved by directly declustering Kv2.1 alone, without inducing injury or altering Kv2.1 channel kinetics (Justice *et al.*, 2017). Because Kv2.1 itself has been observed to traffic to these clusters (Fox *et al.*, 2015), and that declustering of Kv2.1 in neurons prevents the subsequent increase in channel current (Shah & Aizenman, 2014; Justice *et al.*, 2017), it can be inferred that these clusters are required for the cell death-permitting *de novo* trafficking of Kv2.1. Although declustered Kv2.1 may become conducting over time (Zhang *et al.*, 2008), it is unknown whether they contribute significantly in the context of enhanced death-permitting Kv2.1 current.

Interestingly, while it is unknown how the Kv2.1-syntaxin interaction fit into the clustering pathways, VAPA has been previously shown to bind effectively to both v-SNAREs and t-SNAREs, including syntaxin 1A (Weir *et al.*, 2001). All these evidences point towards significant crosstalk between Kv2.1's cell death and clustering pathways. Further investigations are necessary to unravel these two interconnected phenomena.

5.3 Further AAV9-4xMRE-NS5A.eGFP characterization

Several important lingering questions regarding AAV9-4xMRE-NS5A.eGFP remain and may require different approaches to confirm the findings. First, I was surprised with the expression pattern of the virus, which was very widespread but also highly selective. Typically, gene expression with any viral vector in intracerebral injections is very localized and will infect most cell types near the injection site to some degree (Aschauer *et al.*, 2013). Infection of neurons outside of the striatum may be the result of virus diffusion and the relatively large volume (5 uL) of our injection. However, it is strange that we did not observe any expression in the striatum, which may be indicative that the stroke treatment is too severe in the ischemic core, but protease activity is not expected to be this thorough in 3 hr. It is not known if there are any differences in the expression activity of MRE in the striatum vs the cortex caused by zinc buffering activities or other factors. While AAV9 is known to transduce cortical neurons with high efficiency, which we observed, we expected to observe some degrees of NS5A expression in astrocytes or other glia, which was completely absent. In fact, the pathway of oxidative damage-induced release of cytosolic zinc, activating MTF-1, is known to exist in astrocytes as well (Kruczek *et al.*, 2009).

Though the lack of expression in astrocytes may be due to fact that they are more resistance to intracellular zinc liberation (Aizenman *et al.*, 2000).

The combination of virus injection, focal ischemic stroke, and inducible promoter may have caused the expression pattern of the NS5A protein to be too difficult to characterize. Essentially, all three factors must be in effect for the observation of the protein expression. To remedy this, *in situ* hybridization of the *4xMRE-NS5A.eGFP* DNA construct may be used to observe the true infection efficiency of the virus. For the purpose of characterizing the expression pattern only, global ischemia through bilateral carotid artery occlusion may be useful to induce a more consistent ischemic insult throughout the brain parenchyma. In addition, because we have observed infection of large pyramidal neurons in the cortex layers, it may be possible to observe real time expression of the protein during ischemia with a cranial window and a powerful multi-photon microscope. Lastly, because NS5A is known to suppress basal Kv2.1 current (Norris *et al.*, 2012), transient expression of NS5A driven by 4xMRE must be quantified to provide a precise active vs dormant ratio, which then allows for future improvements and comparisons with other inducible promoters. These works will contribute to fully characterize the *in vivo* action of the *4xMRE-NS5A.eGFP* construct and provide the basis for future studies.

AAV9 has been reported to be an effective viral vector in the brain and we sought to see if a more widespread treatments in the CNS is sufficient to provide neuroprotection to a larger brain region. In a separate cohort of animals from the data presented in chapter 4, we injected the same titer of AAV9-4xMRE-NS5A.eGFP virus into the lateral ventricle, induced 50 min MCAO after 3-4 weeks, and quantified the infarct ratio of the total brain as opposed to only the striatum region. Blinded evaluation of the brain sections stained with triphenyltetrazolium chloride found a trending, but not yet significant, effect of the AAV9-4xMRE-NS5A.eGFP virus injection

compared to that of AAV9.CMV.eGFP (Fig. 23). We believe that this finding is promising and warrants further investigation for ways to enhance systemic viral transduction, or even by the conjugation of NS5A with the TAT domain, which is an idea explored by Ma et al. in the nasal delivery of AAV2-TAT-BDNF (Ma *et al.*, 2016).

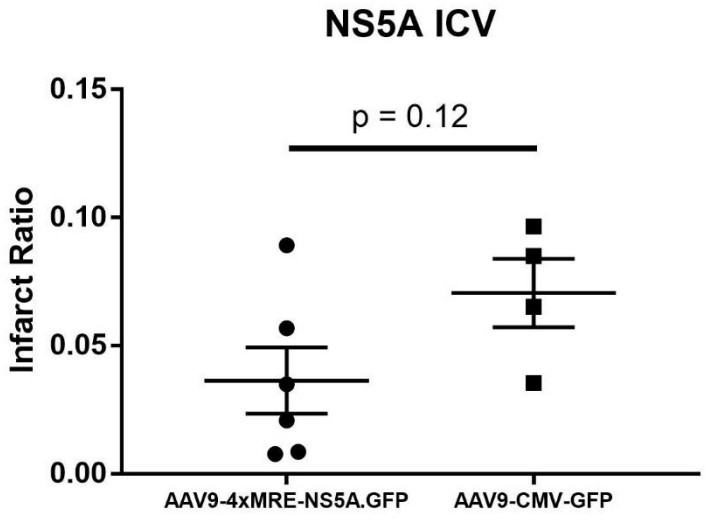

Figure 23. Infusion of AAV9-4xMRE-NS5A.eGFP virus (~5.30x108 GC) into the lateral ventricle did not provide significant neuroprotection against MCAO.

After 3-4 weeks from the virus infusion, mice were treated with 50 min MCAO. Mice brains were stained with TTC 24 hr after stroke and evaluated by a blinded investigator. Infarct ratio mean ± SEM: NS5A 0.036 ± 0.01, GFP 0.071 ± 0.01. N = 6 for NS5A, n = 4 for GFP. Unpaired t-test.

5.4 Gene therapy in clinical trials and AAVs

Since the authorization of the first gene transfer study that took place at the National Institutes of Health in 1989, the number of completed clinical trials on this topic is nearing 3000, with participations in nearly 40 countries (Ginn *et al.*, 2018). Overwhelmingly, cancer and

inherited monogenic diseases are the target of most of these studies, accounting for ~75% of all completed gene therapy clinical trials. Those that targets neurological diseases account for only 1.8% (n = 47) of all completed trials by 2017 (Ginn *et al.*, 2018). While the use of AAV as the viral vector is in only 7.6% of all gene therapy clinical trials (Ginn *et al.*, 2018), it is the most widespread vector for use in neurological diseases today (Choudhury *et al.*, 2017).

Despite the amassing clinical data, only a handful of gene therapies so far have been approved for use in humans. This is a rapidly improving situation. In a statement released by the FDA commissioner Scott Gottlieb on January 15, 2019, the FDA expects to approve 10 to 20 cell and gene therapy products per year by 2025. The first approved gene therapy product, Gendicine (Sibiono), passed its review by the Chinese state FDA in 2003. Gendicine is an adenovirus, a much larger viral vector than AAV, with designations for squamous cell carcinoma and overexpresses p53 to induce cancer cell death with a great safety profile (Zhang *et al.*, 2018). Since then, 6 more gene therapy products have been approved for clinical use, including, with approval by the United States FDA in 2017, Yescarta (an *ex vivo* chimeric antigen receptor T-cell (CAR-T) therapy for large B-cell lymphoma; Gilead) and Kymriah (a CAR-T therapy for B-cell acute lymphoblastic leukemia; Novartis). Just this year, Zolgensma (AVXS-101; Novartis, formerly AveXis) was just approved in May 2019, albeit with the steep price tag of over $2 million dollars.

AVXS-101 is a gene replacement therapy for type 1 spinal muscular atrophy (SMA1), which is the second most common fatal autosomal recessive disorder after cystic fibrosis. Infants afflicted with the SMA1 mutation have homozygous deletion of the survival motor neuron 1 (SMN1) gene in motor neurons and experience rapid muscle atrophy often leading to respiratory failure within two years of age (D'Amico *et al.*, 2011). One-time intravenous infusion of AVXS-101 in patients significantly improved respiratory and motor functions and, at 20 months of age,

all 15 patients in the first clinical trial survived, compared to the 8% historical rate at the same age (NCT02122952) (Mendell *et al.*, 2017). In a later study, the group found treated patients to have reduced hospitalization and improved behavioral outcomes, allowing the infants to preserve respiratory functions, the ability to swallow, and to develop speech (Al-Zaidy *et al.*, 2019). AVXS-101 is a self-complementary AAV9 which expresses the SMN1 gene under the control of the chicken β-actin promoter and has been shown to be able to transduce 60% of motor neurons when injected IV (5×10^{11} GCs) into neonatal mice (Foust *et al.*, 2010). Self-complementary AAV genomes have been shown to have significantly increased transduction efficiency by bypassing the bottleneck of needing the host cell DNA polymerase to generate a double-stranded genome (McCarty *et al.*, 2003). The clinical trial also reported a brief asymptomatic elevation of liver enzymes, which was assumed to be related to the viral vector and was easily overcome with "a brief course of steroids" (Al-Zaidy *et al.*, 2019).

AVXS-101 represents an important success story of utilizing AAV vectors safely and to great effect in the clinical settings. AAV has become a preferred vector for gene therapy for several distinct advantages. AAV-delivered genes can exist in an episomal state with a low rate of genomic integration into the host genome (McCarty *et al.*, 2004). The immunogenicity is very mild due to its small size (Bessis *et al.*, 2004). AAVs in general are also relatively safe to handle, and it is relatively easy to produce titers at high purity. AAV9 have also been found to be able to penetrate the blood brain barrier (Manfredsson *et al.*, 2009), which avoids the highly invasive intracerebral and intrathecal injections. In addition, AAV2 nasal delivery of large TAT-linked proteins can achieve widespread distribution of the cargo (Ma *et al.*, 2016). However, there exist one key shortcoming of the AAV vector and that is its relatively small genomic capacity (4.8 kb) compared to the other popular options in retrovirus (gammaretrovirus and lentivirus; ~8.5 kb), and

adenovirus (10 kb) (Choudhury *et al.*, 2017). Experiments with larger virus particles, such as amplicons based on recombinant herpes simplex virus can carry cargo up to 150 kb but is difficult to purify (Choudhury *et al.*, 2017). This limits the size of cargos for AAV vectors, which practically eliminates its consideration for gene-replacement therapies in some monogenetic diseases.

Recombinant AAVs with different serotypes allow for infectious affinity for specific cell types. Directed evolution forces the brute force generation of AAV capsids with display peptides that has incredible selectivity for almost any cell type desired (Grimm & Zolotukhin, 2015; Deverman *et al.*, 2016). In 2016, Korbelin et al. disclosed a custom AAV capsid (AAV-BR1) generated through directed evolution to specifically target brain endothelial cells. Infected cells by this vector have been shown to express genomic constructs for at least two years. I became interested in this capsid as I was studying the effects of the neuroprotective TAT-linked peptide (TAT-C1aB) in ischemic stroke. I rationalized that the source of brain ischemia begins at the brain vasculature, and brain endothelial cells can be manipulated to induce the expression of TAT-C1aB during ischemic conditions. Dr. Korbelin generously provided me with the plasmid for his capsid. However, I was unable to replicate their results using a simple GFP cargo. Continuing this path has been difficult due to the lack of an *in vitro* system for verifying the virus stock that I have grown, despite PCR confirmation of the genomic load. Nevertheless, I remain optimistic that similar developments in the pool of available AAV capsids will make significant clinical impacts in the near future.

5.5 TAT-linked peptides as AAV cargo

Limitations in cargo size is the predominant shortcoming of AAV vectors. TAT-linked peptides that contain optimized sequences, such as TAT-C1aB (chapter 2) (Yeh *et al.*, 2017), TAT-CDB3 (Brittain *et al.*, 2011b), or TAT-NR2B9c (Ballarin & Tymianski, 2018) may be the ideal cargoes for their significantly reduced length compared to their parent proteins. In the introduction (section 1.8), I presented the workflow of protein binding sequence optimization through techniques such as the SPOT peptide array, followed by the construction of the TAT-linked peptide. Here, I propose the novel transition of encoding the TAT-linked peptides developed in this manner as the genetic cargo for AAV vectors. This strategy has several distinct advantages that makes it the rational continuation. Unlike synthetic molecules commonly used in typical pharmacology, peptide-based treatments can be produced by the patients' own cells. In this setting, treatment expressed from within the cells via an inducible promoter based on cytosolic conditions is, by definition, the fastest treatment possible for a non-preemptive response. Further, AAV treatment represents a nearly permanent solution for the treatment of chronic or subchronic conditions, such is the case with most neurodegenerative diseases. For example, patients with Canavan disease have a mutation of the aspartoacylase gene (ASPA) and accumulates a damaging level of N-acetylaspartate (NAA). With AAV2-mediated gene replacement therapy via direct intraparenchymal infusions, NAA levels were significantly decreased in Canavan disease patients compared to non-treated controls and significantly improved motor functions for 10 years in some (Leone *et al.*, 2012). Lastly, and importantly, this strategy allows for massive optimization of the genetic cargo space, which is an immense opportunity to finetune and extend control over the expression of the TAT-linked molecule through cis-regulatory elements and to have the ability to

express multiple proteins in tandem. An interesting concept is to include means of removing the gene construct as part of the gene itself as a form of reversible gene therapy.

All gene therapies in the clinic today are remarkably simple overexpression constructions with little means of control compared to the various promoters and regulatory elements available in research studies. I would like to highlight an experiment presented by Siprashvili & Khavari in 2004 using a lentiviral vector that contains the erythropoietin (EPO) gene driven by the glucocorticoid regulatory element (GRE) (Siprashvili & Khavari, 2004). Importantly, this GRE-EPO gene construct is placed in tandem with Cre-fused estrogen receptor (Cre-ER) using an internal ribosomal entry sequence (IRES) and flanked by loxP sites. This meant that tamoxifen injection will induce cre-mediated removal of this exact foreign DNA. This viral treatment is injected intradermally into the skin, where topical applications of a glucocorticoid (Clobetasol) can induce expression of EPO for ~1 month. Because the skin has an extensive ability to regenerate itself, it is conceivable that any gene therapy can be totally reversed with the inclusion of an artificial death switch, such as one that have auto-proteolytic activity to release activated caspases after chemical-induced dimerization (CID) of designer molecules that is otherwise biologically inert (Steller, 1998). The GRE-EPO study also highlighted the idea of transducing skin for affecting a distant target (EPO must reach the bone marrow to stimulate red blood cell production). Undoubtedly, TAT-linked peptides can reach the CNS rapidly if expressed by the skin, as intraperineal injections of TAT-C1aB-FitC reach the brain vasculature within 5 minutes (chapter 2) (Yeh *et al.*, 2017). In fact, AAV1 and AAV6 are both effective in transducing skin keratinocytes (Ellis *et al.*, 2013) and can act as the ideal viral vector for this skin-to-CNS treatment concept. With the advent of these novel approaches, future gene therapy may not have to be permanent or even invasive.

Towards the goal of a gene therapy mediated via a TAT-linked peptide, I have attempted to use the chimeric promoter EBS-MRE-2xHRE, which is similar to the EBS-MRE-3xHRE characterized by Lee et al. (Lee *et al.*, 2006), to drive the expression of TAT-C1aB. This plasmid (*pAAV-EBS-MRE-2xHRE-TAT.C1aB*) was found to be neuroprotective in our *in vitro* neuronal culture model (Fig. 24A). However, after injection of the virus (AAV9-EBS-MRE-2xHRE-TAT.C1aB) into the mouse lateral ventricle, the animals inexplicably gained significantly more body weight (Fig. 24B) and exhibited exacerbated infarct size after 50 min MCAO compared to that of the AAV9-CMV-eGFP controls (Fig. 24C). We speculate that the high sensitivity of the chimeric promoter may have led to leak expression and caused long-term systemic effects, such as disrupting the Kv2.1-syntaxin binding in the pancreas, which is known to be important for proper insulin secretion (Greitzer-Antes *et al.*, 2018). Re-construction of this plasmid using the MRE promoter (*4xMRE-TAT.C1aB*) found intrinsic neurotoxicity *in vitro* and was not further pursued *in vivo*. These results are important lessons that while *in vitro* systems can act as surrogates for evaluating cell death mechanisms, it does little to recapitulate the entire animal or reflect the systemic effects of the treatments, which can override any beneficial actions. Nevertheless, because the plasmid cargo itself has been shown to be effective in the many other contexts presented here, I remain optimistic in this approach in future studies.

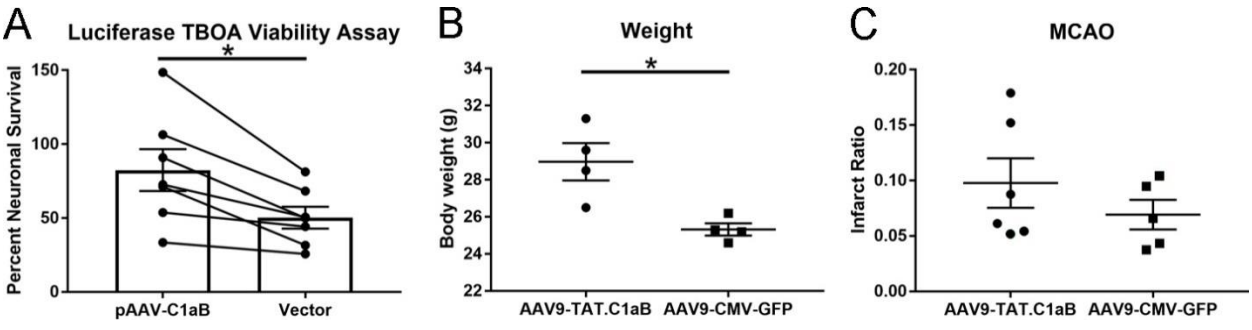

Figure 24. Preliminary evaluation of the gene construct *EBS-MRE-2xHRE-TAT.C1aB*.

A. *In vitro* evaluation of *pAAV-EBS-MRE-2xHRE-TAT.C1aB* found significant neuroprotective actions against overnight applications of 60 uM TBOA. Mean difference in relative luciferase expression ± SEM: 32.14 ± 7.88. *p = 0.0065; paired t-test. N = 7. **B.** *In vivo* infusion of AAV9-EBS-MRE-2xHRE-TAT.C1aB in the mouse brain caused significant weight gain after 3-4 weeks. Mean weight (g) ± SEM: C1aB 28.98 ± 1.0, GFP 25.33 ± 0.33. n = 4 for both groups. Unpaired t-test; *p = 0.0137. C. Mice treated with the experimental virus did not exhibit reduce infarct volume compared with those treated with the control virus. Infarct ratio ± SEM: C1aB 0.098 ± 0.22, GFP 0.069 ± 0.013. n = 6 for C1aB, n = 5 for GFP. Unpaired t-test.

5.6 Closing Remarks

There is an increasing indication of Kv2.1 involvement in several neurodegenerative diseases (McCord & Aizenman, 2014; Shah & Aizenman, 2014; Chao *et al.*, 2018; Yu *et al.*, 2018). As we further understand the role of Kv2.1 in these diseased conditions, it becomes increasingly more important to design and evaluate potential protective agents to target this pathway, such as the three presented here: TAT-C1aB, cpd5, and AAV9-4xMRE-NS5A.eGFP. As these experiments moved forward, we recruited more collaborators and incorporated highly interdisciplinary approaches to reach our goals. I believe this is the case for all translational research today and will be reflected in an increase in the sophistication and the effectiveness of future clinical treatments. I would like to lastly remark that the availability of genomic tools and viral vectors are increasing in a spectacular rate. Together with the increasing understanding of constructing properly regulated gene elements, this technology may one day become a customizable retail product for the layperson to both design and administer.

Bibliography

Aarts, M., Liu, Y., Liu, L., Besshoh, S., Arundine, M., Gurd, J.W., Wang, Y.T., Salter, M.W. & Tymianski, M. (2002) Treatment of ischemic brain damage by perturbing NMDA receptor-PSD-95 protein interactions. *Science (New York, N.Y.)*, 298, 846-850.

Aizenman, E., Hartnett, K.A. & Reynolds, I.J. (1990) Oxygen free radicals regulate NMDA receptor function via a redox modulatory site. *Neuron*, 5, 841-846.

Aizenman, E., Stout, A.K., Hartnett, K.A., Dineley, K.E., McLaughlin, B. & Reynolds, I.J. (2000) Induction of neuronal apoptosis by thiol oxidation: putative role of intracellular zinc release. *Journal of neurochemistry*, 75, 1878-1888.

Al-Zaidy, S., Pickard, A.S., Kotha, K., Alfano, L.N., Lowes, L., Paul, G., Church, K., Lehman, K., Sproule, D.M., Dabbous, O., Maru, B., Berry, K., Arnold, W.D., Kissel, J.T., Mendell, J.R. & Shell, R. (2019) Health outcomes in spinal muscular atrophy type 1 following AVXS-101 gene replacement therapy. *Pediatric pulmonology*, 54, 179-185.

Allen, J.W., Eldadah, B.A., Huang, X., Knoblach, S.M. & Faden, A.I. (2001) Multiple caspases are involved in β-amyloid-induced neuronal apoptosis. *Journal of neuroscience research*, 65, 45-53.

Amako, Y., Igloi, Z., Mankouri, J., Kazlauskas, A., Saksela, K., Dallas, M., Peers, C. & Harris, M. (2013) Hepatitis C virus NS5A inhibits mixed lineage kinase 3 to block apoptosis. *Journal of Biological Chemistry*, 288, 24753-24763.

Andreini, C., Banci, L., Bertini, I. & Rosato, A. (2006) Counting the zinc-proteins encoded in the human genome. *Journal of proteome research*, 5, 196-201.

Aras, M., Hartnett, K. & Aizenman, E. (2008) Assessment of cell viability in primary neuronal cultures. *Current protocols in neuroscience/editorial board, Jacqueline N. Crawley...[et al.]*, Unit 7.18.

Aras, M.A. & Aizenman, E. (2005) Obligatory role of ASK1 in the apoptotic surge of K+ currents. *Neurosci Lett*, 387, 136-140.

Aras, M.A., Hara, H., Hartnett, K.A., Kandler, K. & Aizenman, E. (2009a) Protein kinase C regulation of neuronal zinc signaling mediates survival during preconditioning. *J Neurochem*, 110, 106-117.

Aras, M.A., Hartnett, K.A. & Aizenman, E. (2001) Assessment of Cell Viability in Primary Neuronal Cultures *Current Protocols in Neuroscience*. John Wiley & Sons, Inc.

Aras, M.A., Saadi, R.A. & Aizenman, E. (2009b) Zn2+ regulates Kv2. 1 voltage-dependent gating and localization following ischemia. *European Journal of Neuroscience*, 30, 2250-2257.

Aschauer, D.F., Kreuz, S. & Rumpel, S. (2013) Analysis of transduction efficiency, tropism and axonal transport of AAV serotypes 1, 2, 5, 6, 8 and 9 in the mouse brain. *PloS one*, 8, e76310.

Bach, A., Clausen, B.H., Møller, M., Vestergaard, B., Chi, C.N., Round, A., Sørensen, P.L., Nissen, K.B., Kastrup, J.S. & Gajhede, M. (2012) A high-affinity, dimeric inhibitor of PSD-95 bivalently interacts with PDZ1-2 and protects against ischemic brain damage. *Proceedings of the National Academy of Sciences*, 109, 3317-3322.

Ballarin, B. & Tymianski, M. (2018) Discovery and development of NA-1 for the treatment of acute ischemic stroke. *Acta Pharmacologica Sinica*.

Batey, A.J. & Coker, S.J. (2002) Proarrhythmic potential of halofantrine, terfenadine and clofilium in a modified in vivo model of torsade de pointes. *British journal of pharmacology*, 135, 1003-1012.

Berendsen, H.J., Postma, J.v., van Gunsteren, W.F., DiNola, A. & Haak, J. (1984) Molecular dynamics with coupling to an external bath. *The Journal of chemical physics*, 81, 3684-3690.

Bessis, N., GarciaCozar, F.J. & Boissier, M.C. (2004) Immune responses to gene therapy vectors: influence on vector function and effector mechanisms. *Gene Ther*, 11 Suppl 1, S10-17.

Bierbower, S.M., Choveau, F.S., Lechleiter, J.D. & Shapiro, M.S. (2015) Augmentation of M-type (KCNQ) potassium channels as a novel strategy to reduce stroke-induced brain injury. *The Journal of Neuroscience*, 35, 2101-2111.

Blitzblau, R., Gupta, S., Djali, S., Robinson, M.B. & Rosenberg, P.A. (1996) The glutamate transport inhibitor L-trans-pyrrolidine-2,4-dicarboxylate indirectly evokes NMDA receptor mediated neurotoxicity in rat cortical cultures. *Eur J Neurosci*, 8, 1840-1852.

Bocksteins, E. (2016) Kv5, Kv6, Kv8, and Kv9 subunits: No simple silent bystanders. *The Journal of general physiology*, 147, 105-125.

Bonaventura, P., Benedetti, G., Albarède, F. & Miossec, P. (2015) Zinc and its role in immunity and inflammation. *Autoimmunity reviews*, 14, 277-285.

Bonfoco, E., Krainc, D., Ankarcrona, M., Nicotera, P. & Lipton, S.A. (1995) Apoptosis and necrosis: two distinct events induced, respectively, by mild and intense insults with N-methyl-D-aspartate or nitric oxide/superoxide in cortical cell cultures. *Proceedings of the National Academy of Sciences*, 92, 7162-7166.

Bortner, C.D. & Cidlowski, J.A. (2002) Apoptotic volume decrease and the incredible shrinking cell. Nature Publishing Group.

Bortner, C.D. & Cidlowski, J.A. (2007) Cell shrinkage and monovalent cation fluxes: role in apoptosis. *Archives of Biochemistry and Biophysics*, 462, 176-188.

Bortner, C.D., Gómez-Angelats, M. & Cidlowski, J.A. (2001) Plasma membrane depolarization without repolarization is an early molecular event in anti-Fas-induced apoptosis. *Journal of Biological Chemistry*, 276, 4304-4314.

Bossy-Wetzel, E., Talantova, M.V., Lee, W.D., Schölzke, M.N., Harrop, A., Mathews, E., Götz, T., Han, J., Ellisman, M.H. & Perkins, G.A. (2004) Crosstalk between nitric oxide and zinc pathways to neuronal cell death involving mitochondrial dysfunction and p38-activated K+ channels. *Neuron*, 41, 351-365.

Bratosin, D., Estaquier, J., Petit, F., Arnoult, D., Quatannens, B., Tissier, J., Slomianny, C., Sartiaux, C., Alonso, C. & Huart, J. (2001) Programmed cell death in mature erythrocytes: a model for investigating death effector pathways operating in the absence of mitochondria. *Cell death and differentiation*, 8, 1143.

Bretón, R.R. & Rodríguez, J.C.G. (2012) Excitotoxicity and oxidative stress in acute ischemic stroke. *stroke*, 8, 9.

Brittain, J.M., Chen, L., Wilson, S.M., Brustovetsky, T., Gao, X., Ashpole, N.M., Molosh, A.I., You, H., Hudmon, A. & Shekhar, A. (2011a) Neuroprotection against traumatic brain injury by a peptide derived from the collapsin response mediator protein 2 (CRMP2). *Journal of Biological Chemistry*, 286, 37778-37792.

Brittain, J.M., Duarte, D.B., Wilson, S.M., Zhu, W., Ballard, C., Johnson, P.L., Liu, N., Xiong, W., Ripsch, M.S., Wang, Y., Fehrenbacher, J.C., Fitz, S.D., Khanna, M., Park, C.K., Schmutzler, B.S., Cheon, B.M., Due, M.R., Brustovetsky, T., Ashpole, N.M., Hudmon, A., Meroueh, S.O., Hingtgen, C.M., Brustovetsky, N., Ji, R.R., Hurley, J.H., Jin, X., Shekhar, A., Xu, X.M., Oxford, G.S., Vasko, M.R., White, F.A. & Khanna, R. (2011b) Suppression of inflammatory and neuropathic pain by uncoupling CRMP-2 from the presynaptic Ca(2)(+) channel complex. *Nat Med*, 17, 822-829.

Brittain, J.M., Pan, R., You, H., Brustovetsky, T., Brustovetsky, N., Zamponi, G.W., Lee, W.H. & Khanna, R. (2012a) Disruption of NMDAR-CRMP-2 signaling protects against focal cerebral ischemic damage in the rat middle cerebral artery occlusion model. *Channels (Austin)*, 6, 52-59.

Brittain, J.M., Piekarz, A.D., Wang, Y., Kondo, T., Cummins, T.R. & Khanna, R. (2009) An atypical role for collapsin response mediator protein 2 (CRMP-2) in neurotransmitter release via interaction with presynaptic voltage-gated calcium channels. *Journal of Biological Chemistry*, 284, 31375-31390.

Brittain, M.K., Brustovetsky, T., Sheets, P.L., Brittain, J.M., Khanna, R., Cummins, T.R. & Brustovetsky, N. (2012b) Delayed calcium dysregulation in neurons requires both the NMDA receptor and the reverse Na+/Ca2+ exchanger. *Neurobiol Dis*, 46, 109-117.

Burkhardt, P., Hattendorf, D.A., Weis, W.I. & Fasshauer, D. (2008) Munc18a controls SNARE assembly through its interaction with the syntaxin N-peptide. *The EMBO journal*, 27, 923-933.

Caccamo, A., Branca, C., Piras, I.S., Ferreira, E., Huentelman, M.J., Liang, W.S., Readhead, B., Dudley, J.T., Spangenberg, E.E. & Green, K.N. (2017) Necroptosis activation in Alzheimer's disease. *Nature neuroscience*, 20, 1236.

Cain, K., Langlais, C., Sun, X.-M., Brown, D.G. & Cohen, G.M. (2001) Physiological concentrations of K+ inhibit cytochrome c-dependent formation of the apoptosome. *Journal of Biological Chemistry*, 276, 41985-41990.

Calhoun, J.D., Vanoye, C.G., Kok, F., George, A.L. & Kearney, J.A. (2017) Characterization of a KCNB1 variant associated with autism, intellectual disability, and epilepsy. *Neurology Genetics*, 3, e198.

Case, D.A., Babin, V., Berryman, J., Betz, R., Cai, Q., Cerutti, D., Cheatham Iii, T., Darden, T., Duke, R. & Gohlke, H. (2014) Amber 14.

Cerda, O. & Trimmer, J.S. (2011) Activity-dependent phosphorylation of neuronal Kv2.1 potassium channels by CDK5. *The Journal of biological chemistry*, 286, 28738-28748.

Chao, R.Y., Cheng, C.H., Wu, S.N. & Chen, P.C. (2018) Defective trafficking of Kv2. 1 channels in MPTP-induced nigrostriatal degeneration. *Journal of neurochemistry*, 144, 483-497.

Chen, X. & Wang, K. (2016) The fate of medications evaluated for ischemic stroke pharmacotherapy over the period 1995–2015. *Acta Pharmaceutica Sinica B*, 6, 522-530

Chi, H., Chang, H.-Y. & Sang, T.-K. (2018) Neuronal cell death mechanisms in major neurodegenerative diseases. *International journal of molecular sciences*, 19, 3082.

Chi, X.X. & Xu, Z.C. (2000) Differential changes of potassium currents in CA1 pyramidal neurons after transient forebrain ischemia. *Journal of neurophysiology*, 84, 2834-2843.

Choi, B.-Y., Kim, H.-Y., Lee, K.-H., Cho, Y.-H. & Kong, G. (1999) Clofilium, a potassium channel blocker, induces apoptosis of human promyelocytic leukemia (HL-60) cells via Bcl-2-insensitive activation of caspase-3. *Cancer letters*, 147, 85-93.

Choi, D.W. (1987) Ionic dependence of glutamate neurotoxicity. *Journal of Neuroscience*, 7, 369-379.

Choudhury, S.R., Hudry, E., Maguire, C.A., Sena-Esteves, M., Breakefield, X.O. & Grandi, P. (2017) Viral vectors for therapy of neurologic diseases. *Neuropharmacology*, 120, 63-80.

Cook, D.J., Teves, L. & Tymianski, M. (2012) Treatment of stroke with a PSD-95 inhibitor in the gyrencephalic primate brain. *Nature*, 483, 213-217.

Craddock, T.J., Tuszynski, J.A., Chopra, D., Casey, N., Goldstein, L.E., Hameroff, S.R. & Tanzi, R.E. (2012) The zinc dyshomeostasis hypothesis of Alzheimer's disease. *PloS one*, 7, e33552.

D'Amico, A., Mercuri, E., Tiziano, F.D. & Bertini, E. (2011) Spinal muscular atrophy. *Orphanet Journal of Rare Diseases*, 6, 71.

Danysz, W. & Parsons, C.G. (2003) The NMDA receptor antagonist memantine as a symptomatological and neuroprotective treatment for Alzheimer's disease: preclinical evidence. *International journal of geriatric psychiatry*, 18, S23-S32.

Deb, A., Thornton, J.D., Sambamoorthi, U. & Innes, K. (2017) Direct and indirect cost of managing Alzheimer's disease and related dementias in the United States. *Expert review of pharmacoeconomics & outcomes research*, 17, 189-202.

Deverman, B.E., Pravdo, P.L., Simpson, B.P., Kumar, S.R., Chan, K.Y., Banerjee, A., Wu, W.L., Yang, B., Huber, N., Pasca, S.P. & Gradinaru, V. (2016) Cre-dependent selection yields AAV variants for widespread gene transfer to the adult brain. *Nature biotechnology*, 34, 204-209.

Dong, X., Milholland, B. & Vijg, J. (2016) Evidence for a limit to human lifespan. *Nature*, 538, 257.

Ebadi, M., Iversen, P., Hao, R., Cerutis, D., Rojas, P., Happe, H., Murrin, L. & Pfeiffer, R. (1995) Expression and regulation of brain metallothionein. *Neurochemistry international*, 27, 1-22.

Editorial, N.N. (2018) Focus on neurodegenerative disease. *Nature Neuroscience*, 21, 1293-1293.

Elliot, J. & Higgins, C. (2003) IKCa1 activity is required for cell shrinkage, phosphatidylserine translocation and death in T lymphocytes apoptosis. *EMBO Rep*, 4, 189-194.

Ellis, B.L., Hirsch, M.L., Barker, J.C., Connelly, J.P., Steininger, R.J., 3rd & Porteus, M.H. (2013) A survey of ex vivo/in vitro transduction efficiency of mammalian primary cells and cell lines with Nine natural adeno-associated virus (AAV1-9) and one engineered adeno-associated virus serotype. *Virol J*, 10, 74.

Elmore, S. (2007) Apoptosis: a review of programmed cell death. *Toxicologic pathology*, 35, 495-516.

Feinshreiber, L., Singer-Lahat, D., Friedrich, R., Matti, U., Sheinin, A., Yizhar, O., Nachman, R., Chikvashvili, D., Rettig, J. & Ashery, U. (2010) Non-conducting function of the Kv2. 1 channel enables it to recruit vesicles for release in neuroendocrine and nerve cells. *J Cell Sci*, 123, 1940-1947.

Foust, K.D., Wang, X., McGovern, V.L., Braun, L., Bevan, A.K., Haidet, A.M., Le, T.T., Morales, P.R., Rich, M.M., Burghes, A.H. & Kaspar, B.K. (2010) Rescue of the spinal muscular atrophy phenotype in a mouse model by early postnatal delivery of SMN. *Nature biotechnology*, 28, 271-274.

Fox, P.D., Haberkorn, C.J., Akin, E.J., Seel, P.J., Krapf, D. & Tamkun, M.M. (2015) Induction of stable ER–plasma-membrane junctions by Kv2. 1 potassium channels. *J Cell Sci*, 128, 2096-2105.

Fox, P.D., Loftus, R.J. & Tamkun, M.M. (2013) Regulation of Kv2. 1 K+ conductance by cell surface channel density. *Journal of Neuroscience*, 33, 1259-1270.

Franco, R., Bortner, C. & Cidlowski, J. (2006) Potential roles of electrogenic ion transport and plasma membrane depolarization in apoptosis. *The Journal of membrane biology*, 209, 43-58.

Francois-Moutal, L., Dustrude, E.T., Wang, Y., Brustovetsky, T., Dorame, A., Ju, W., Moutal, A., Perez-Miller, S., Brustovetsky, N., Gokhale, V., Khanna, M. & Khanna, R. (2018) Inhibition of the Ubc9 E2 SUMO-conjugating enzyme-CRMP2 interaction decreases NaV1.7 currents and reverses experimental neuropathic pain. *Pain*, 159, 2115-2127.

Frank, R. (2002) The SPOT-synthesis technique: synthetic peptide arrays on membrane supports—principles and applications. *Journal of immunological methods*, 267, 13-26.

Frank, R., Güler, S., Krause, S. & Lindenmaier, W. (1990) Facile and rapid "spot-synthesis" of large numbers of peptides on membrane sheets. *Peptides*, 2, 151-152.

Frazzini, V., Guarnieri, S., Bomba, M., Navarra, R., Morabito, C., Mariggiò, M. & Sensi, S. (2016) Altered Kv2. 1 functioning promotes increased excitability in hippocampal neurons of an Alzheimer's disease mouse model. *Cell death & disease*, 7, e2100.

Fueta, Y. & Avoli, M. (1993) Tetraethylammonium-induced epileptiform activity in young and adult rat hippocampus. *Developmental brain research*, 72, 51-58.

Galasso, S.L. & Dyck, R.H. (2007) The role of zinc in cerebral ischemia. *Molecular medicine*, 13, 380-387.

Ginn, S.L., Amaya, A.K., Alexander, I.E., Edelstein, M. & Abedi, M.R. (2018) Gene therapy clinical trials worldwide to 2017: An update. *The journal of gene medicine*, 20, e3015.

Glinka, Y., Gassen, M. & Youdim, M.B. (1997) Mechanism of 6-hydroxydopamine neurotoxicity. *Journal of neural transmission. Supplementum*, 50, 55-66.

Götz, A.W., Williamson, M.J., Xu, D., Poole, D., Le Grand, S. & Walker, R.C. (2012) Routine microsecond molecular dynamics simulations with AMBER on GPUs. 1. Generalized born. *Journal of chemical theory and computation*, 8, 1542-1555.

Graham, A.J. (1950) Toxic Effects of Tetraethylammonium Bromide. *British medical journal*, 2, 321.

Granzotto, A. & Sensi, S.L. (2015) Intracellular zinc is a critical intermediate in the excitotoxic cascade. *Neurobiology of disease*, 81, 25-37.

Gray, J.T. & Zolotukhin, S. (2012) Design and construction of functional AAV vectors *Adeno-Associated Virus*. Springer, pp. 25-46.

Greitzer-Antes, D., Xie, L., Qin, T., Xie, H., Zhu, D., Dolai, S., Liang, T., Kang, F., Hardy, A.B. & He, Y. (2018) Kv2. 1 clusters on β-cell plasma membrane act as reservoirs that replenish pools of newcomer insulin granule through their interaction with syntaxin-3. *Journal of Biological Chemistry*, jbc. RA118. 002703.

Gribkoff, V.K. & Kaczmarek, L.K. (2017) The need for new approaches in CNS drug discovery: why drugs have failed, and what can be done to improve outcomes. *Neuropharmacology*, 120, 11-19.

Grimm, D. & Zolotukhin, S. (2015) E Pluribus Unum: 50 Years of Research, Millions of Viruses, and One Goal--Tailored Acceleration of AAV Evolution. *Molecular therapy : the journal of the American Society of Gene Therapy*, 23, 1819-1831.

Hartnett, K., Stout, A., Rajdev, S., Rosenberg, P., Reynolds, I. & Aizenman, E. (1997) NMDA receptor-mediated neurotoxicity: a paradoxical requirement for extracellular Mg2+ in Na+/Ca2+-free solutions in rat cortical neurons in vitro. *Journal of neurochemistry*, 68, 1836-1845.

He, K., McCord, M.C., Hartnett, K.A. & Aizenman, E. (2015) Regulation of pro-apoptotic phosphorylation of Kv2. 1 K+ channels. *PloS one*, 10, e0129498.

He, W., Goodkind, D. & Kowal, P.R. (2016) *An aging world: 2015*. United States Census Bureau Washington, DC.

He, Y., Staschke, K.A. & Tan, S.-L. (2006) HCV NS5A: a multifunctional regulator of cellular pathways and virus replication. *Hepatitis C viruses: genomes and molecular biology*, 267-292.

Hessler, J.A., Budor, A., Putchakayala, K., Mecke, A., Rieger, D., Banaszak Holl, M.M., Orr, B.G., Bielinska, A., Beals, J. & Baker, J. (2005) Atomic force microscopy study of early morphological changes during apoptosis. *Langmuir*, 21, 9280-9286.

Hill, M.D., Martin, R.H., Mikulis, D., Wong, J.H., Silver, F.L., Milot, G., Clark, W.M., MacDonald, R.L., Kelly, M.E. & Boulton, M. (2012) Safety and efficacy of NA-1 in patients with iatrogenic stroke after endovascular aneurysm repair (ENACT): a phase 2, randomised, double-blind, placebo-controlled trial. *The Lancet Neurology*, 11, 942-950.

Hughes, F.M., Bortner, C.D., Purdy, G.D. & Cidlowski, J.A. (1997) Intracellular K+ suppresses the activation of apoptosis in lymphocytes. *Journal of Biological Chemistry*, 272, 30567-30576.

Hughes, F.M., Jr. & Cidlowski, J.A. (1999) Potassium is a critical regulator of apoptotic enzymes in vitro and in vivo. *Adv Enzyme Regul*, 39, 157-171.

Irwin, J.J. & Shoichet, B.K. (2005) ZINC− A free database of commercially available compounds for virtual screening. *Journal of chemical information and modeling*, 45, 177-182.

Iwaki, M., Mizobuchi, S., Nakaya, Y., Kawano, K., Niki, T. & Mori, H. (1987) Tetraethylammonium induced coronary spasm in isolated perfused rabbit heart: a hypothesis for the mechanism of coronary spasm. *Cardiovascular research*, 21, 130-139.

Javan, B. & Shahbazi, M. (2017) Hypoxia-inducible tumour-specific promoters as a dual-targeting transcriptional regulation system for cancer gene therapy. *Ecancermedicalscience*, 11, 751.

Jensen, C.S., Watanabe, S., Stas, J.I., Klaphaak, J., Yamane, A., Schmitt, N., Olesen, S.-P., Trimmer, J.S., Rasmussen, H.B. & Misonou, H. (2017) Trafficking of Kv2. 1 Channels to the Axon Initial Segment by a Novel Nonconventional Secretory Pathway. *Journal of Neuroscience*, 37, 11523-11536.

Jiao, J., He, M., Port, S.A., Baker, R.W., Xu, Y., Qu, H., Xiong, Y., Wang, Y., Jin, H. & Eisemann, T.J. (2018) Munc18-1 catalyzes neuronal SNARE assembly by templating SNARE association. *eLife*, 7, e41771.

Jiao, S., Liu, Z., Ren, W.H., Ding, Y., Zhang, Y.Q., Zhang, Z.H. & Mei, Y.A. (2007) cAMP/protein kinase A signalling pathway protects against neuronal apoptosis and is associated with modulation of Kv2. 1 in cerebellar granule cells. *Journal of neurochemistry*, 100, 979-991.

Johnson, B., Leek, A.N., Solé, L., Maverick, E.E., Levine, T.P. & Tamkun, M.M. (2018) Kv2 potassium channels form endoplasmic reticulum/plasma membrane junctions via interaction with VAPA and VAPB. *Proceedings of the National Academy of Sciences*, 115, E7331-E7340.

Jorgensen, W.L., Chandrasekhar, J., Madura, J.D., Impey, R.W. & Klein, M.L. (1983) Comparison of simple potential functions for simulating liquid water. *The Journal of chemical physics*, 79, 926-935.

Joshi, A., Kalappa, B.I., Anderson, C.T. & Tzounopoulos, T. (2016) Cell-specific cholinergic modulation of excitability of layer 5B principal neurons in mouse auditory cortex. *Journal of Neuroscience*, 36, 8487-8499.

Joshi, A., Middleton, J.W., Anderson, C.T., Borges, K., Suter, B.A., Shepherd, G.M. & Tzounopoulos, T. (2015) Cell-specific activity-dependent fractionation of layer 2/3→ 5B excitatory signaling in mouse auditory cortex. *Journal of Neuroscience*, 35, 3112-3123.

Joshi, C.N., Jain, S.K. & Murthy, P.S.R. (2004) An optimized triphenyltetrazolium chloride method for identification of cerebral infarcts. *Brain research protocols*, 13, 11-17.

Justice, J.A., Manjooran, D.T., Yeh, C.-Y., Hartnett-Scott, K.A., Schulien, A.J., Kosobucki, G.J., Mammen, S., Palladino, M.J. & Aizenman, E. (2018) Molecular Neuroprotection Induced by Zinc-Dependent Expression of Hepatitis C–Derived Protein NS5A Targeting Kv2. 1 Potassium Channels. *Journal of Pharmacology and Experimental Therapeutics*, 367, 348-355.

Justice, J.A., Schulien, A.J., He, K., Hartnett, K.A., Aizenman, E. & Shah, N.H. (2017) Disruption of K V 2.1 somato-dendritic clusters prevents the apoptogenic increase of potassium currents. *Neuroscience*, 354, 158-167.

Kambe, T., Tsuji, T., Hashimoto, A. & Itsumura, N. (2015) The physiological, biochemical, and molecular roles of zinc transporters in zinc homeostasis and metabolism. *Physiological reviews*, 95, 749-784.

Kaukinen, P., Sillanpää, M., Kotenko, S., Lin, R., Hiscott, J., Melén, K. & Julkunen, I. (2006) Hepatitis C virus NS2 and NS3/4A proteins are potent inhibitors of host cell cytokine/chemokine gene expression. *Virology journal*, 3, 66.

Kihira, Y., Hermanstyne, T.O. & Misonou, H. (2010) Formation of heteromeric Kv2 channels in mammalian brain neurons. *Journal of Biological Chemistry*, 285, 15048-15055.

Kikuchi, K., Tanaka, E., Murai, Y. & Tancharoen, S. (2014) Clinical trials in acute ischemic stroke. *CNS drugs*, 28, 929-938

Kilic, E., Kilic, U. & Hermann, D.M. (2006) TAT fusion proteins against ischemic stroke: current status and future perspectives. *Front Biosci*, 11, 1716-1721.

Kim, J.-A., Kang, Y.S., Jung, M.-W., Kang, G.-H., Lee, S.H. & Lee, Y.S. (2000) Ca2+ influx mediates apoptosis induced by 4-aminopyridine, a K+ channel blocker, in HepG2 human hepatoblastoma cells. *Pharmacology*, 60, 74-81.

Kirmiz, M., Vierra, N.C., Palacio, S. & Trimmer, J.S. (2018) Identification of VAPA and VAPB as Kv2 channel-interacting proteins defining endoplasmic reticulum–plasma membrane junctions in mammalian brain neurons. *Journal of Neuroscience*, 38, 7562-7584.

Kjaergaard, M. & Kragelund, B.B. (2017) Functions of intrinsic disorder in transmembrane proteins. *Cellular and Molecular Life Sciences*, 74, 3205-3224.

Knoch, M.E., Hartnett, K.A., Hara, H., Kandler, K. & Aizenman, E. (2008) Microglia induce neurotoxicity via intraneuronal Zn2+ release and a K+ current surge. *Glia*, 56, 89-96.

Koeberle, P. & Schlichter, L.C. (2010) Targeting KV channels rescues retinal ganglion cells in vivo directly and by reducing inflammation. *Channels*, 4, 337-346.

Koes, D.R., Baumgartner, M.P. & Camacho, C.J. (2013) Lessons learned in empirical scoring with smina from the CSAR 2011 benchmarking exercise. *Journal of chemical information and modeling*, 53, 1893-1904.

Koes, D.R. & Camacho, C.J. (2012) ZINCPharmer: pharmacophore search of the ZINC database. *Nucleic acids research*, 40, W409-W414.

Koh, J.-Y., Suh, S.W., Gwag, B.J., He, Y.Y., Hsu, C.Y. & Choi, D.W. (1996) The role of zinc in selective neuronal death after transient global cerebral ischemia. *Science (New York, N.Y.)*, 272, 1013-1016.

Koh, J.Y. & Choi, D.W. (1987) Quantitative determination of glutamate mediated cortical neuronal injury in cell culture by lactate dehydrogenase efflux assay. *Journal of neuroscience methods*, 20, 83-90.

Krosl, J., Austin, P., Beslu, N., Kroon, E., Humphries, R.K. & Sauvageau, G. (2003) In vitro expansion of hematopoietic stem cells by recombinant TAT-HOXB4 protein. *Nature medicine*, 9, 1428-1432.

Kruczek, C., Görg, B., Keitel, V., Pirev, E., Kröncke, K.D., Schliess, F. & Häussinger, D. (2009) Hypoosmotic swelling affects zinc homeostasis in cultured rat astrocytes. *Glia*, 57, 79-92.

Lang, F., Lang, K.S., Wieder, T., Myssina, S., Birka, C., Lang, P.A., Kaiser, S., Kempe, D., Duranton, C. & Huber, S.M. (2003) Cation channels, cell volume and the death of an erythrocyte. *Pflügers Archiv*, 447, 121-125.

Langmade, S.J., Ravindra, R., Daniels, P.J. & Andrews, G.K. (2000) The transcription factor MTF-1 mediates metal regulation of the mouse ZnT1 gene. *Journal of Biological Chemistry*, 275, 34803-34809.

Leary, S., Underwood, W., Anthony, R., Cartner, S., Corey, D., Grandin, T., Greenacre, C.B., Gwaltney-Bran, S., McCrackin, M.A. & Meyer, R. (2013) AVMA guidelines for the euthanasia of animals: 2013 edition.

Lee, J., Lee, Y., Kim, J., Kim, K., Lee, J., Jang, H., Shin, I., Suh, W., Jeon, E. & Byun, J. (2006) A novel chimeric promoter that is highly responsive to hypoxia and metals. *Gene therapy*, 13, 857.

Leist, M. & Nicotera, P. (1998) Apoptosis, excitotoxicity, and neuropathology. *Exp Cell Res*, 239, 183-201.

Leone, P., Shera, D., McPhee, S.W., Francis, J.S., Kolodny, E.H., Bilaniuk, L.T., Wang, D.J., Assadi, M., Goldfarb, O., Goldman, H.W., Freese, A., Young, D., During, M.J., Samulski, R.J. & Janson, C.G. (2012) Long-term follow-up after gene therapy for canavan disease. *Science translational medicine*, 4, 165ra163.

Leung, Y.M., Kang, Y., Gao, X., Xia, F., Xie, H., Sheu, L., Tsuk, S., Lotan, I., Tsushima, R.G. & Gaisano, H.Y. (2003) Syntaxin 1A binds to the cytoplasmic C terminus of Kv2. 1 to regulate channel gating and trafficking. *Journal of Biological Chemistry*, 278, 17532-17538.

Lim, S.T., Antonucci, D.E., Scannevin, R.H. & Trimmer, J.S. (2000) A novel targeting signal for proximal clustering of the Kv2. 1 K+ channel in hippocampal neurons. *Neuron*, 25, 385-397.

Liu, Z., Zhou, T., Ziegler, A.C., Dimitrion, P. & Zuo, L. (2017) Oxidative stress in neurodegenerative diseases: from molecular mechanisms to clinical applications. *Oxidative medicine and cellular longevity*, 2017.

Loncharich, R.J., Brooks, B.R. & Pastor, R.W. (1992) Langevin dynamics of peptides: The frictional dependence of isomerization rates of N-acetylalanyl-N′-methylamide. *Biopolymers: Original Research on Biomolecules*, 32, 523-535.

Longa, E.Z., Weinstein, P.R., Carlson, S. & Cummins, R. (1989) Reversible middle cerebral artery occlusion without craniectomy in rats. *stroke*, 20, 84-91.

Love, R.A., Brodsky, O., Hickey, M.J., Wells, P.A. & Cronin, C.N. (2009) Crystal structure of a novel dimeric form of NS5A domain I protein from hepatitis C virus. *Journal of virology*, 83, 4395-4403.

Lvov, A., Chikvashvili, D., Michaelevski, I. & Lotan, I. (2008) VAMP2 interacts directly with the N terminus of Kv2. 1 to enhance channel inactivation. *Pflügers Archiv-European Journal of Physiology*, 456, 1121.

Ma, X.C., Liu, P., Zhang, X.L., Jiang, W.H., Jia, M., Wang, C.X., Dong, Y.Y., Dang, Y.H. & Gao, C.G. (2016) Intranasal Delivery of Recombinant AAV Containing BDNF Fused with HA2TAT: a Potential Promising Therapy Strategy for Major Depressive Disorder. *Scientific reports*, 6, 22404.

Macdonald, A., Crowder, K., Street, A., McCormick, C. & Harris, M. (2004) The hepatitis C virus NS5A protein binds to members of the Src family of tyrosine kinases and regulates kinase activity. *Journal of General Virology*, 85, 721-729.

MacDonald, P.E., Wang, G., Tsuk, S., Dodo, C., Kang, Y., Tang, L., Wheeler, M.B., Cattral, M.S., Lakey, J.R. & Salapatek, A.M.F. (2002) Synaptosome-associated protein of 25 kilodaltons modulates Kv2. 1 voltage-dependent K+ channels in neuroendocrine islet β-cells through an interaction with the channel N terminus. *Molecular endocrinology*, 16, 2452-2461.

Maeno, E., Ishizaki, Y., Kanaseki, T., Hazama, A. & Okada, Y. (2000) Normotonic cell shrinkage because of disordered volume regulation is an early prerequisite to apoptosis. *Proceedings of the National Academy of Sciences*, 97, 9487-9492.

Manfredsson, F.P., Rising, A.C. & Mandel, R.J. (2009) AAV9: a potential blood-brain barrier buster. *Molecular therapy : the journal of the American Society of Gene Therapy*, 17, 403-405.

Mankouri, J., Dallas, M.L., Hughes, M.E., Griffin, S.D., Macdonald, A., Peers, C. & Harris, M. (2009) Suppression of a pro-apoptotic K+ channel as a mechanism for hepatitis C virus persistence. *Proceedings of the National Academy of Sciences*, 106, 15903-15908.

Mann, C.L., Bortner, C.D., Jewell, C.M. & Cidlowski, J.A. (2001) Glucocorticoid-induced plasma membrane depolarization during thymocyte apoptosis: association with cell shrinkage and degradation of the Na+/K+-adenosine triphosphatase. *Endocrinology*, 142, 5059-5068.

Maret, W. (2019) The redox biology of redox-inert zinc ions. *Free Radical Biology and Medicine*.

Marini, C., Romoli, M., Parrini, E., Costa, C., Mei, D., Mari, F., Parmeggiani, L., Procopio, E., Metitieri, T. & Cellini, E. (2017) Clinical features and outcome of 6 new patients carrying de novo KCNB1 gene mutations. *Neurology Genetics*, 3, e206.

Marreiro, D., Cruz, K., Morais, J., Beserra, J., Severo, J. & de Oliveira, A. (2017) Zinc and oxidative stress: current mechanisms. *Antioxidants*, 6, 24.

Matthews, K.A., Xu, W., Gaglioti, A.H., Holt, J.B., Croft, J.B., Mack, D. & McGuire, L.C. (2019) Racial and ethnic estimates of Alzheimer's disease and related dementias in the United States (2015–2060) in adults aged≥ 65 years. *Alzheimer's & Dementia*, 15, 17-24.

McCarty, D.M., Fu, H., Monahan, P.E., Toulson, C.E., Naik, P. & Samulski, R.J. (2003) Adeno-associated virus terminal repeat (TR) mutant generates self-complementary vectors to overcome the rate-limiting step to transduction in vivo. *Gene Ther*, 10, 2112-2118.

McCarty, D.M., Young, S.M., Jr. & Samulski, R.J. (2004) Integration of adeno-associated virus (AAV) and recombinant AAV vectors. *Annual review of genetics*, 38, 819-845.

McCord, M.C. & Aizenman, E. (2013) Convergent Ca2+ and Zn2+ signaling regulates apoptotic Kv2. 1 K+ currents. *Proceedings of the National Academy of Sciences*, 110, 13988-13993.

McCord, M.C. & Aizenman, E. (2014) The role of intracellular zinc release in aging, oxidative stress, and Alzheimer's disease. *Frontiers in aging neuroscience*, 6, 77.

McCord, M.C., Kullmann, P.H., He, K., Hartnett, K.A., Horn, J.P., Lotan, I. & Aizenman, E. (2014) Syntaxin-binding domain of Kv2. 1 is essential for the expression of apoptotic K+ currents. *The Journal of physiology*, 592, 3511-3521.

McLaughlin, B., Pal, S., Tran, M.P., Parsons, A.A., Barone, F.C., Erhardt, J.A. & Aizenman, E. (2001) p38 activation is required upstream of potassium current enhancement and caspase cleavage in thiol oxidant-induced neuronal apoptosis. *The Journal of Neuroscience*, 21, 3303-3311.

Medvedeva, Y.V., Ji, S.G., Yin, H.Z. & Weiss, J.H. (2017) Differential Vulnerability of CA1 versus CA3 Pyramidal Neurons After Ischemia: Possible Relationship to Sources of Zn2+ Accumulation and Its Entry into and Prolonged Effects on Mitochondria. *The Journal of neuroscience : the official journal of the Society for Neuroscience*, 37, 726-737.

Meldrum, B.S., Evans, M.C., Swan, J.H. & Simon, R.P. (1987) Protection against hypoxic/ischaemic brain damage with excitatory amino acid antagonists. *Medical biology*, 65, 153-157.

Mendell, J.R., Al-Zaidy, S., Shell, R., Arnold, W.D., Rodino-Klapac, L.R., Prior, T.W., Lowes, L., Alfano, L., Berry, K., Church, K., Kissel, J.T., Nagendran, S., L'Italien, J., Sproule, D.M., Wells, C., Cardenas, J.A., Heitzer, M.D., Kaspar, A., Corcoran, S., Braun, L., Likhite, S., Miranda, C., Meyer, K., Foust, K.D., Burghes, A.H.M. & Kaspar, B.K. (2017) Single-Dose Gene-Replacement Therapy for Spinal Muscular Atrophy. *The New England journal of medicine*, 377, 1713-1722.

Michaelevski, I., Chikvashvili, D., Tsuk, S., Singer-Lahat, D., Kang, Y., Linial, M., Gaisano, H.Y., Fili, O. & Lotan, I. (2003) Direct interaction of target SNAREs with the Kv2.1 channel. Modal regulation of channel activation and inactivation gating. *J Biol Chem*, 278, 34320-34330.

Misonou, H., Mohapatra, D.P., Menegola, M. & Trimmer, J.S. (2005) Calcium- and metabolic state-dependent modulation of the voltage-dependent Kv2.1 channel regulates neuronal excitability in response to ischemia. *The Journal of neuroscience : the official journal of the Society for Neuroscience*, 25, 11184-11193.

Misonou, H., Mohapatra, D.P., Park, E.W., Leung, V., Zhen, D., Misonou, K., Anderson, A.E. & Trimmer, J.S. (2004) Regulation of ion channel localization and phosphorylation by neuronal activity. *Nat Neurosci*, 7, 711-718.

Misura, K.M., Scheller, R.H. & Weis, W.I. (2000) Three-dimensional structure of the neuronal-Sec1–syntaxin 1a complex. *Nature*, 404, 355.

Mitsios, N., Gaffney, J., Krupinski, J., Mathias, R., Wang, Q., Hayward, S., Rubio, F., Kumar, P., Kumar, S. & Slevin, M. (2007) Expression of signaling molecules associated with apoptosis in human ischemic stroke tissue. *Cell biochemistry and biophysics*, 47, 73-85.

Mohapatra, D.P., Misonou, H., Sheng-Jun, P., Held, J.E., Surmeier, D.J. & Trimmer, J.S. (2009) Regulation of intrinsic excitability in hippocampal neurons by activity-dependent modulation of the KV2. 1 potassium channel. *Channels*, 3, 46-56.

Moutal, A., Wang, Y., Yang, X., Ji, Y., Luo, S., Dorame, A., Bellampalli, S.S., Chew, L.A., Cai, S., Dustrude, E.T., Keener, J.E., Marty, M.T., Vanderah, T.W. & Khanna, R. (2017) Dissecting the role of the CRMP2-neurofibromin complex on pain behaviors. *Pain*, 158, 2203-2221.

Murakoshi, H. & Trimmer, J.S. (1999) Identification of the Kv2. 1 K+ channel as a major component of the delayed rectifier K+ current in rat hippocampal neurons. *Journal of Neuroscience*, 19, 1728-1735.

Murphy, S.L., Xu, J., Kochanek, K.D. & Arias, E. (2018) Mortality in the United States, 2017.

Nathwani, A.C., Tuddenham, E.G., Rangarajan, S., Rosales, C., McIntosh, J., Linch, D.C., Chowdary, P., Riddell, A., Pie, A.J. & Harrington, C. (2011) Adenovirus-associated virus vector–mediated gene transfer in hemophilia B. *New England Journal of Medicine*, 365, 2357-2365.

Nattel, S. (2008) Delayed-rectifier potassium currents and the control of cardiac repolarization: Noble and Tsien 40 years after. *The Journal of physiology*, 586, 5849-5852.

Nobel, C.S.I., Aronson, J.K., Van Den Dobbelsteen, D.J. & Slater, A.F. (2000) Inhibition of Na+/K+-ATPase may be one mechanism contributing to potassium efflux and cell shrinkage in CD95-induced apoptosis. *Apoptosis*, 5, 153-163.

Norris, C.A., He, K., Springer, M.G., Hartnett, K.A., Horn, J.P. & Aizenman, E. (2012) Regulation of neuronal proapoptotic potassium currents by the hepatitis C virus nonstructural protein 5A. *Journal of Neuroscience*, 32, 8865-8870.

O'Connell, K.M., Loftus, R. & Tamkun, M.M. (2010) Localization-dependent activity of the Kv2. 1 delayed-rectifier K+ channel. *Proceedings of the National Academy of Sciences*, 107, 12351-12356.

O'Connell, K.M., Rolig, A.S., Whitesell, J.D. & Tamkun, M.M. (2006) Kv2. 1 potassium channels are retained within dynamic cell surface microdomains that are defined by a perimeter fence. *Journal of Neuroscience*, 26, 9609-9618.

Obulesu, M. & Lakshmi, M.J. (2014) Apoptosis in Alzheimer's disease: an understanding of the physiology, pathology and therapeutic avenues. *Neurochemical research*, 39, 2301-2312.

Ottschytsch, N., Raes, A., Van Hoorick, D. & Snyders, D. (2002) Obligatory heterotetramerization of three previously uncharacterized Kv channel α-subunits identified in the human genome. *Proceedings of the National Academy of Sciences*, 99, 7986-7991.

Ovbiagele, B., Goldstein, L.B., Higashida, R.T., Howard, V.J., Johnston, S.C., Khavjou, O.A., Lackland, D.T., Lichtman, J.H., Mohl, S. & Sacco, R.L. (2013) Forecasting the future of stroke in the United States: a policy statement from the American Heart Association and American Stroke Association. *Stroke*, 44, 2361-2375.

Pabon, N.A. & Camacho, C.J. (2017) Probing protein flexibility reveals a mechanism for selective promiscuity. *Elife*, 6, e22889.

Pachori, A.S., Melo, L.G., Hart, M.L., Noiseux, N., Zhang, L., Morello, F., Solomon, S.D., Stahl, G.L., Pratt, R.E. & Dzau, V.J. (2004) Hypoxia-regulated therapeutic gene as a preemptive treatment strategy against ischemia/reperfusion tissue injury. *Proceedings of the National Academy of Sciences*, 101, 12282-12287.

Pal, S., Hartnett, K.A., Nerbonne, J.M., Levitan, E.S. & Aizenman, E. (2003) Mediation of neuronal apoptosis by Kv2. 1-encoded potassium channels. *Journal of Neuroscience*, 23, 4798-4802.

Pal, S., Takimoto, K., Aizenman, E. & Levitan, E.S. (2006) Apoptotic surface delivery of K+ channels. *Cell Death & Differentiation*, 13, 661-667.

Park, K.-S., Mohapatra, D.P., Misonou, H. & Trimmer, J.S. (2006) Graded regulation of the Kv2. 1 potassium channel by variable phosphorylation. *Science (New York, N.Y.)*, 313, 976-979.

Peltola, M.A., Kuja-Panula, J., Lauri, S.E., Taira, T. & Rauvala, H. (2011) AMIGO is an auxiliary subunit of the Kv2.1 potassium channel. *EMBO Rep*, 12, 1293-1299.

Perry, V.H., Nicoll, J.A. & Holmes, C. (2010) Microglia in neurodegenerative disease. *Nature Reviews Neurology*, 6, 193.

Pologruto, T.A., Sabatini, B.L. & Svoboda, K. (2003) ScanImage: Flexible software for operating laser scanning microscopes. *BioMedical Engineering OnLine*, 2, 13.

Portbury, S. & Adlard, P. (2017) Zinc signal in brain diseases. *International journal of molecular sciences*, 18, 2506.

Prentice, H., Bishopric, N.H., Hicks, M.N., Discher, D.J., Wu, X., Wylie, A.A. & Webster, K.A. (1997) Regulated expression of a foreign gene targeted to the ischaemic myocardium. *Cardiovascular research*, 35, 567-574.

Quillinan, N., Herson, P.S. & Traystman, R.J. (2016) Neuropathophysiology of Brain Injury. *Anesthesiology clinics*, 34, 453-464.

Radak, D., Katsiki, N., Resanovic, I., Jovanovic, A., Sudar-Milovanovic, E., Zafirovic, S., A Mousad, S. & R Isenovic, E. (2017) Apoptosis and acute brain ischemia in ischemic stroke. *Current vascular pharmacology*, 15, 115-122.

Radtke, F., Heuchel, R., Georgiev, O., Hergersberg, M., Gariglio, M., Dembic, Z. & Schaffner, W. (1993) Cloned transcription factor MTF-1 activates the mouse metallothionein I promoter. *The EMBO journal*, 12, 1355-1362.

Redman, P.T., Hartnett, K.A., Aras, M.A., Levitan, E.S. & Aizenman, E. (2009) Regulation of apoptotic potassium currents by coordinated zinc-dependent signalling. *The Journal of physiology*, 587, 4393-4404.

Redman, P.T., He, K., Hartnett, K.A., Jefferson, B.S., Hu, L., Rosenberg, P.A., Levitan, E.S. & Aizenman, E. (2007) Apoptotic surge of potassium currents is mediated by p38 phosphorylation of Kv2. 1. *Proceedings of the National Academy of Sciences*, 104, 3568-3573.

Redman, P.T., Jefferson, B.S., Ziegler, C.B., Mortensen, O.V., Torres, G.E., Levitan, E.S. & Aizenman, E. (2006) A vital role for voltage-dependent potassium channels in dopamine transporter-mediated 6-hydroxydopamine neurotoxicity. *Neuroscience*, 143, 1-6.

Repantis, D., Laisney, O. & Heuser, I. (2010) Acetylcholinesterase inhibitors and memantine for neuroenhancement in healthy individuals: a systematic review. *Pharmacological research*, 61, 473-481.

Reynolds, I.J., Rush, E.A. & Aizenman, E. (1990) Reduction of NMDA receptors with dithiothreitol increases [3H]-MK-801 binding and NMDA-induced Ca2+ fluxes. *Br J Pharmacol*, 101, 178-182.

Rohn, T.T. & Head, E. (2009) Caspases as therapeutic targets in Alzheimer's disease: is it time to "cut" to the chase? *International journal of clinical and experimental pathology*, 2, 108.

Romer, S.H., Deardorff, A.S. & Fyffe, R.E. (2016) Activity-dependent redistribution of Kv2.1 ion channels on rat spinal motoneurons. *Physiological reports*, 4.

Ross-Thriepland, D. & Harris, M. (2015) Hepatitis C virus NS5A: enigmatic but still promiscuous 10 years on! *Journal of General Virology*, 96, 727-738.

Ruttkay-Nedecky, B., Nejdl, L., Gumulec, J., Zitka, O., Masarik, M., Eckschlager, T., Stiborova, M., Adam, V. & Kizek, R. (2013) The role of metallothionein in oxidative stress. *International journal of molecular sciences*, 14, 6044-6066.

Ryckaert, J.-P., Ciccotti, G. & Berendsen, H.J. (1977) Numerical integration of the cartesian equations of motion of a system with constraints: molecular dynamics of n-alkanes. *Journal of Computational Physics*, 23, 327-341.

Sattler, R. & Tymianski, M. (2001) Molecular mechanisms of glutamate receptor-mediated excitotoxic neuronal cell death. *Molecular neurobiology*, 24, 107-129.

Schrodinger (2010) The PyMOL Molecular Graphics System, Version 1.7. 4. Schrodinger LLC.

Schwarze, S.R., Ho, A., Vocero-Akbani, A. & Dowdy, S.F. (1999) In vivo protein transduction: delivery of a biologically active protein into the mouse. *Science (New York, N.Y.)*, 285, 1569-1572.

Segawa, K. & Nagata, S. (2015) An apoptotic 'eat me'signal: phosphatidylserine exposure. *Trends in cell biology*, 25, 639-650.

Sensi, S.L., Ton-That, D., Sullivan, P.G., Jonas, E.A., Gee, K.R., Kaczmarek, L.K. & Weiss, J.H. (2003) Modulation of mitochondrial function by endogenous Zn2+ pools. *Proc Natl Acad Sci U S A*, 100, 6157-6162.

Sesti, F. (2016) Oxidation of K(+) Channels in Aging and Neurodegeneration. *Aging and disease*, 7, 130-135.

Shah, N.H. & Aizenman, E. (2014) Voltage-gated potassium channels at the crossroads of neuronal function, ischemic tolerance, and neurodegeneration. *Translational stroke research*, 5, 38-58.

Shah, N.H., Schulien, A.J., Clemens, K., Aizenman, T.D., Hageman, T.M., Wills, Z.P. & Aizenman, E. (2014) Cyclin e1 regulates Kv2.1 channel phosphorylation and localization in neuronal ischemia. *The Journal of neuroscience : the official journal of the Society for Neuroscience*, 34, 4326-4331.

Sheline, C.T., Zhu, J., Zhang, W., Shi, C. & Cai, A.-L. (2013) Mitochondrial inhibitor models of Huntington's disease and Parkinson's disease induce zinc accumulation and are attenuated by inhibition of zinc neurotoxicity in vitro or in vivo. *Neurodegenerative Diseases*, 11, 49-58.

Shen, J., Rathore, S.S., Khandan, L. & Rothman, J.E. (2010) SNARE bundle and syntaxin N-peptide constitute a minimal complement for Munc18-1 activation of membrane fusion. *The Journal of cell biology*, 190, 55-63.

Shen, Q.J., Zhao, Y.M., Cao, D.X. & Wang, X.L. (2009) Contribution of Kv channel subunits to glutamate-induced apoptosis in cultured rat hippocampal neurons. *Journal of neuroscience research*, 87, 3153-3160.

Shepherd, A.J., Loo, L., Gupte, R.P., Mickle, A.D. & Mohapatra, D.P. (2012) Distinct modifications in Kv2.1 channel via chemokine receptor CXCR4 regulate neuronal survival-death dynamics. *The Journal of neuroscience : the official journal of the Society for Neuroscience*, 32, 17725-17739.

Shi, P.-y., Zhou, X.-c., Yin, X.-x., Xu, L.-l., Zhang, X.-m. & Bai, H.-y. (2016) Early application of citicoline in the treatment of acute stroke: a meta-analysis of randomized controlled trials. *Journal of Huazhong University of Science and Technology [Medical Sciences]*, 36, 270-277.

Shimamoto, K., Lebrun, B., Yasuda-Kamatani, Y., Sakaitani, M., Shigeri, Y., Yumoto, N. & Nakajima, T. (1998) DL-threo-β-benzyloxyaspartate, a potent blocker of excitatory amino acid transporters. *Molecular pharmacology*, 53, 195-201.

Simola, N., Morelli, M. & Carta, A.R. (2007) The 6-hydroxydopamine model of Parkinson's disease. *Neurotoxicity research*, 11, 151-167.

Singer-Lahat, D., Chikvashvili, D. & Lotan, I. (2008) Direct interaction of endogenous Kv channels with syntaxin enhances exocytosis by neuroendocrine cells. *PLoS One*, 3, e1381.

Singer-Lahat, D., Sheinin, A., Chikvashvili, D., Tsuk, S., Greitzer, D., Friedrich, R., Feinshreiber, L., Ashery, U., Benveniste, M. & Levitan, E.S. (2007) K+ channel facilitation of exocytosis by dynamic interaction with syntaxin. *Journal of Neuroscience*, 27, 1651-1658.

Sinor, J.D., Du, S., Venneti, S., Blitzblau, R.C., Leszkiewicz, D.N., Rosenberg, P.A. & Aizenman, E. (2000) NMDA and glutamate evoke excitotoxicity at distinct cellular locations in rat cortical neurons in vitro. *Journal of Neuroscience*, 20, 8831-8837.

Siprashvili, Z. & Khavari, P.A. (2004) Lentivectors for regulated and reversible cutaneous gene delivery. *Molecular Therapy*, 9, 93-100.

Speca, D.J., Ogata, G., Mandikian, D., Bishop, H.I., Wiler, S.W., Eum, K., Wenzel, H.J., Doisy, E.T., Matt, L., Campi, K.L., Golub, M.S., Nerbonne, J.M., Hell, J.W., Trainor, B.C., Sack, J.T., Schwartzkroin, P.A. & Trimmer, J.S. (2014) Deletion of the Kv2.1 delayed rectifier potassium channel leads to neuronal and behavioral hyperexcitability. *Genes Brain Behav*, 13, 394-408.

Stalmans, S., Bracke, N., Wynendaele, E., Gevaert, B., Peremans, K., Burvenich, C., Polis, I. & De Spiegeleer, B. (2015) Cell-penetrating peptides selectively cross the blood-brain barrier in vivo. *PloS one*, 10, e0139652.

Stas, J.I., Bocksteins, E., Jensen, C.S., Schmitt, N. & Snyders, D.J. (2016) The anticonvulsant retigabine suppresses neuronal KV2-mediated currents. *Scientific Reports*, 6.

Steller, H. (1998) Artificial death switches: induction of apoptosis by chemically induced caspase multimerization. *Proceedings of the National Academy of Sciences of the United States of America*, 95, 5421-5422.

Su, H., Arakawa-Hoyt, J. & Kan, Y.W. (2002) Adeno-associated viral vector-mediated hypoxia response element-regulated gene expression in mouse ischemic heart model. *Proceedings of the National Academy of Sciences*, 99, 9480-9485.

Szabò, I., Lepple-Wienhues, A., Kaba, K.N., Zoratti, M., Gulbins, E. & Lang, F. (1998) Tyrosine kinase-dependent activation of a chloride channel in CD95-induced apoptosis in T lymphocytes. *Proceedings of the National Academy of Sciences*, 95, 6169-6174.

Tellinghuisen, T.L., Evans, M.J., von Hahn, T., You, S. & Rice, C.M. (2007) Studying hepatitis C virus: making the best of a bad virus. *Journal of virology*, 81, 8853-8867.

Tellinghuisen, T.L., Marcotrigiano, J. & Rice, C.M. (2005) Structure of the zinc-binding domain of an essential component of the hepatitis C virus replicase. *Nature*, 435, 374-379.

Thompson, G.J., LANGLAIS, C., Kelvin, C., CONLEY, E.C. & COHEN, G.M. (2001) Elevated extracellular [K+] inhibits death-receptor-and chemical-mediated apoptosis prior to caspase activation and cytochrome c release. *Biochemical Journal*, 357, 137-145.

Thrift, A.G., Thayabaranathan, T., Howard, G., Howard, V.J., Rothwell, P.M., Feigin, V.L., Norrving, B., Donnan, G.A. & Cadilhac, D.A. (2016) Global stroke statistics. *International journal of stroke : official journal of the International Stroke Society*.

Toonen, R.F. & Verhage, M. (2007) Munc18-1 in secretion: lonely Munc joins SNARE team and takes control. *Trends in neurosciences*, 30, 564-572.

Tsuda, M., Imaizumi, K., Katayama, T., Kitagawa, K., Wanaka, A., Tohyama, M. & Takagi, T. (1997) Expression of zinc transporter gene, ZnT-1, is induced after transient forebrain ischemia in the gerbil. *Journal of Neuroscience*, 17, 6678-6684.

Tymianski, M. (2013) Novel approaches to neuroprotection trials in acute ischemic stroke. *Stroke*, 44, 2942-2950.

Tymianski, M. (2014) Stroke in 2013: disappointments and advances in acute stroke intervention. *Nature reviews. Neurology*, 10, 66-68.

Uversky, V.N. (2015) Intrinsically disordered proteins and their (disordered) proteomes in neurodegenerative disorders. *Frontiers in aging neuroscience*, 7, 18.

Valentine, J.S. & Hart, P.J. (2003) Misfolded CuZnSOD and amyotrophic lateral sclerosis. *Proceedings of the National Academy of Sciences*, 100, 3617-3622.

Verhage, M., Maia, A.S., Plomp, J.J., Brussaard, A.B., Heeroma, J.H., Vermeer, H., Toonen, R.F., Hammer, R.E., Missler, M. & Geuze, H.J. (2000) Synaptic assembly of the brain in the absence of neurotransmitter secretion. *Science (New York, N.Y.)*, 287, 864-869.

Wang, G.J., Chung, H.J., Schnuer, J., Lea, E., Robinson, M.B., Potthoff, W.K., Aizenman, E. & Rosenberg, P.A. (1998) Dihydrokainate-sensitive neuronal glutamate transport is required for protection of rat cortical neurons in culture against synaptically released glutamate. *The European journal of neuroscience*, 10, 2523-2531.

Wang, M., Zhi, D., Wang, H., Ru, Y., Ren, H., Wang, N., Liu, Y., Li, Y. & Li, H. (2016) TAT-HSA-α-MSH fusion protein with extended half-life inhibits tumor necrosis factor-α in brain inflammation of mice. *Applied microbiology and biotechnology*, 1-9.

Waszkielewicz, M., Gunia, A., Szkaradek, N., Sloczynska, K., Krupinska, S. & Marona, H. (2013) Ion channels as drug targets in central nervous system disorders. *Current medicinal chemistry*, 20, 1241-1285.

Wegmann, S., Eftekharzadeh, B., Tepper, K., Zoltowska, K. M., Bennett, R. E., Dujardin, S., … Hyman, B. T. (2018). Tau protein liquid-liquid phase separation can initiate tau aggregation. *The EMBO journal*, *37*(7), e98049. doi:10.15252/embj.201798049

Wei, G., Hough, C., Li, Y. & Sarvey, J. (2004a) Characterization of extracellular accumulation of Zn2+ during ischemia and reperfusion of hippocampus slices in rat. *Neuroscience*, 125, 867-877.

Wei, L., Xiao, A.Y., Jin, C., Yang, A., Lu, Z.Y. & Yu, S.P. (2004b) Effects of chloride and potassium channel blockers on apoptotic cell shrinkage and apoptosis in cortical neurons. *Pflügers Archiv*, 448, 325-334.

Wei, L., Yu, S.P., Gottron, F., Snider, B.J., Zipfel, G.J. & Choi, D.W. (2003) Potassium channel blockers attenuate hypoxia-and ischemia-induced neuronal death in vitro and in vivo. *Stroke*, 34, 1281-1286.

Weimer, R.M., Richmond, J.E., Davis, W.S., Hadwiger, G., Nonet, M.L. & Jorgensen, E.M. (2003) Defects in synaptic vesicle docking in unc-18 mutants. *Nature neuroscience*, 6, 1023-1030.

Weir, M.L., Xie, H., Klip, A. & Trimble, W.S. (2001) VAP-A binds promiscuously to both v- and tSNAREs. *Biochemical and biophysical research communications*, 286, 616-621.

Wilson, S.M., Brittain, J.M., Piekarz, A.D., Ballard, C.J., Ripsch, M.S., Cummins, T.R., Hurley, J.H., Khanna, M., Hammes, N.M., Samuels, B.C., White, F.A. & Khanna, R. (2011) Further insights into the antinociceptive potential of a peptide disrupting the N-type calcium channel-CRMP-2 signaling complex. *Channels*, 5, 449-456.

Wilson, S.M., Schmutzler, B.S., Brittain, J.M., Dustrude, E.T., Ripsch, M.S., Pellman, J.J., Yeum, T.S., Hurley, J.H., Hingtgen, C.M., White, F.A. & Khanna, R. (2012) Inhibition of transmitter release and attenuation of anti-retroviral-associated and tibial nerve injury-related painful peripheral neuropathy by novel synthetic Ca2+ channel peptides. *The Journal of biological chemistry*, 287, 35065-35077.

Wolf-Goldberg, T., Michaelevski, I., Sheu, L., Gaisano, H.Y., Chikvashvili, D. & Lotan, I. (2006) Target soluble N-ethylmaleimide-sensitive factor attachment protein receptors (t-SNAREs) differently regulate activation and inactivation gating of Kv2.2 and Kv2.1: Implications on pancreatic islet cell Kv channels. *Mol Pharmacol*, 70, 818-828.

Wu, K., Yang, P., Li, S., Liu, C. & Sun, F. (2015) VEGF attenuated increase of outward delayed-rectifier potassium currents in hippocampal neurons induced by focal ischemia via PI3-K pathway. *Neuroscience*, 298, 94-101.

Wu, X., Hernandez-Enriquez, B., Banas, M., Xu, R. & Sesti, F. (2013) Molecular mechanisms underlying the apoptotic effect of KCNB1 K+ channel oxidation. *The Journal of biological chemistry*, 288, 4128-4134.

Xia, C.-F., Smith, R.S., Shen, B., Yang, Z.-R., Borlongan, C.V., Chao, L. & Chao, J. (2006) Postischemic brain injury is exacerbated in mice lacking the kinin B2 receptor. *Hypertension*, 47, 752-761.

Yao, H., Zhou, K., Yan, D., Li, M. & Wang, Y. (2009) The Kv2. 1 channels mediate neuronal apoptosis induced by excitotoxicity. *Journal of neurochemistry*, 108, 909-919.

Ye, Z., Baumgartner, M.P., Wingert, B.M. & Camacho, C.J. (2016) Optimal strategies for virtual screening of induced-fit and flexible target in the 2015 D3R Grand Challenge. *Journal of computer-aided molecular design*, 30, 695-706.

Yeh, C.Y., Bulas, A.M., Moutal, A., Saloman, J.L., Hartnett, K.A., Anderson, C.T., Tzounopoulos, T., Sun, D., Khanna, R. & Aizenman, E. (2017) Targeting a Potassium Channel/Syntaxin Interaction Ameliorates Cell Death in Ischemic Stroke. *J Neurosci*.

Yu, S.P. (2003) Regulation and critical role of potassium homeostasis in apoptosis. *Progress in neurobiology*, 70, 363-386.

Yu, S.P., Farhangrazi, Z.S., Ying, H.S., Yeh, C.-H. & Choi, D.W. (1998) Enhancement of outward potassium current may participate in β-amyloid peptide-induced cortical neuronal death. *Neurobiology of disease*, 5, 81-88.

Yu, S.P. & Kerchner, G.A. (1998) Endogenous voltage-gated potassium channels in human embryonic kidney (HEK293) cells. *Journal of neuroscience research*, 52, 612-617.

Yu, S.P., Yeh, C.-H., Sensi, S.L., Gwag, B.J., Canzoniero, L.M., Farhangrazi, Z.S., Ying, H.S., Tian, M., Dugan, L.L. & Choi, D.W. (1997) Mediation of neuronal apoptosis by enhancement of outward potassium current. *Science (New York, N.Y.)*, 278, 114-117.

Yu, W., Parakramaweera, R., Teng, S., Gowda, M., Sharad, Y., Thakker-Varia, S., Alder, J. & Sesti, F. (2016) Oxidation of KCNB1 Potassium Channels Causes Neurotoxicity and Cognitive Impairment in a Mouse Model of Traumatic Brain Injury. *The Journal of neuroscience: the official journal of the Society for Neuroscience*, 36, 11084.

Yu, W., Shin, M.R. & Sesti, F. (2018) Oxidation of KCNB1 channels in the human brain and in mouse model of Alzheimer's disease. *Cell death & disease*, 9, 820.

Yu, W., Zhang, H., Shin, M.R. & Sesti, F. (2019) Oxidation of KCNB1 potassium channels in the murine brain during aging is associated with cognitive impairment. *Biochemical and Biophysical Research Communications*.

Yuan, H., Wang, W.-P., Feng, N., Wang, L. & Wang, X.-L. (2011) Donepezil attenuated oxygen–glucose deprivation insult by blocking Kv2. 1 potassium channels. *European journal of pharmacology*, 657, 76-83.

Zhang, W.W., Li, L., Li, D., Liu, J., Li, X., Li, W., Xu, X., Zhang, M.J., Chandler, L.A., Lin, H., Hu, A., Xu, W. & Lam, D.M. (2018) The First Approved Gene Therapy Product for Cancer Ad-p53 (Gendicine): 12 Years in the Clinic. *Human gene therapy*, 29, 160-179.

Zhang, Y., McKay, S.E., Bewley, B. & Kaczmarek, L.K. (2008) Repetitive firing triggers clustering of Kv2. 1 potassium channels in Aplysia neurons. *Journal of Biological Chemistry*, 283, 10632-10641.

Zhu, D., Koo, E., Kwan, E., Kang, Y., Park, S., Xie, H., Sugita, S. & Gaisano, H. (2013) Syntaxin-3 regulates newcomer insulin granule exocytosis and compound fusion in pancreatic beta cells. *Diabetologia*, 56, 359-369.

Zincarelli, C., Soltys, S., Rengo, G. & Rabinowitz, J.E. (2008) Analysis of AAV Serotypes 1–9 Mediated Gene Expression and Tropism in Mice After Systemic Injection. *Molecular Therapy*, 16, 1073-1080.

Zou, H., Li, Y., Liu, X. & Wang, X. (1999) An APAF-1· cytochrome c multimeric complex is a functional apoptosome that activates procaspase-9. *Journal of Biological Chemistry*, 274, 11549-11556.

Zou, L.-l., Ma, J.-L., Wang, T., Yang, T.-B. & Liu, C.-B. (2013) Cell-penetrating peptide-mediated therapeutic molecule delivery into the central nervous system. *Current neuropharmacology*, 11, 197-208.